Chapter 4 Strong Motion Velocity Instrument Performance in 2003 M8.3 Tokachi-Oki Earthquake

4.1 Introduction

The M8.3 Tokachi-Oki earthquake hit the South-East side of the Northern Japanese island of Hokkaido on 04:50AM on the morning of the 26^{th} September 2003, local time (25 September at 19:50:06.2, UTC). The epicentre was about 145km SSW of the the town of Kushiro, 41.775^{o}Lat, 143.904^{o}Long, at a depth of $27km$ (`neic.usgs.gov`). The reverse-thrust earthquake occurred on a fault at the plate interface between the over-riding North American plate, which extends into the North-East corner of the Eurasian land-mass, including Hokkaido Island, and the subducting Pacific plate. Tectonic measurements indicate that at this boundary, the Pacific plate moves WNW at a rate of about $8.2cm/year$ relative to the the North American plate (`earthquake.usgs.gov`).

This earthquake occurred in a region extraordinarily well instrumented, and provided an excellent set of strong motion records and GPS displacements. Three large networks operate strong motion instrumentation under the National Research Institute for Earth Science and Disaster Prevention, NIED (Okada et al, 2003). Currently, all NIED data is openly available to the community through their Web-site (`www.bosai.go.jp`). One of these networks, FREESIA, or F-NET, operates Tokyo-Sokushin VSE-355G and VSE-355G2 instruments. Independent of NIED, another network, the Warning Information System of Earthquakes (WISE, `www.ceri.go.jp`), operated by the Structural Division of the Civil Engineering Research Institute of Hokkaido, in Sapporo, provides about 140 single instrument stations also with Tokyo-Sokushin strong motion velocity (VSE-355EI) instruments.

This Chapter evaluates the field performance of VSE series of instruments during the

earthquake. Some major areas of concern, highlighted in the previous two Chapters, are investigated. The ability of the instrument to recover ground displacements is investigated by comparing the permanent offsets after strong motion has passed with the GPS network in the region. It is obvious that the Tokyo Sokushin sensors, with corners at about $56s$ for the VSE-355EI, and at about $94s$ for the VSE-355G and VSE-355G2, have problems recovering large static offsets even using the time-domain deconvolved timeseries. They are also highly sensitive to tilt, in a similar manner to accelerometers (shown in Figure 3.7). The character of the instrument during strong motion is also investigated. In all cases where the VSE-355G2 records velocities above $17cm/s$ (though only at 2 stations), the timeseries is observed to be unstable. This was also observed in the laboratory (Figure 3.21). In this event, spikes are also often observed in the timeseries, though unlike in the cart test clipping, only a very short (if any) flat-line is seen. Only one VSE-355G instrument was subjected to velocities above $10cm/s$, and it performed without apparent problem reaching $21.7cm/s$ (Station URH in Figure 4.35). Many VSE-355EI in the WISE array recorded motions above $10cm/s$, some even above $100cm/s$ — the network is more dense, and as the stations are located on structures, the response is often dominated by the structural resonances, unlike the $40m$ deep F-Net vaults. This local, large effect means the WISE array may not be readily compared with data from the free-field stations. Static offsets are also more unstable, partly due to this as well as the short corner frequency at $56s$.

The usefulness of the strong motion sensor in a broadband network is also discussed. All high-gain broadband instruments are saturated within a $500km$ radius, and some instruments out to a distance of nearly $1000km$ are clipped. An earthquake of this magnitude has strong motion signals with good signal-to-noise thousands of kilometers from the epicenter for a $144dB$ quality sensor. Consequently, comparing the broadband and strong motion signals from large events for all stations within a network is demonstrated to be a useful way to determine the operational health the network. In this network, the VSE sensors and some broadband instruments (the STS-1 and CMG-1T), show evidence of signal non-linearities at levels well below their expected clip level. The broadband sensors also exhibit a lot more variability in signal calibration than the widely deployed STS-2.

4.2 The Available Networks

A map of Japan with all the NIED and WISE station locations is presented in Figure 4.1. Figure 4.2 shows the same data for Hokkaido Island. The characteristics of a typical station in each network is described as follows:

4.2.1 F-Net

This is a 'full-range' seismographic network, with every station consisting of a broadband instrument as well as a strong motion instrument. Each of the 6 channels are recorded with 27-bit dataloggers (originally the Quanterra Q680 was used, but to ensure compatibility with other networks, a Japanese manufactured digitiser is now used). There are about 80 stations throughout Japan, spaced at about $100km$ intervals. The instruments are co-located in tunnels $30-50m$ deep to reduce noise. Data is continuously telemetered to NIED in Tsukuba and archived. The dynamic and frequency range covered by these stations are very similar to a typical CISN station in Southern California. $100Hz$ data is available.

4.2.2 K-Net

'Kyoshin Net' is a dense strong motion network consisting of over 1000 accelerometer stations at free-field sites at intervals of $20km$ covering the country. These instruments are located on the ground surface. The stations have K-NET95 accelerometers, with $144dB$ dynamic range and a clip of $2g$. Frequency bandwidth is from about $20Hz$ to DC. The on-site digitiser is 24bits with a sampling frequency of $100Hz$. Data is triggered, with automatic dial-in once an event has been recorded. Most K-Net stations are located on thick sedimentary sites in urban areas.

4.2.3 KiK-Net

'Kiban Kyoshin-Net' is also a nationwide strong motion Network, with about 650 stations. Each station consists of an up-hole and down-hole accelerometer, with 6 channels of data. The depth of the boreholes range from a minimum of $100m$, to a maximum of $2000m$.

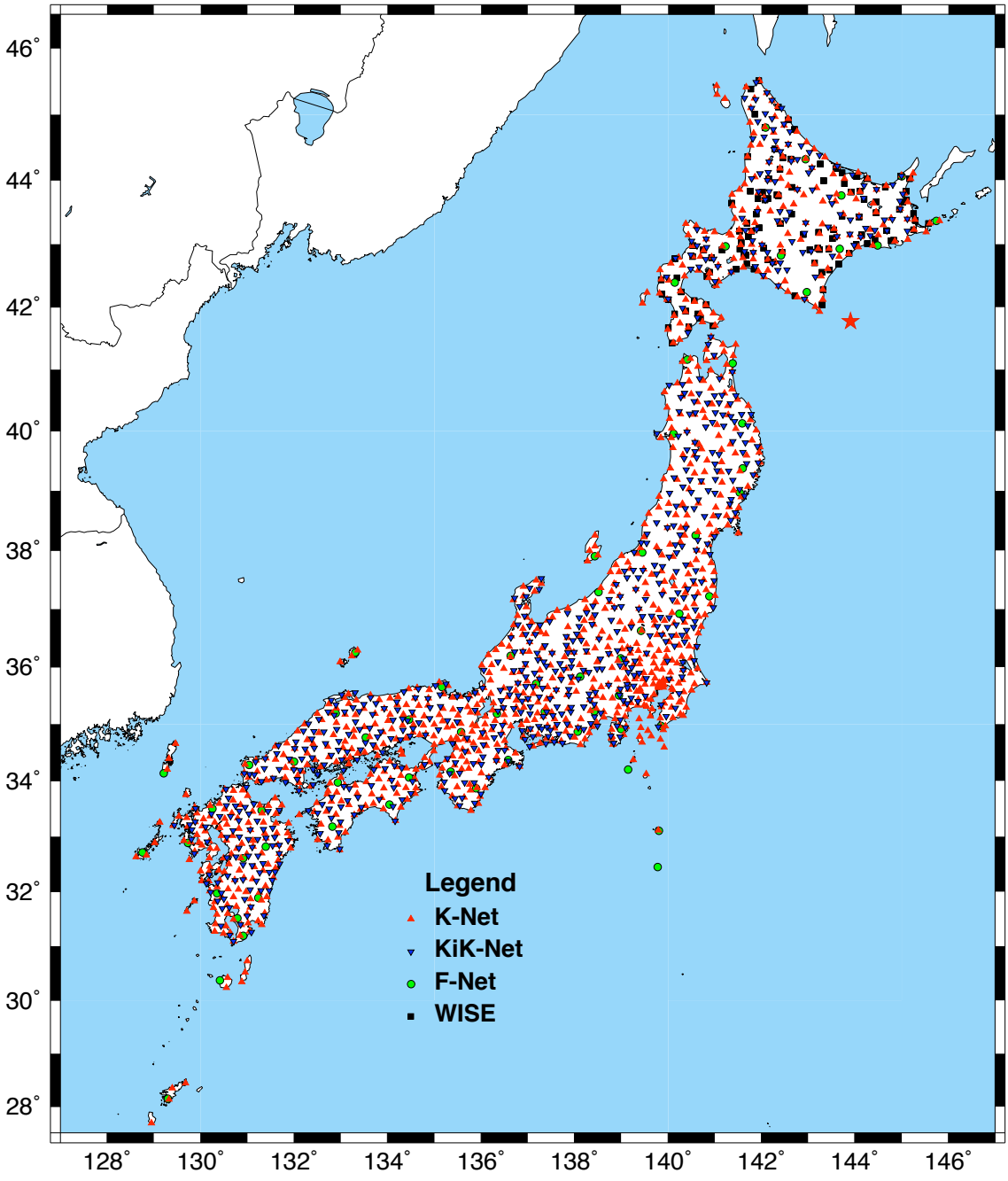

Figure 4.1: Strong motion stations in Japan: F-Net, K-Net, KiK-Net and WISE. Star indicates M8.3 Epicenter.

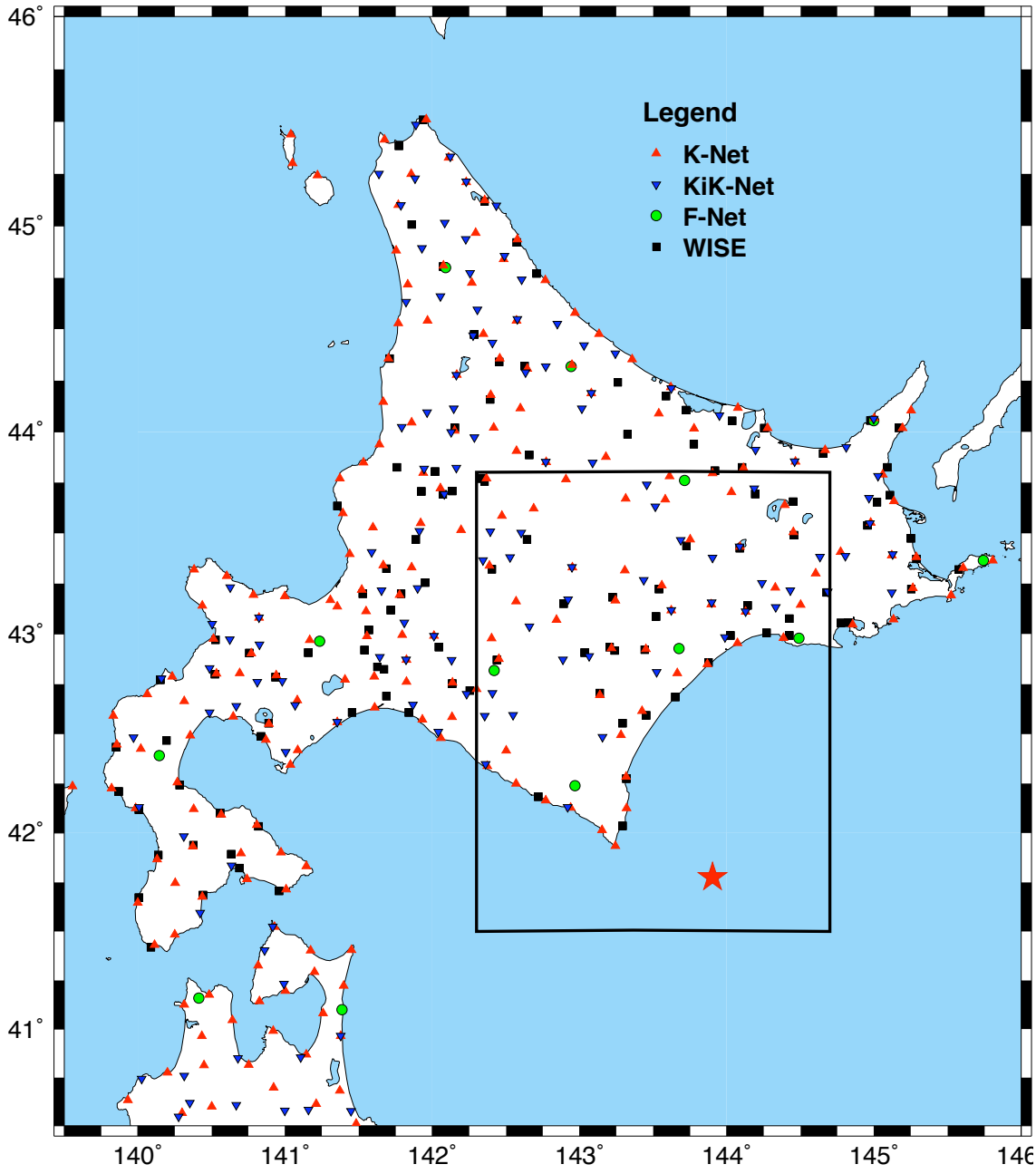

Figure 4.2: Strong motion stations in Hokkaido: WISE Network, F-Net, K-Net and KiK-Net stations. Star indicates M8.3 Epicenter. Box is outline of the boundaries of the south-eastern Hokkaido Plot, Figure 4.11.

The modal depth is about 300m. KiK-Net stations piggy-back on the existing Hi-Net (high sensitivity network) boreholes, and so are located mainly on rock or thin sedimentary sites. Instrumentation is the same as in the K-Net sites, with K-Net95 accelerometers, though sampling is at 200Hz. Automatic dial-in ISDN phone line transmission is used to retrieve the data, as in K-Net.

4.2.4 WISE

The Warning Information System of Earthquakes (WISE) is a strong motion network consisting of VSE-355EI instruments in single sensor stations, with 16-bits dataloggers digitising at 100Hz (*personal communication, Isamu Yokoi, 2003*). The 140 stations, approximately at 40km spacing, are at important civil infrastructure locations throughout Hokkaido, such as highway embankments, dams and bridges. Unfortunately, a station list with details of the structure being monitored by each sensor, and the proximity of the sensor to the structure, is not available. The timeseries data indicates many of the sensors are located on the structures, as there are strong resonances dominating the response. The VSE-355EI is a velocity strong motion seismometer, like the VSE-355G2 but with a more limited frequency range, from 0.0188Hz (56s) to 100Hz. The dynamic range is just below the VSE-355G2, at 136dB (`www.to-soku.co.jp/english.html`), with expected clip at 200cm/s. The digitiser is only 16bits, so the output data has only about 90dB dynamic range. ISDN packet lines are used to transmit data once the sensor has triggered in near-real time. The network was primarily developed to rapidly determine damage levels of critical civil infrastructure on the island in the event of a large earthquake.

Stations from all 4 of these networks obtained multiple records from within 100km of epicenter.

4.3 Static Offset — GPS and Seismometers

In Japan, the Geographical Survey Institute measures crustal deformation using GEONET, the GPS Earth Observation Network. This is a dense network of GPS stations located throughout the country. GPS data is collected and distributed to the public through their Web-site `mekira.gsi.go.jp/ENGLISH/index.html`. Data from the Website is available in Cartesian co-ordinates (X,Y,Z) at a sampling rate of 1 sample per day.

The method outlined in Strang and Borre (1997), which employs a reference ellipsoid, is used to convert these Cartesian co-ordinates to a latitude, longitude and height. The reference ellipsoid selected is the World Geodetic System (1984) ellipsoid, with ellipsoid parameters $a = 6378137m$ and $1/f = 298.257223568$; a is the major axis length (the radius of earth at the equator), and f is the dimensionless flattening of the earth. The Matlab function TOGEOID.M, from `kom.auc.dk/~borre/matlab/sat_cons/`, is used to perform the conversion.

The deformation in cm along the lines of latitude (corresponds to E-W component) and longitude (N-S) are then determined from the relative change in the geographical co-ordinates. At $43.5^o Latitude$, the length of a degree of latitude is $111.102km$ and the length of a degree of longitude is $80.877km$ (National Geospatial-Intelligence Agency, `pollux.nss.nima.mil/calc/degree.html`).

There is some variation between each daily recording that appears to be due to measurement error. Thus, to reduce this, an average co-ordinate change over the seven days before and after the earthquake is used. Figure 4.3 shows the variation over this period for several stations at varying distances from the epicenter. For simplicity, it is assumed all the drift that occurs is due to the dynamic tectonic movement associated with the earthquake rupture, and the displacement caused by aftershocks is negligible. This assumption is satisfactory for the accuracy involved in this study, though Figure 4.4 shows there is significant further displacements at nearby stations due to the M7.1 aftershock.

The GPS displacement field can be compared to the displacement field from the strong motion records once these calculations have been made. As there is static offset, the instrument responses of each seismometer need to be removed. This deconvolution is performed

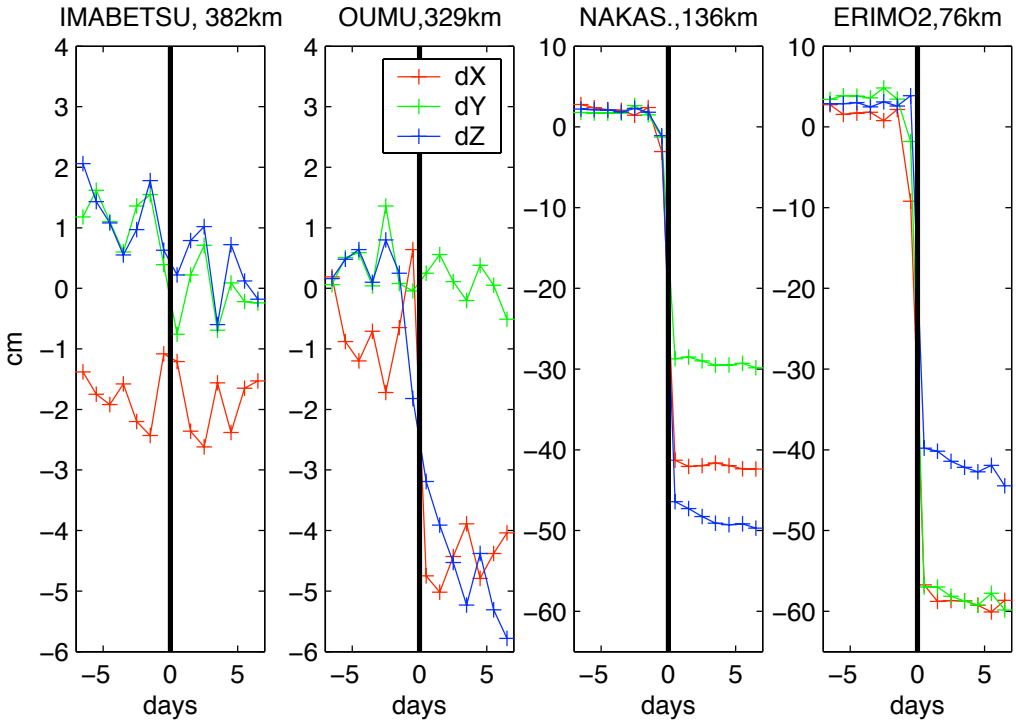

Figure 4.3: Variation of GPS readings at 4 stations of varying distance from the mainshock, in the week before and the week after the M8.3 earthquake. Data is 1 sample/day, obtained from the Web.

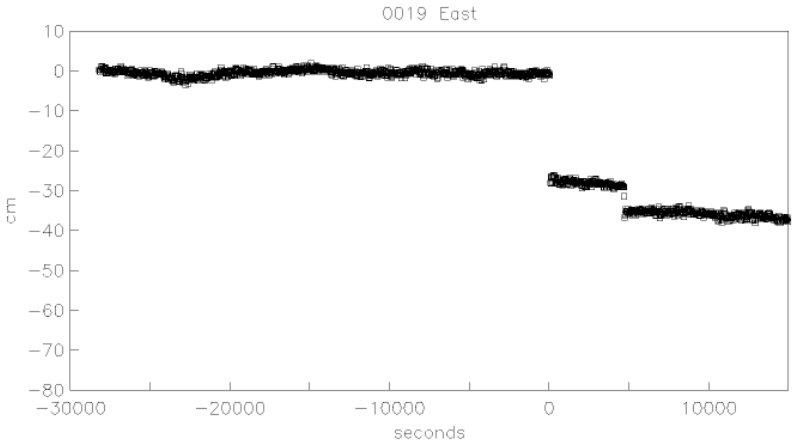

Figure 4.4: Variation of GPS sampled every 30*s* at station Erimo1 (closest stations to mainshock) from a 12.5*hr* period centered around the mainshock. E-W only. Note large offsets mainshock as well as M7.1 aftershock. From K. Larson (*personal communication*)

by a time domain direct integration of the equivalent equation of motion for the seismometer. The method is described in detail in Chapter 3. As illustrated in Figures 3.5 — 3.10, as the accelerometers have very high natural frequencies, only the instrument gain needs to be removed, and then the signal is integrated twice to recover displacement. For the VSE sensors, the output, $y(t)$, can be converted to ground displacement, $u(t)$ using Equation 3.12, reproduced here —

$$u(t) = \frac{1}{G}\left(\int_0^T y(t)\,dt + 2\beta \iint_0^T y(t)\,dt^2 + \omega_0^2 \iiint_0^T y(t)\,dt^3\right) \tag{4.1}$$

Strong motion VSE sensors are deployed by both the F-Net (with more recent VSE-355G and VSE-355G2), and the WISE Network (all stations deploy older VSE-355EI sensors). There are 13 F-Net stations in the Hokkaido region, and over 100 Hokkaido strong motion stations. After removal of the pre-event mean from the whole signal $y(t)$, the ground displacement $u(t)$ is determined from Equation 4.1. As the VSE-355EI has a much shorter equivalent natural period ($56s$ compared to $\sim 94s$), the parameters β and ω_0^2 are significantly larger, and so are the sizes of the double and triple integral terms, and consequently the permanent displacements are less stable.

The permanent offsets for all the records from the seismometers tend to be unstable. With increasing time, every record becomes unstable. Some records become unstable as soon as the strong motion begins, due to instrument malfunction, clipping, or tilting, others develop numerical instabilities after the strong motion has passed, and the permanent offset can then be more easily estimated. A final estimation of permanent offset for each record is always somewhat subjective. After about $100s$, most records have developed quadratic or at least linear trends, which can swamp the physically plausible offsets. Usually, an offset is taken from about $30s - 100s$ after the strong motion begins, which in the near-field region is after the strongest motions, and the majority of the co-seismic static offset, have occurred. Even when the quality of the displacement record is good, the accuracy of any offset is at best of the order of $0.5cm - 2cm$. Permanent offsets are determined independently of the nearby GPS stations to reduce estimation bias.

Figure 4.5 shows a map of Hokkaido island, where the length and direction of the

arrows emanating from each station represents the static horizontal offsets due to the earthquake. The black arrows are from GPS stations, and the blue and green arrows represent the estimated final horizontal offsets from the WISE and F-Net VSE seismometers respectively. Figure 4.6 presents the vertical components of the final offset for each station. For the VSE stations, a circle surrounding the station indicates a static displacement value was too difficult to estimate, usually due to wild trends leading to non-physically large displacements occurring near the onset of motions. This indicates instrument malfunction, or, in certain regions close to the epicenter, ground failure. Some examples of stations with this response will be shown in the next Section (e.g. Station KMU in Figure 4.23)

It is obvious that in general the VSE instruments do not give an accurate view of the permanent ground displacements as measured by the GPS. The longer period VSE-355G/G2 sensors, located in vaults, perform better than the WISE sensor, although as is shown later, some of these instruments clip at low velocities near the epicenter. It is very difficult to estimate static offset from the WISE VSE-355EI, as the sensors have a comparably short period, and are located at noisy civil infrastructure sites. Though the magnitudes are generally of similar order as the GPS, the azimuths tend to wildly differ from the GPS. Resonances from the structures dominate many WISE records. Another obvious problem is selecting permanent offsets before the major displacements have been recorded — many WISE records are unstable, with large tilts occurring shortly after the strong motion begins. Even if the selected static deformation estimate before instabilities dominant is correct for that time, it may not be the final offset for that site. This may partly explain why motions appear to be the opposite direction for many WISE stations. Another complication is there is strong evidence that the WISE VSE instruments are not oriented correctly. In particular, the E-W and N-S components seem to be recording west and south as positive at certain sites, opposite to the standard convention. Further, in (rectangular) structures, the horizontal channels are usually aligned parallel to the external walls, or main structural orientation. In the case of buildings, bridges and dams, this may not coincide with East and West. Also, all Sokushin instruments have default horizontal channel polarity which produces a negative N-S channel output (or S-N), and this needs to be accounted for in any network, which can easily be forgotten. The individual station timeseries analyses in the next section illus-

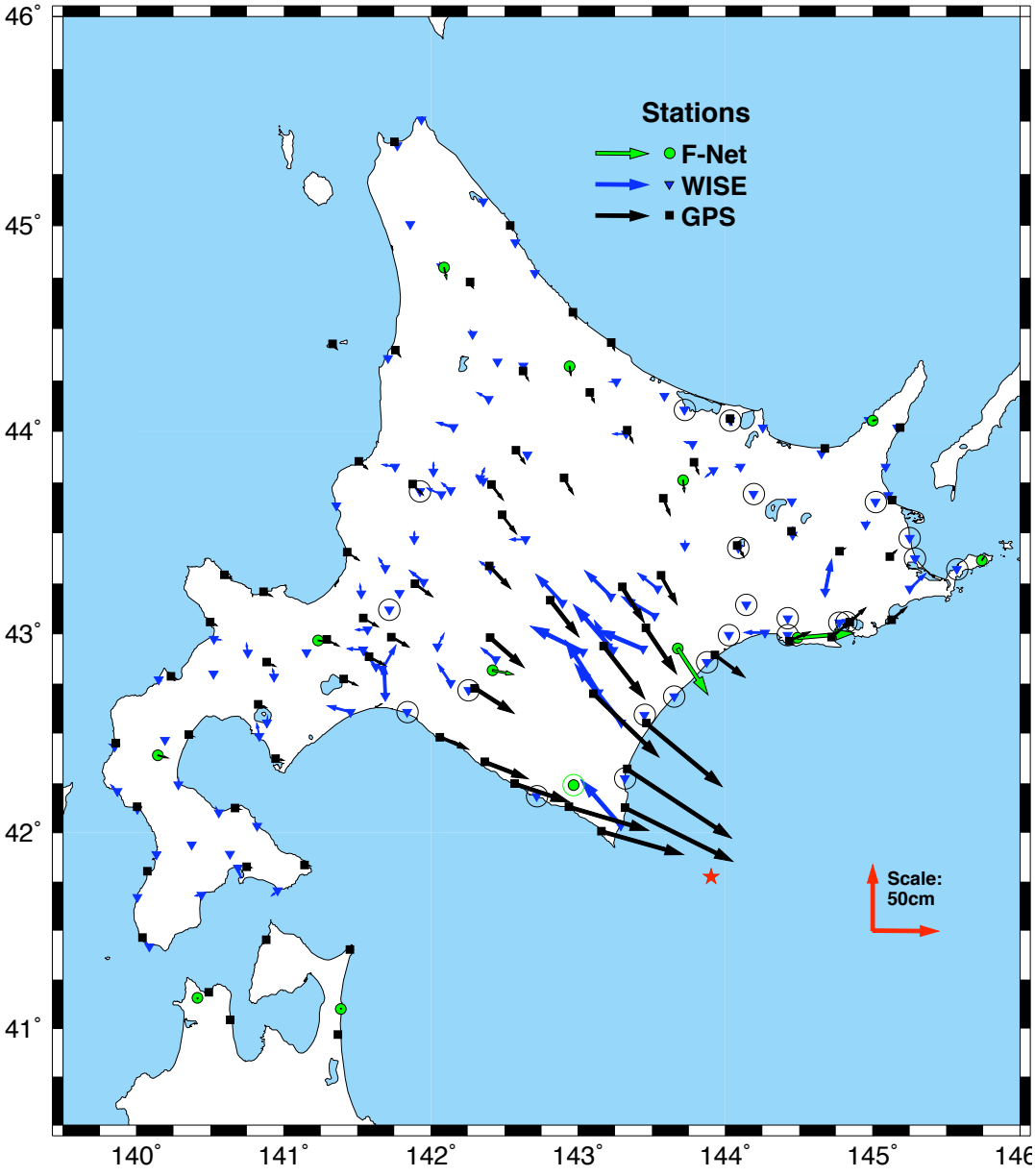

Figure 4.5: Comparison of static horizontal offset due to M8.3 Tokachi-Oki earthquake, as recorded from GPS and strong motion velocity instruments (deconvolved). A circle around a station indicates static offset cannot be estimated, or is non-physically large, indicating serious ground failure or instrument malfunction.

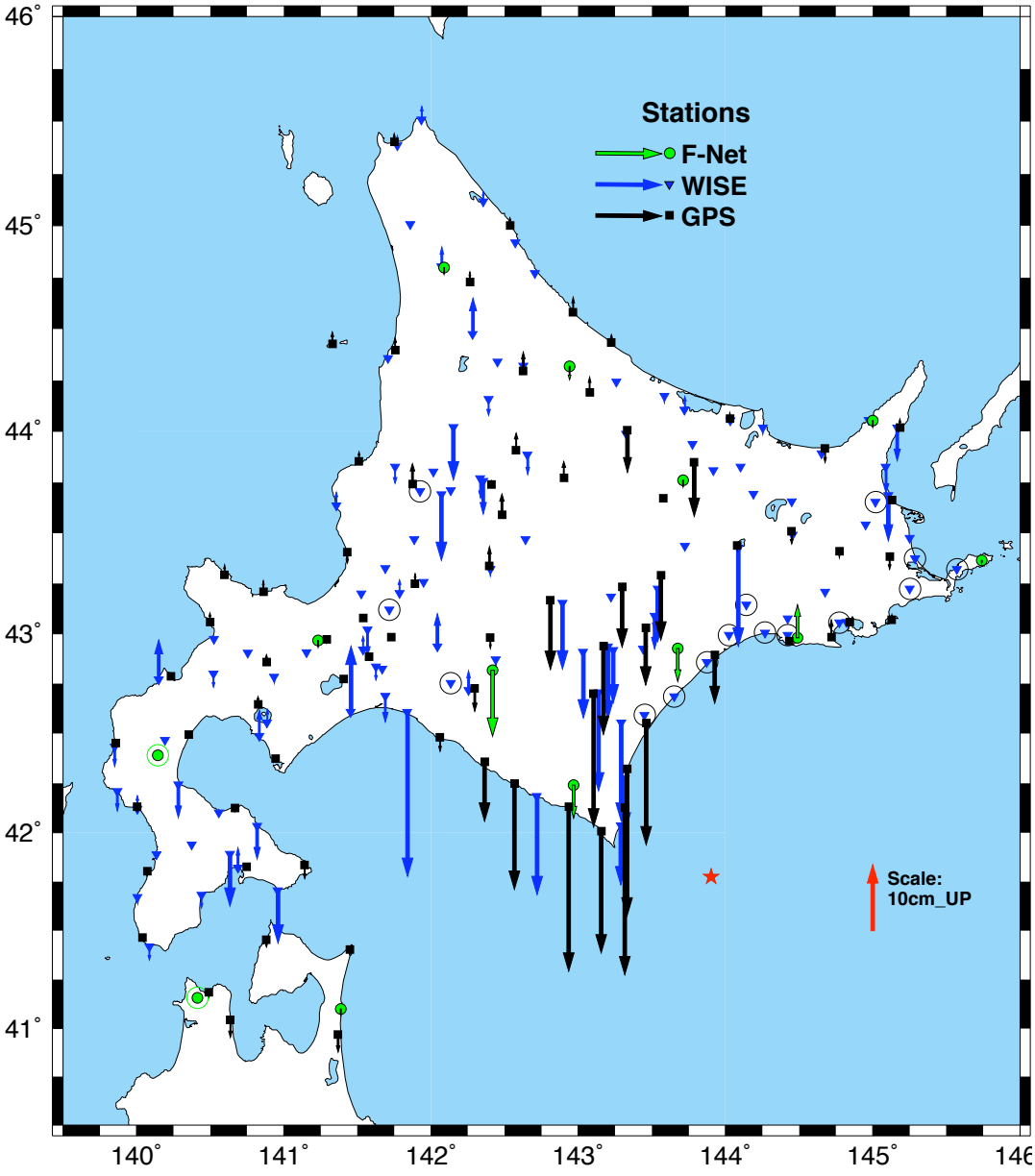

Figure 4.6: Comparison of static vertical offset due to the M8.3 Tokachi-Oki earthquake, as recorded from GPS and strong motion velocity instruments (deconvolved). A circle around a station indicates static offset cannot be estimated, or is non-physically large, indicating serious ground failure or instrument malfunction.

trate evidence for all these problems. It will also be shown that some stations have reversed polarity for both horizontal channels (see Figure 4.42), which explains why many stations have almost exactly reversed azimuth in Figure 4.5. The vertical stations are all properly oriented, and this produces a better displacement field. This improved data quality exposes other deficiencies away from the epicenter in the north and south-west of Hokkaido, where large differences in magnitude and orientation of the final vertical offset of the seismometers is observed with the GPS in Figure 4.5. Note this cannot be blamed on ground tilt, as this would not be widespread at these distances, and further the vertical component is not sensitive to small tilts.

In order to observe how the VSE sensors compare to the accelerometers in terms of static displacement recovery, some K-Net and KiK-Net accelerometer data near the epicentral region were also integrated up to displacement. These data are presented alongside the GPS and VSE static offsets in Figures 4.7 and 4.8. As expected, the double integration leads to serious instabilities commonly observed in accelerometers. This is a well-known problem, and may be due to non-linear behaviour of the accelerometer (though this has not been noted before for this particular instrument), or may be due to a real tilting of the ground (Iwan et al, 1985; Boore, 2001) from the serious and widespread ground failure associated with the event. Even so, many stations, including even the relatively noisy surface free-field K-Net stations close to the epicenter, have remarkable good final estimations.

In particular, the down-hole KiK-Net sites, at depths of over $100m$, are shown as yellow arrows with black outline, show excellent correlation with the GPS field.

Figures 4.9 and 4.10 present the VSE data for the entire island again, but without any instrument correction. For the F-Net stations, continuous data is available, and to estimate the permanent offset, the average displacement from a $10s$ period long after the strong motion shaking is over $(590-600s)$ is used. For the WISE Strong Motion Array, data is available for $200s$, so after a single integration, the permanent offset is defined as the average displacement of the last $10s$ $(190s-200s)$. As expected for instruments insensitive to DC offsets, all F-Net stations, and almost all VSE-355EI stations, have very stable final offsets on all channels after the single integration. It is noted that not all these are zero offsets though. Permanent offsets are observed at numerous stations, even far away from

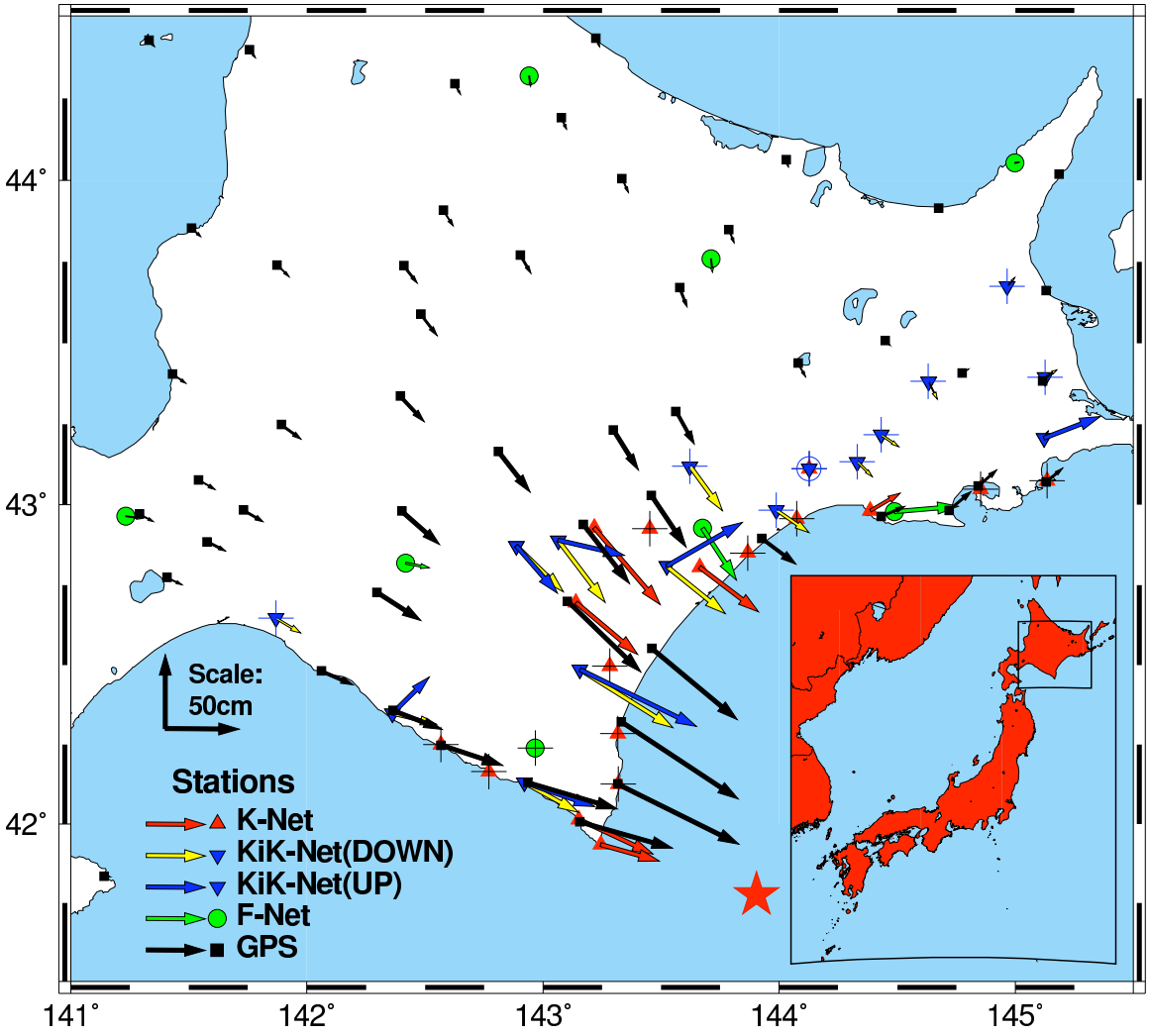

Figure 4.7: Comparison of static horizontal offset due to the M8.3 Tokachi-Oki earthquake, as recorded from GPS, velocity instruments (deconvolved), and accelerometers (deconvolved). Circle around a station indicates it was impossible to estimate a static offset, suggesting serious ground failure or instrument malfunction (for KiK-Net down-hole, '+' indicates impossible to estimate static offset).

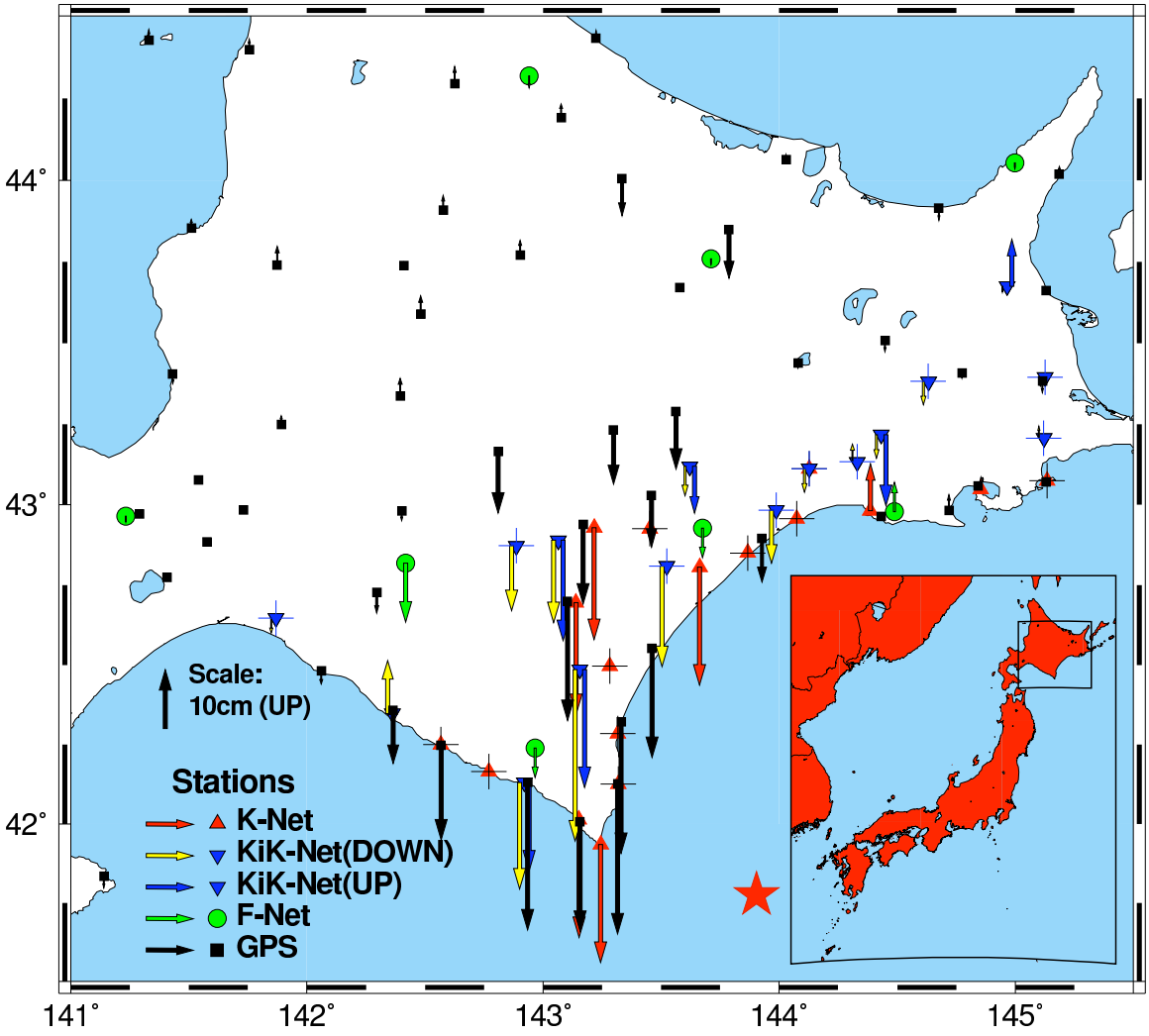

Figure 4.8: Comparison of static vertical offset due to the M8.3 Tokachi-Oki earthquake, as recorded from GPS, velocity instruments (deconvolved), and accelerometers (deconvolved). Circle around a station indicates it was impossible to estimate a static offset, suggesting serious ground failure or instrument malfunction (for KiK-Net down-hole, '+' indicates impossible to estimate static offset).

the mainshock, which recorded peak velocities well under the low clip level of $15cm/s$. These offsets most likely indicate poor instrument performance. One example is from the F-Net VSE-355G2 at station HID, in the south-center of the island.

Recording GPS positions at high frequencies, for example at about $1sps$, is a current area of research. During this earthquake, all the GEONET GPS stations were recording locally at this rate. Unfortunately, without a local power supply back-up at the stations, as there were widespread power outages in the near-field of the event, many stations briefly lost power after a few seconds of strong motion, as parts of the national grid failed. Many stations thus do not record a full uninterrupted time series for the event.

The daily GPS data point for each station is composed of an average of all the high-rate measurements, which minimises as far as possible the many errors, such as atmospheric effects, instantaneous satellite configuration etc. For the high-rate $1sps$ GPS data, no such averaging is possible, so much care must be taken when analysing the data. As there is some concern to quality (and interpretation) of the $1sps$ data, as well as the sheer volume of data this would present, this data is not readily made available. Through personal communication with Kristine Larson, who has obtained and worked on this $1sps$ data, several GPS stations in the near field are seen to have displacement time-series very similar to nearby seismic data. In future, if GPS recording at high sample rates, and seismic instruments are co-located, a general inversion would be possible, solving for for the three linear degrees of freedom, and two rotational degrees of freedom (defined by rotation about the horizontal axes). At this time, this would be the optimal station configuration for recording ground motions.

Larson et al. (2003) presents data showing that seismic deformations recorded during the M7.9 Denali earthquake in November 2002 are indeed similar to nearby high-rate GPS,with similar long period waves being observed by both sensors. The Tokachi-Oki dataset has a far greater network density, and much improved station quality. Further, displacements of over $1m$ are widespread over a very large area encompassing many diverse types of seismic stations. This dataset provides ample information to produce and test an inversion scheme to determine translations and rotations measured at a site using both GPS and seismic records.

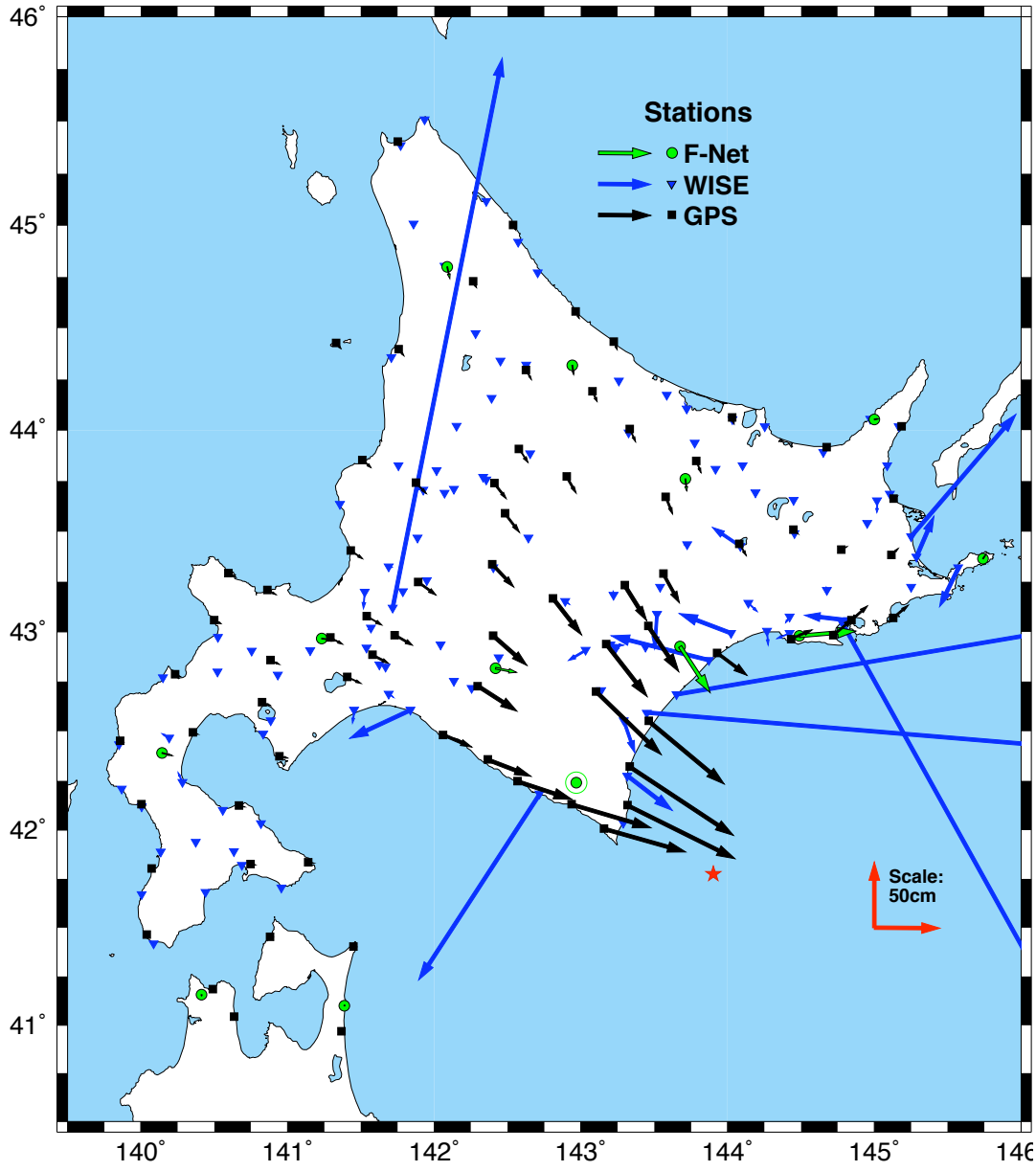

Figure 4.9: Comparison of static horizontal offset as recorded from GPS and strong motion VSE velocity instruments (no deconvolution). Black arrows: GPS, blue: WISE stations, green: F-Net. As expected, without deconvolution, VSE sensors show no static offset unless instrument malfunction or serious site failure occurs.

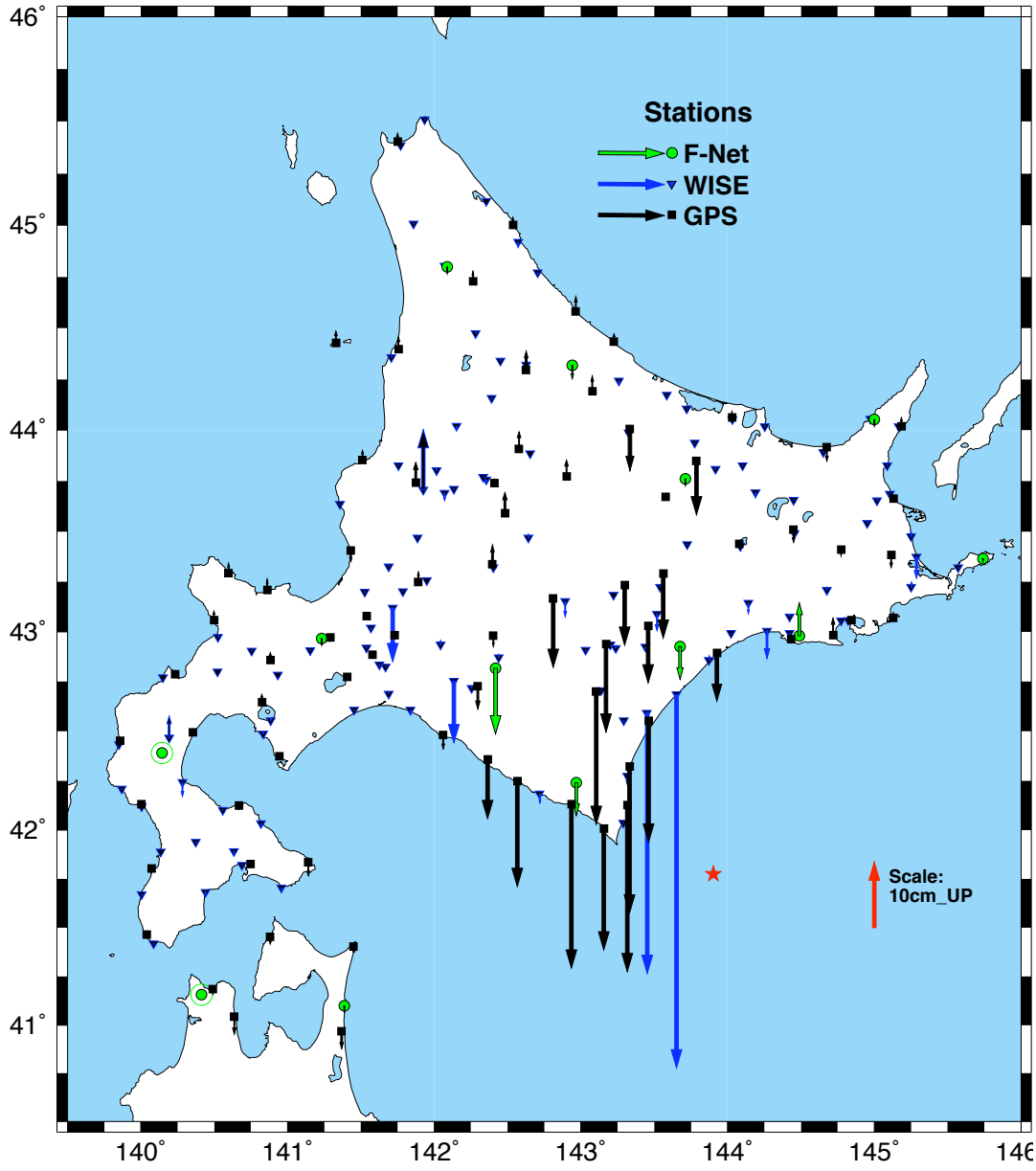

Figure 4.10: Comparison of static vertical offset as recorded from GPS and strong motion VSE velocity instruments (no deconvolution). Black arrows: GPS, blue: WISE stations, green: F-Net. As expected, without deconvolution, VSE sensors show no static offset unless instrument malfunction or serious site failure occurs.

An example of a high-rate GPS record will be presented later in the Chapter (Figure 4.44), where the similarity of the GPS displacement timeseries with that from nearby accelerometers is illustrated.

4.4 Strong Motion around Hokkaido

In this section the VSE performance in general is evaluated from timeseries analysis. Regions nearest the epicenter with a high density of stations, are selected for a comparison of records from the various sensors. The VSE series instruments are compared to each other, as well as to nearby data from accelerometer and GPS stations. By analysis of the individual timeseries, both the dynamic and static performance of the sensor can be evaluated. For the VSE-355G2, errors similar to those observed in the laboratory are repeated during the strong motions.

Though there are two networks that deploy Sokushin VSE instruments — F-Net and WISE — the most reliable indication of the performance of the instrument can be determined from the F-Net stations, as they contain sensors exactly the same as the model tested at Caltech (VSE-355G2), or the most recent predecessor (VSE-355G). Plus, these stations are located at quiet free-field vault sites. Unfortunately, there are few of them in the region of largest motions. The F-Net stations KSR and KMU (both with VSE-355G2 sensors) recorded the strongest velocities, though both instruments exhibit large velocity spikes consistent with low clipping instrument malfunction observed at Caltech. The largest motions that seem to be uncorrupted are from URH (VSE-355G), with peak velocity of $21.7 cm/s$.

All subsequent timeseries data in this sections have the instrument responses removed using the time domain method, unless stated otherwise. Timing is not synchronised between network stations, but is synchronised within networks.

In general the VSE range of instruments have a similar capacity to recover permanent displacements as accelerometers. The F-Net VSE-355G/G2 instruments, once deconvolved, are about as reliable as the K-Net and up-hole KiK-Net accelerometers. Unfortunately only a few of these instruments are located in the near-field. The WISE VSE-355EI are less capable, which may be due to being located at extremely noisy sites, having inexact

orientations, as well as having a short corner period.

The regions investigated in detail are all located in East Hokkaido, as shown in Figure 4.11. Altitude is included on this map. A range of mountains sweep southwards from the centre of the island to the southern tip closest to the epicenter. Assuming relief correlates with station site quality, this tip is the only area with many hard rock stations looked at in detail in the following analysis. It is probably no coincidence that static displacements are well recovered from this region. Unfortunately, only accelerometers are located here. Flat topography, possibly indicating basin geology, dominate the other selected regions, where ground failure was widely reported in the aftermath of the mainshock. This is reflected in general from the displacements in these regions seemingly being contaminated by large tilts.

The damage to civil infrastructure in the near-field cited in this section is from an EQE/ABS Consulting Reconnaissance Report,
`www.eqe.co.jp/pressservice/pressreport/2003Tokachi/tokachi_reportE.pdf`.
Fortunately the region was relatively sparsely populated, with few towns with large structures. Some structures, such as town halls and schools, were damaged. Widespread liquefaction and lateral spreading caused foundation failure of roads, railroads, structures, bridges and ports. A tsunami washed many fishing boats onto the ports. In general though, thanks to the sparse population and infrastructure and the good quality of construction technique (partly due to the known earthquake risk and thick wall construction for insulation against the harsh climate), damage from this large earthquake was limited.

Chapter 1 includes a discussion on how tectonic tilt can be measured from GPS, and then compared to local tilts determined by linear and quadratic trends in the seismic records. Many tilts observed in the field appear not to be due to the tectonic tilt, as they are many times larger. This is shown to include KiK-Net down-hole sites.

4.4.1 Stations near Kushiro town

There is a cluster of stations around the fishing town of Kushiro, the largest town on the East Coast of Hokkaido, about 145km directly North of the epicenter (Figure 4.12). F-

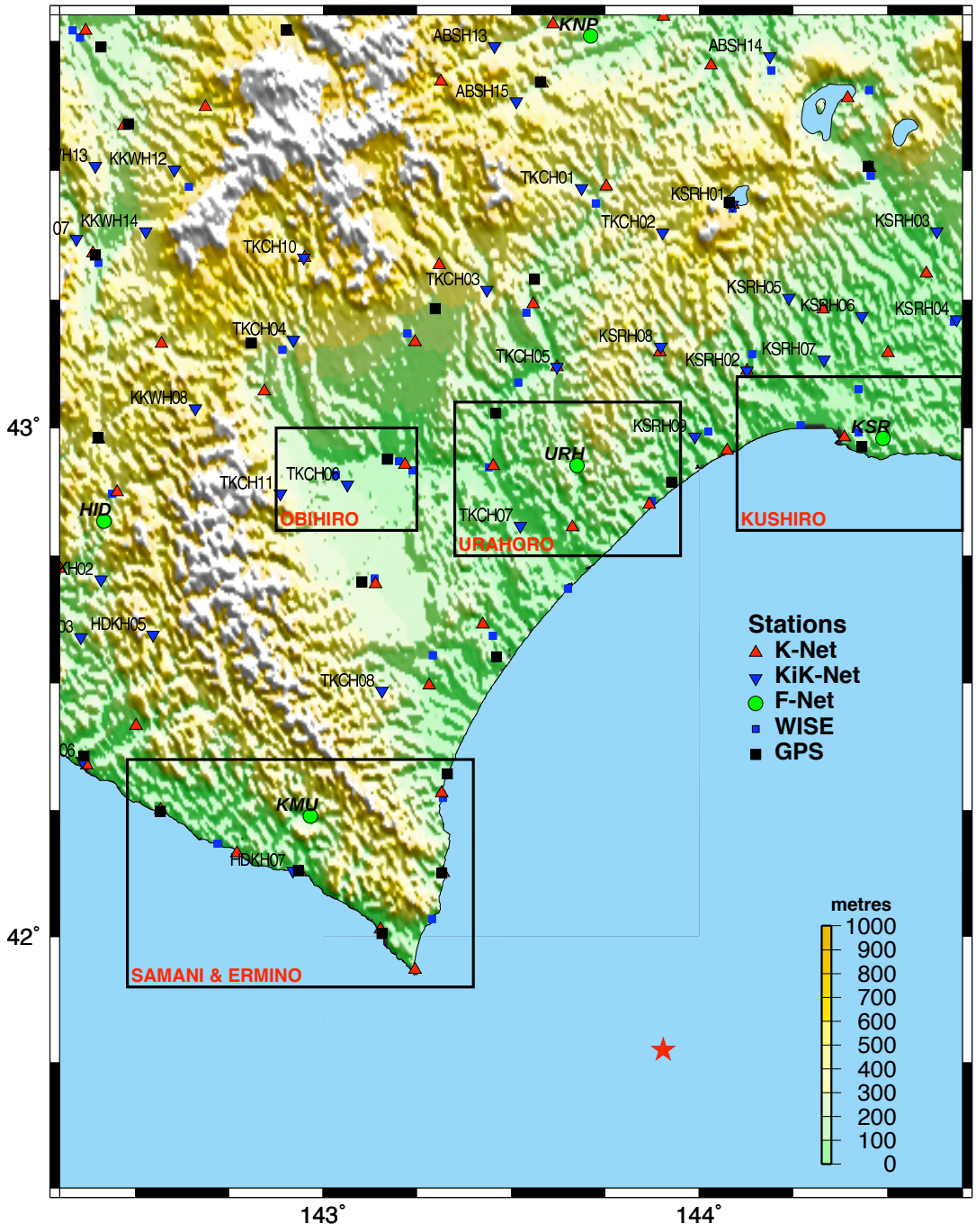

Figure 4.11: Topography and strong motion stations in East Hokkaido. Elevation in *m*. Station names for F-Net and KiK-Net stations. Star indicates M8.3 Epicenter. Boxes outline the regions where stations are compared in detail.

Net station KSR, K-Net station HKD077, and 3 WISE stations, i902k004, i907k002, and i907k003, are all within 15km kilometres of each other. GPS station Kushiroshi is also located in the town. Liquefaction was reported at the fishing port, and ceilings at the local airport collapsed.

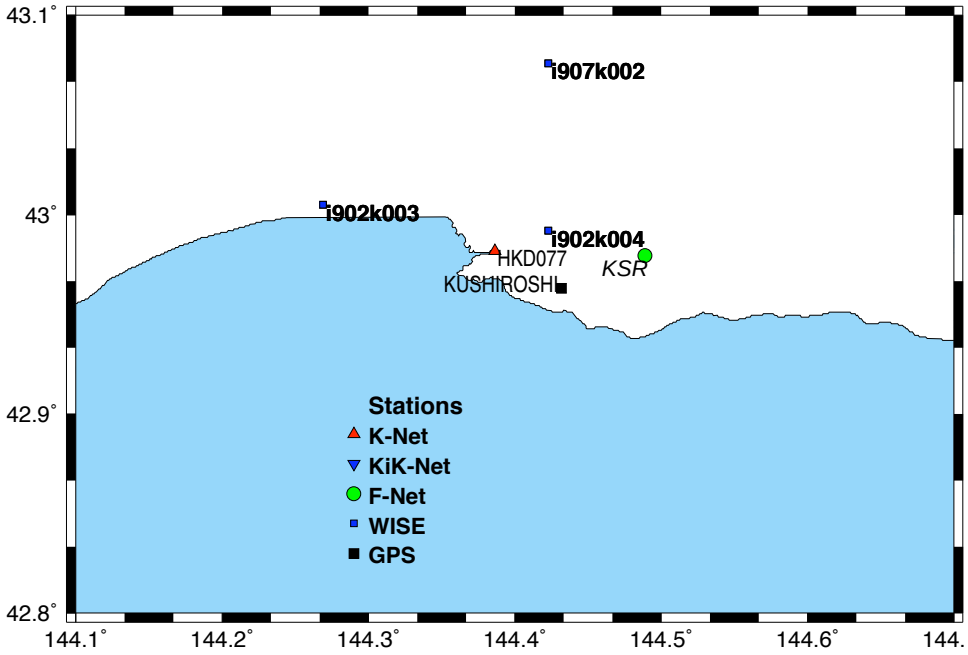

Figure 4.12: Stations near Kushiro town. Blue stations from WISE, green: F-Net, red: K-Net, black: GPS. All stations are within 15km of each other, and about 145km from the epicenter.

The F-Net station KSR has a VSE-355G2. Figure 4.13 shows the strong motion portion of the velocity trace during the earthquake. There appears to be a non-linearity in the E-W component, when the velocity swings from $-20cm/s$ rapidly to $+16cm/s$, at which stage a high frequency spike is recorded. Note the N-S component, as well as the negative E-W component, reach greater velocities (max. $23.6cm/s$), without any obvious non-linearity. Clearly a spike like this could also be caused by the sensor being struck by an object during the strong station, but this is unlikely as the spike is not observed in the other 2 components. Also, it is curious the spike occurs at about the same velocity that caused the problems in the lab. Further, spikes at this frequency are observed at the other F-Net station with a VSE-355G2, KMU, as described in the next case study.

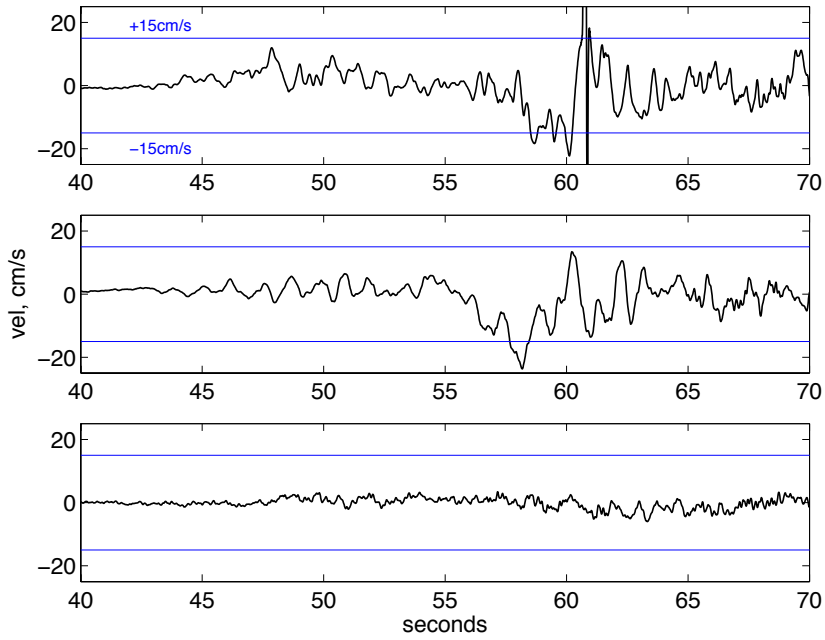

Figure 4.13: Close up of velocity trace showing F-Net KSR VSE-355G2 clipping during M8.3 earthquake. Only E-W component clips, with a high frequency spike at 61s. N-S component reaches 23.6cm/s without clipping. Top: E-W; middle: N-S; bottom: vertical.

Figures 4.14, 4.15 and 4.16 present the deconvolved acceleration, velocity and displacement records from all the Kushiro town stations. Timing is not synchronised between networks. In the figures, WISE station i902k003 clearly has a strong resonance frequency, which indicates it is located at a structure, and does not have a free-field response. The response at high frequencies is dominated by the structural response, as seen from the velocity and acceleration. Due to this resonance, velocities over 150cm/s, and accelerations over 0.4g, are recorded (without clipping) for this VSE-355EI.

The acceleration and velocity traces are very noisy for all the stations other than the F-Net KSR — from this group of stations, only KSR is located at a quiet site. Nonetheless, velocities of similar size to the KSR spike are observed at the other stations. The acceleration spike caused by the velocity jump at KSR is anomalously high though, near 6g, many times larger than any other peaks at KSR, or at any other nearby station.

The GPS station Kushiroshi records a static offset of 16.1cm to the East, 7.09cm to the North and 1.2cm of uplift. In Figure 4.16, it is clear no instrument exactly recovers this

displacement once the strong shaking has stopped. The K-Net station HKD077 and the F-Net station KSR displacements are similar to the GPS offset about $30-40s$ after strong motion begins, after which the time domain integration scheme becomes unstable, or the land tilts, causing the observed non-physical deviations. The E-W F-Net channel, shown to clip in Figure 4.13, is initially similar to the K-Net station, but becomes unstable after $60s$, when the clipping occurs. Permanent offsets are difficult to estimate from the WISE stations, which have very unstable displacement timeseries.

Figures 4.17 and 4.18 are similar to Figures 4.15 and 4.16, but a bandpass filter between $50s$ and $5s$ has been applied, to remove the static offset and the high frequecy components that are highly variable from site to site. In these plots, the K-Net and the F-Net stations (the only stations assured to be in free-field sites) are very similar for all 3 components. The WISE station i902k003 has a response dominated by a $3-4s$ resonance, the structural resonance previously mentioned. The two other WISE stations have similar Z-component velocities and displacements, but it seems the N-S channel on i902k004 and the E-W channel on i907k002 are inverted, as well as the i907k002 E-W channel. These problems illustrate why the displacement field from the WISE network in Figure 4.5 is characterised by highly variable azimuths not commensurate with the GPS.

4.4.2 Stations near Samani town

There are a number of stations in the vicinity of the small fishing village of Samani, near the South-East tip of Hokkaido, one of the regions closest to the epicenter — see Figure 4.19. This section analyses waveforms from the stations nearby and to the west of Samani village: F-Net station KMU, K-Net stations HKD109 and HKD108 (HKD110 did not record during the event), KiK-Net station HDKH07, and WISE station i306k003, are all within $20km$ of each other, except HKD108, which is about $30km$ directly west of KMU. Stations to the East, the closest set of stations to the epicenter, are discussed in the next subsection. Schools in this region reported minor damage.

The F-Net station KMU, at Kamikineusu, has a VSE-355G2. Figure 4.20 shows the strong motion portion of the velocity trace during the event. All 3 channels on the sensor

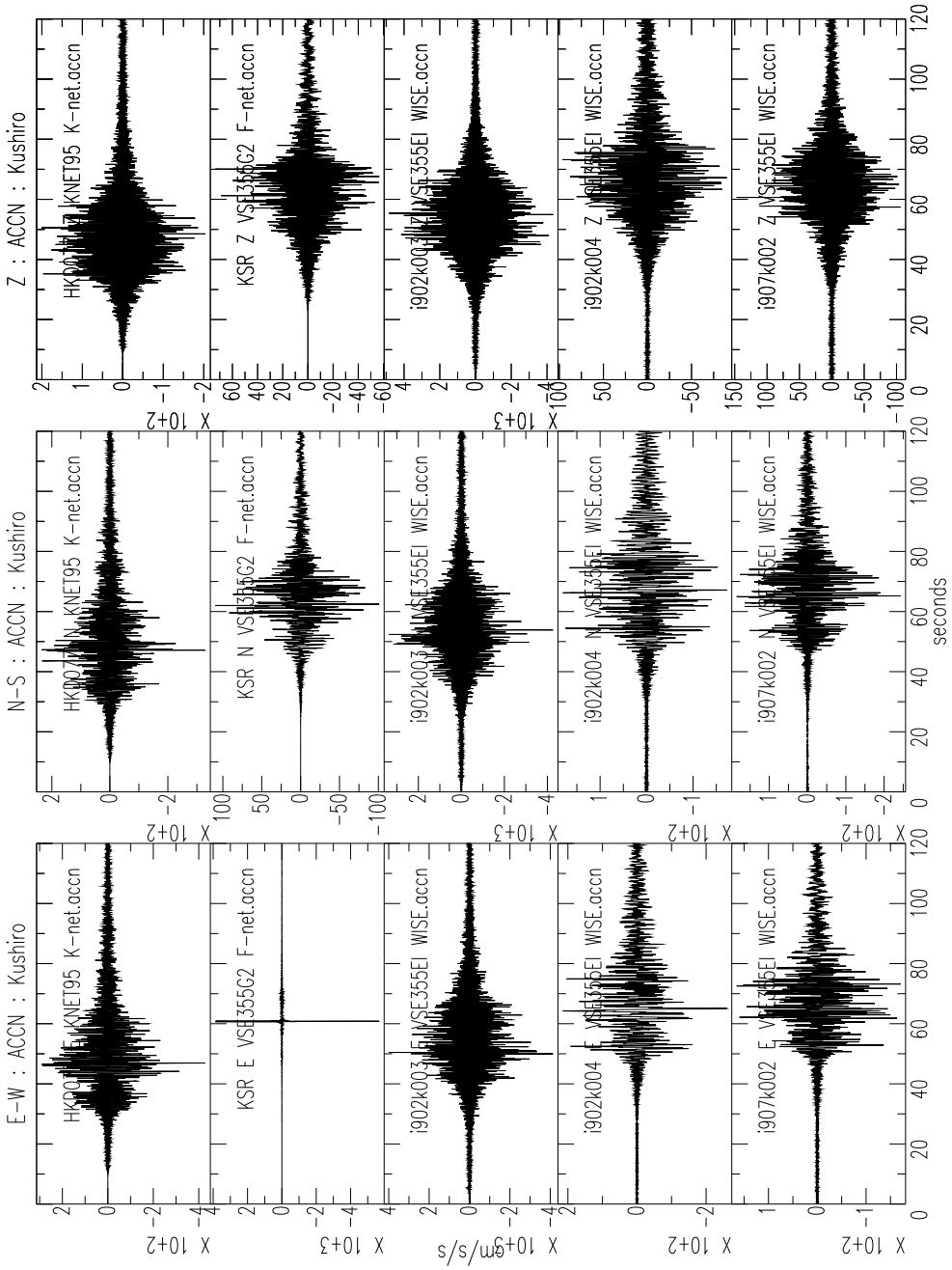

Figure 4.14: Acceleration timeseries from the stations located near Kushiro town. Note the anomalously large acceleration spike at KSR E-W component.

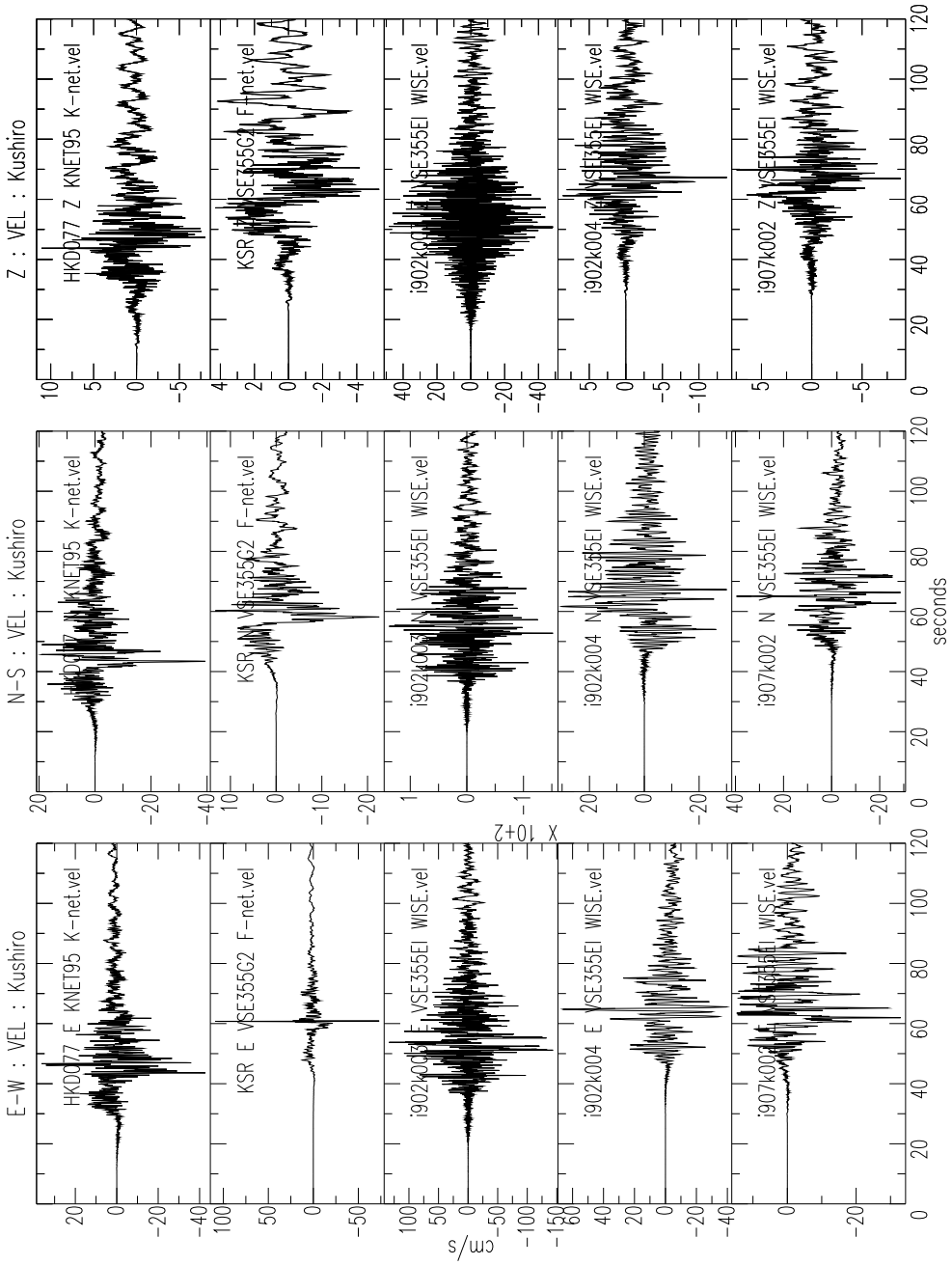

Figure 4.15: Velocity timeseries from the stations located near Kushiro town. Note the anomalously large velocity spike at KSR E-W component.

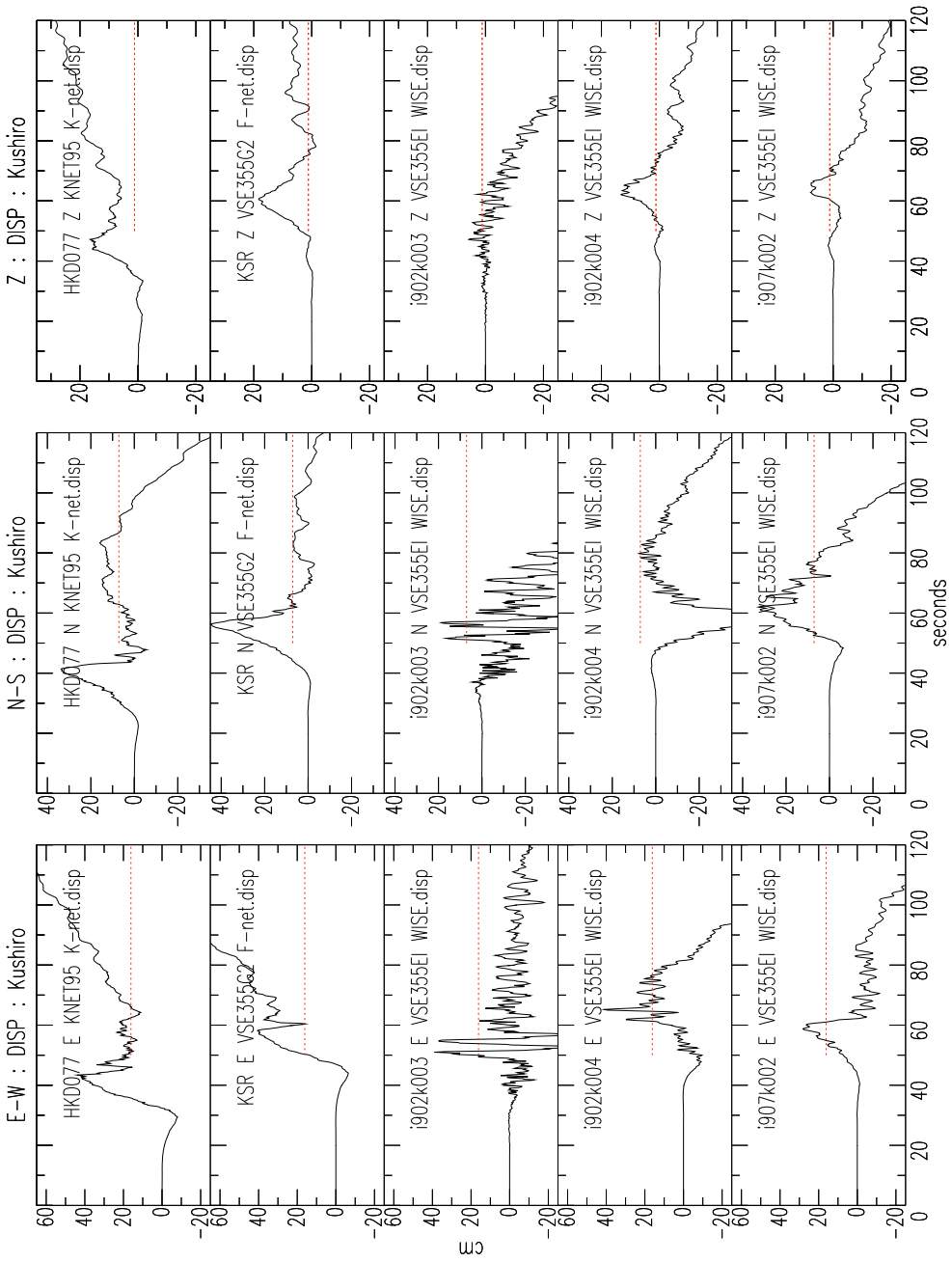

Figure 4.16: Displacement timeseries from stations near Kushiro town. GPS Stn Kushiroshi offsets are 16.1cm East, 7.09cm North and 1.2cm uplift, indicated by the dotted lines. No seismometer measures this change exactly. The K-Net components show similar displacements after 70s, although then the signal deviates. The F-Net N and Z components are also close to the static offset after about 90s before deviating, and the E component, has similar to behaviour to the K-Net E component until clipping occurs at $\sim 60s$. WISE instruments all perform poorly.

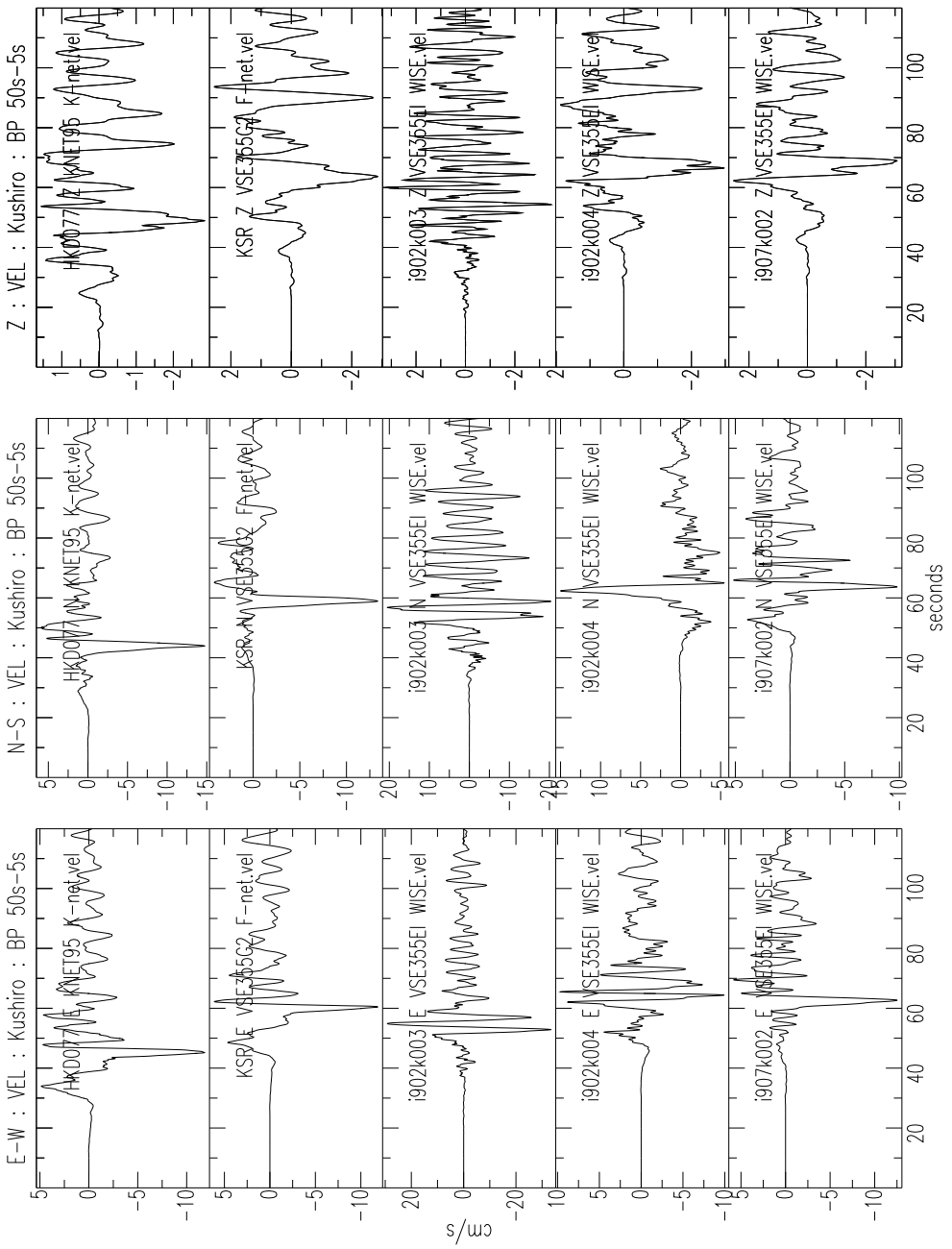

Figure 4.17: Velocity timeseries from the stations located near Kushiro town. Bandpass from $50s - 5s$. Note similarities between K-Net (top trace) and F-Net (2^{nd} trace) stations, the free-field sites. WISE station i902k003 is dominated by a structural resonsnace at $\approx 3.5s$

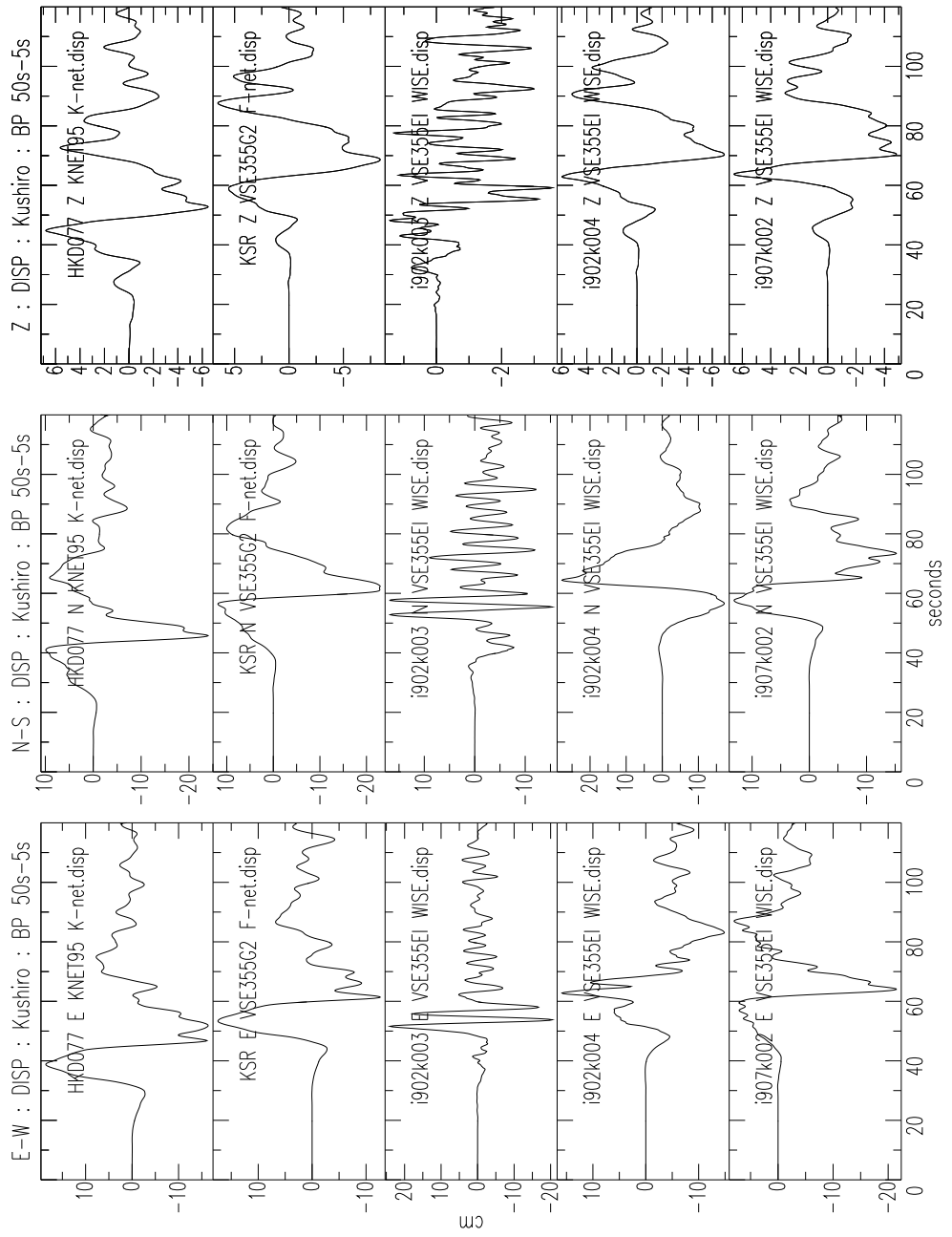

Figure 4.18: Displacement timeseries from the stations located near Kushiro town. Band-pass from $50s - 5s$. Note similarities between K-Net (top trace) and F-Net (2^{nd} trace) stations, the free-field sites. i902k003 is dominated by a structural resonance. i902k004 N-S and i907k002 E-W appear to be inverted.

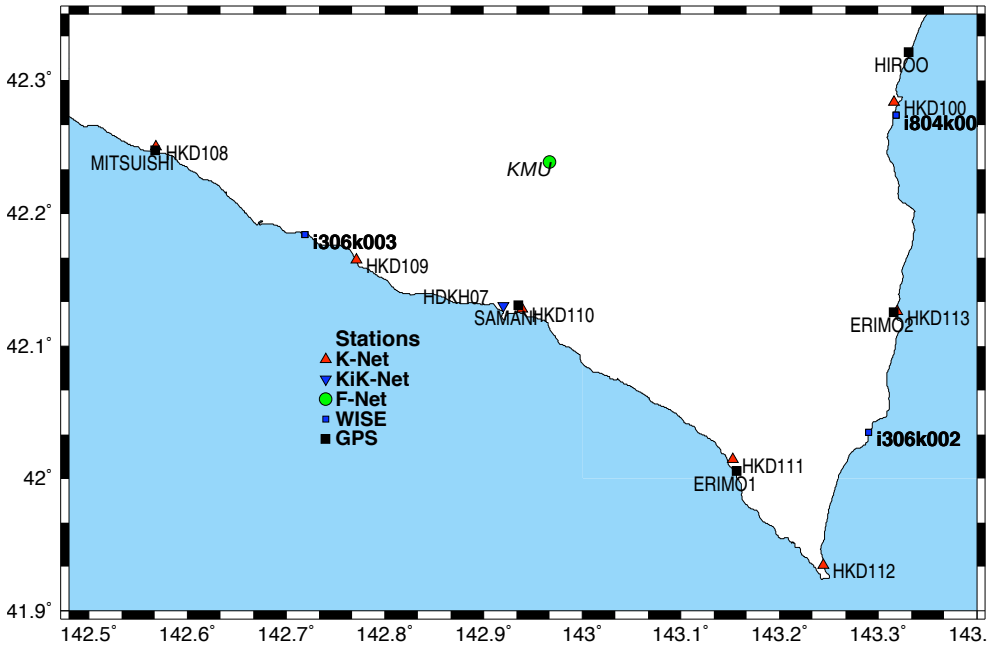

Figure 4.19: Stations near Samani and Erimo towns. Blue stations from WISE, green: F-Net, red: K-Net, black triangle: KiK-Net, black square: GPS. The villages are near the GPS stations with the same name. Station KMU is 94km from the epicenter.

show some corruption, a 'clip' occurs when the velocity exceeds $\sim \pm 16 cm/s$ — as seen by the spikes in velocity, often followed by a short rest at this 'clip velocity', as if the mechanical pendulum is resting at its maximum displacement 'stop'. This is similar to the behaviour observed at Caltech, though in the lab the rest at clip velocity was longer (Figure 3.21). This may be due to the violent high frequency velocity cycles characteristic of this strong motion — velocity reversals move the pendulum away from the 'stops' back 'on-scale'. These velocity reversals were not present in our cart tests — the cart was pushed with monotonically increasing displacement, with much smaller changes in accelerations. The likelihood of these clips being caused by external objects banging the sensor is small, as at times only certain channels clip at a given instant, and, unlike at station KSR, there are very many clip spikes on all 3 components.

Figures 4.21, 4.22 and 4.23 present the acceleration, velocity and displacement records from all the Kushiro town stations. Timing is not synchronised between networks. For the F-Net station KMU, the clipping is observed to produce non-physical (at least from

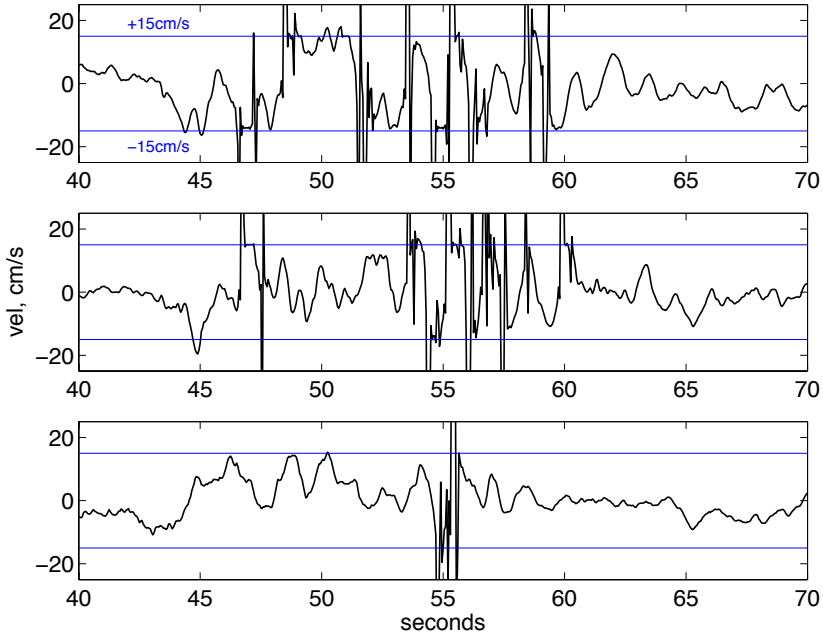

Figure 4.20: Close up of velocity trace showing F-Net KMU VSE-355G2 clipping during M8.3 earthquake. Clipping occurs when velocities are greater than $\sim \pm 15 cm/s$, with short plateau at this level after clip, until a velocity reversal. Top: E-W; middle: N-S; bottom: vertical.

the earthquake) high frequency spikes in the acceleration record of at least $3g$ in every channel. The clips do not have much obvious impact on the displacement time series, as stable (though incorrect) static displacements are recorded on 2 channels.

The velocity and acceleration timeseries from the down-hole KiK-Net site look very much like the up-hole with a lowpass filter. The filtered velocity and displacement traces, with bandpass of $50s$ to$5s$, in Figures 4.24 and 4.25 show this is indeed the case. The K-Net station has a linear trend in velocity beginning during the strongest motion, which is a good indication of tilting at the site. The slope of the velocity is $\sim 0.2 cm/s^2$, equivalent to a tilt of 0.01^o. A tilt 10 times bigger, of 0.1^o would cause the linear trend observed at the WISE station. The tectonic tilt in the region can be determined from the GPS stations at Samani and Mitsuishi. The elevation change due to the earthquake is $-22.2cm$ at Samani, and $-14.4cm$ at Mitsuishi, so there is a rise of $7.8cm$ from Samani to Mitsuishi. Samani is about $10km$ south, and about $30km$ east of Mitsuishi, so the maximum tectonic tilt (Equation 1.16) should be in the N-S component, and be of the order of 0.00045^o, with tilting to the north,

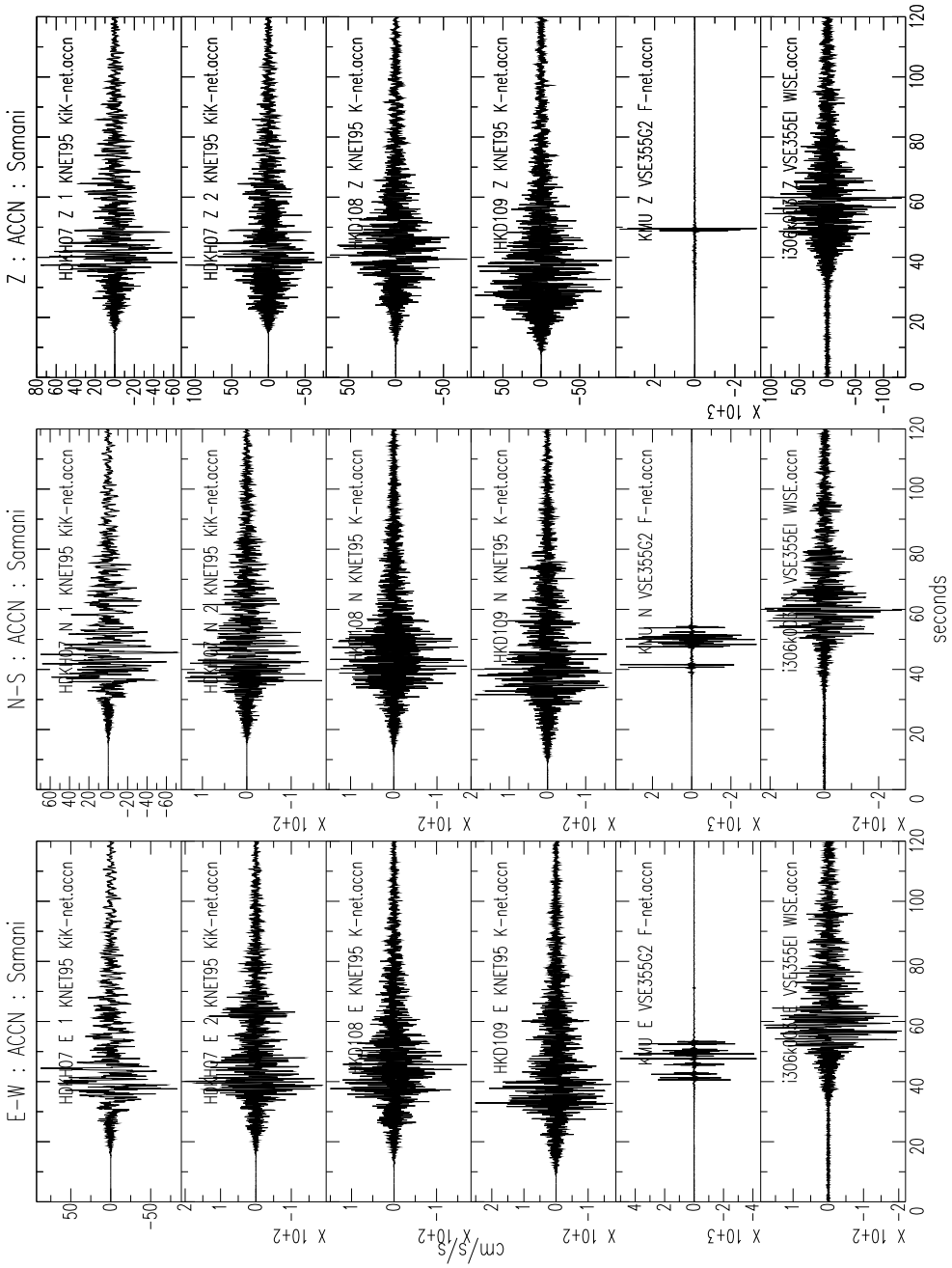

Figure 4.21: Acceleration timeseries from the stations located near Samani town. Note the anomalously large acceleration spikes in all KMU channels. KiK-Net stations: '1': Down-Hole, '2': Up-Hole.

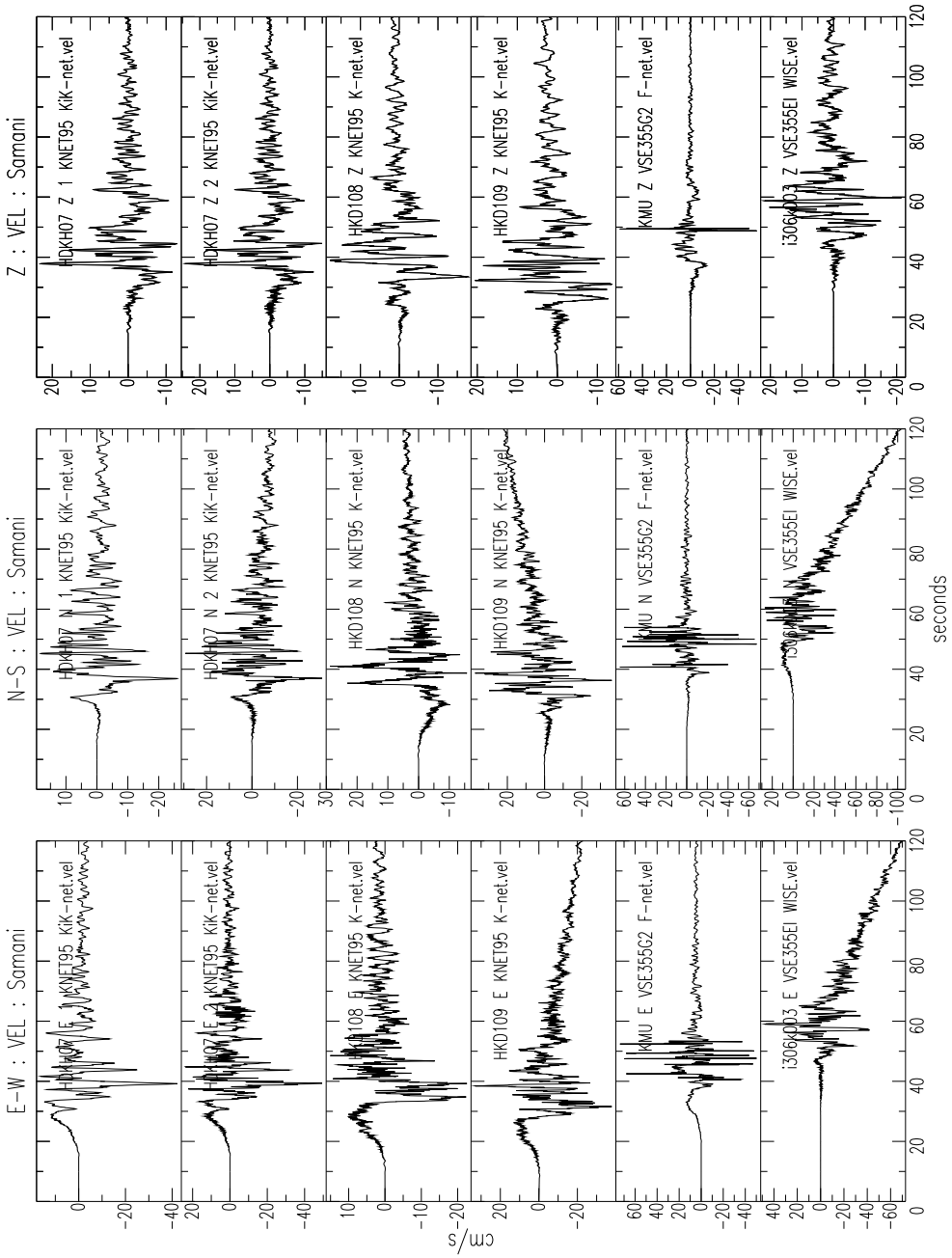

Figure 4.22: Velocity timeseries from the stations located near Samani town. Note the anomalously large velocity spikes in all KMU channels. KiK-Net stations: ‘1’: Down-Hole, ‘2’: Up-Hole.

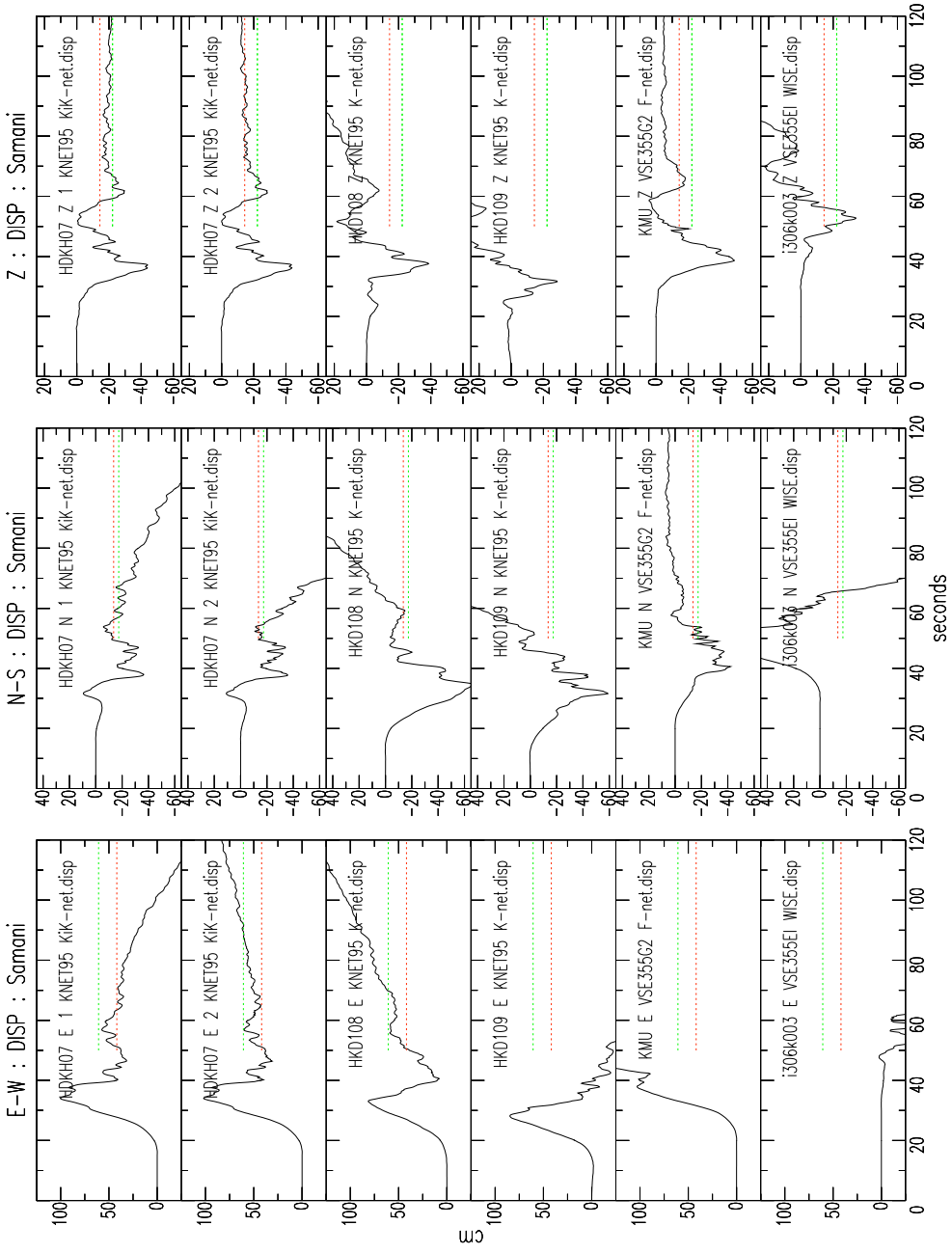

Figure 4.23: Displacements from stations near Samani town. GPS stations Samani records 60.7*cm* East, 17.4*cm* South and 22.2*cm* vertical drop, Mitsuishi records 41.8*cm* East, 13.6*cm* South and 14.4*cm* vertical drop, with similar final displacements for HKD111, and HKD109 after $\sim 70s$ (although then the signal deviates). The VSE instruments perform poorly, only KMU N-S and Z have stable offsets, which differ from GPS. KiK-Net stations: '1': Down-Hole, '2': Up-Hole.

leading to positive offsets for the N-S channels. The tilts observed in practice are well over an order of magnitude higher than this, and for the WISE station, in the other direction.

In Figure 4.23, the KiK-Net stations also appear to suffer some tilt, though for the E-W channels, do so in opposite directions. If it assumed the general form of the deviation from the permanent offset is due to a quadratic function, as expected for a tilt, the tilt can be estimated using Equation 1.19. For the N-S down-hole KiK-Net channel, a displacement of $-70cm$ occurs from time $50s$ to $100s$. This is equivalent to 0.0033^o, and not only is this still an order of magnitude higher then the tectonic tilt, it is in the wrong direction. The tectonic tilt has a negligible effect at these levels of displacements.

The GPS station Samani records a static offset of $60.7cm$ to the East, $17.4cm$ to the South and $22.2cm$ of vertical drop. In Figure 4.23, it is clear no instrument nearby recovers the horizontal displacements once the strong shaking has stopped. Both the up-hole and the down-hole KiK-Net station HDKH07 do record a large, stable permanent offset for the vertical channel, of $15cm$ drop up-hole, and $19.8cm$ drop down-hole. These are remarkably similar to the Samani GPS station only a few km away. In contrast, although the VSE-355G2 F-Net instrument recorded a relatively stable static offset in 2 components, both components are at least $15cm$ offset from the closest GPS.

The WISE station i306k003 has a very sharp change in velocity at $70s$, when a large linear trend begins. The displacement timeseries in Figure 4.25 show that after about $70s$, both the E-W and N-S components have a sharp change in displacement that is not consistent with other station displacements, deviating away from the expected zero displacements observed for the other instruments. The onset of this unusual behaviour coincides with a small amplitude long period response in the velocity, which is very similar to the response of the instrument to a step in acceleration. This was illustrated in the lab in the top sub-figure of Figure 3.12. The resultant integrated output, as seen in the lower subplot, has a permanent offset, which explains the observed displacement for these channels. [Note these are VSE-355EI, with corner frequency at $55s$, not the $\sim 80s$ period of the VSE-355G2.] This could arise from some instrument error, or severe ground failure at the site.

Kristine Larson (*personal communication*) has determined the $1sps$ high-rate GPS data from Mitsuishi. In Figure 4.26, this GPS data and the K-Net station HKD106 displacement

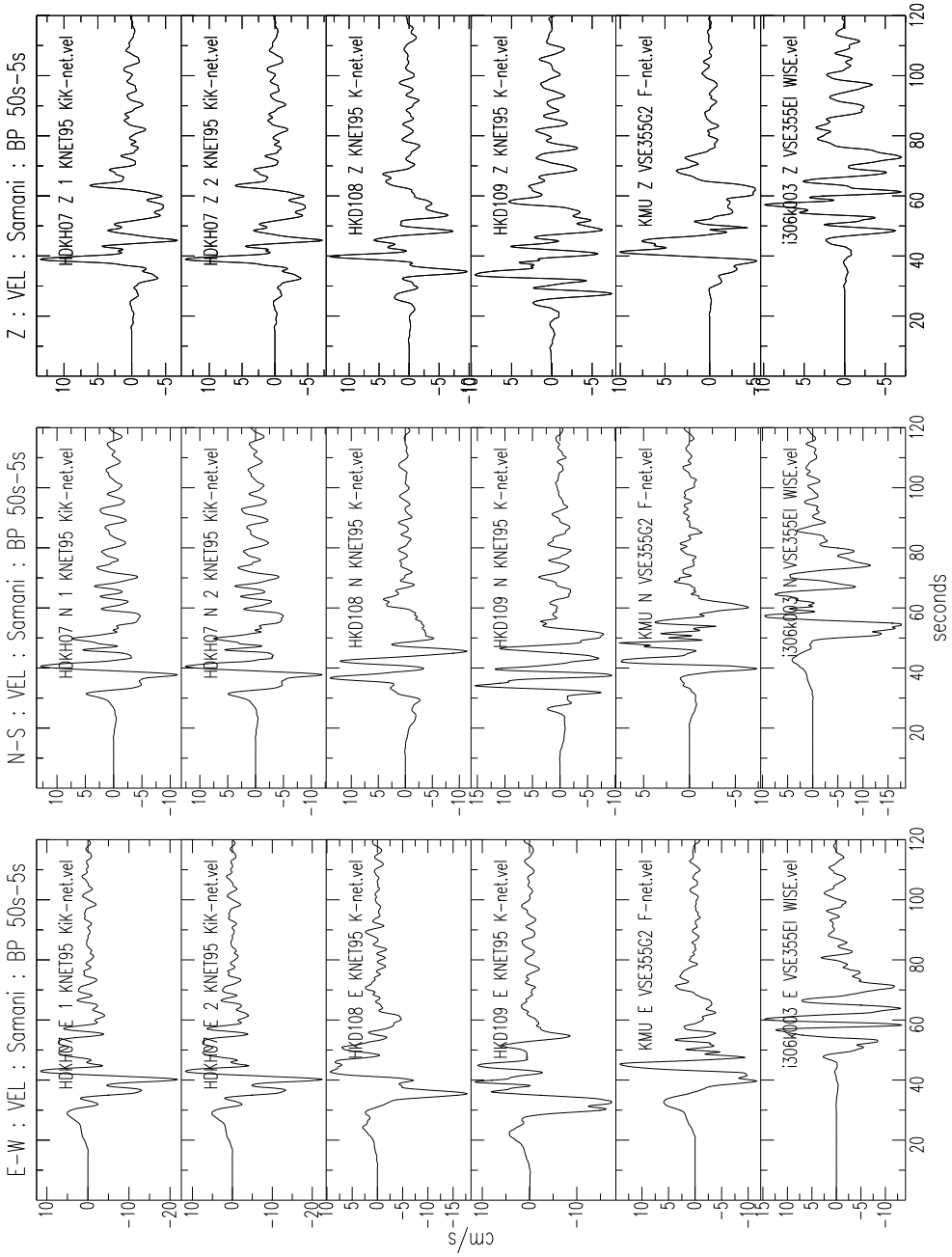

Figure 4.24: Velocity timeseries from the stations located near Samani town. Bandpass from $50s$ — $5s$. Note similarities between KiK-Net (top 2 traces), K-Net (3^{rd}, 4^{th} traces) and F-Net (bottom trace) stations, at free-field sites. KiK-Net stations: '1': Down-Hole, '2': Up-Hole.

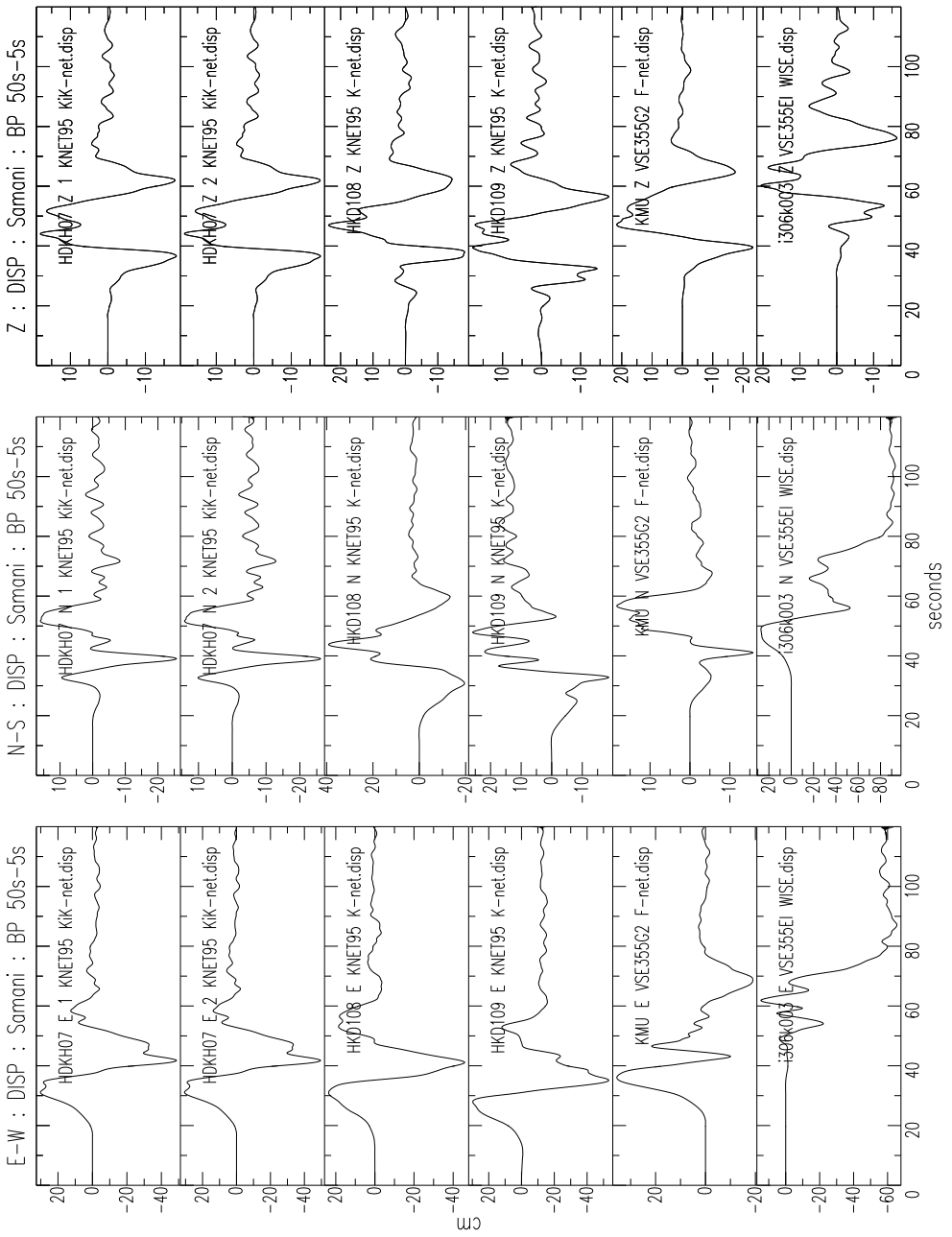

Figure 4.25: Displacement timeseries from the stations located near Samani town. Band-pass from $50s$ — $5s$. Note similarities between KiK-Net (top 2 traces), K-Net (3^{rd}, 4^{th} traces) and F-Net (bottom trace) stations, at free-field sites. KiK-Net stations: '1' : Down-Hole, '2': Up-Hole.

timeseries are compared. These stations are within $1km$ of each other. The K-Net station has apparent tilt, which distorts the records after about $50s$ of motion. The GPS station suffered a power outage about $20s$ after the strong motion began, but regained transmission after about $170s$, recording the static offset for the earthquake.

In the early part of the motions, which is well recorded by both sensors, the displacements are similar, especially for the Vertical motions. The timing and shape of the E-W motion are also similar, though the peak magnitude of the initial swing is reduced from about $100cm$ on the GPS to about $85cm$ in the accelerometer. The N-S motions are quite different for both stations. It is expected large offsets in this direction would take place concurrently with the E-W component. This is the case for the K-Net station, though the GPS station does not record large N-S motion for about $10s$ after the E-W motions begin, which is the same time as the Vertical motion begins. Further investigation showed that if the horizontal components of the accelerometer is rotated, a much better fit can be obtained. The timing problem was also resolved, once the GPS leap seconds were taken into account, and actual trigger times were found for the accelerometers. Figure 4.27 presents this rotated data. Amplitudes and phase are very well matched. Tilting is clearly a problem at this site, though for the E-W channels, the offset at $80s$, just before the tilting becomes large, is very similar to the $7day$ GPS average. For the N-S component, the accelerometer displacements deviated from the GPS very early on in the strong motion, before the $1sps$ GPS data is lost, indicating tilting concurrent with the onset of the strong motion. If this quality data can be determined for the entire timeseries, timeseries for both rotations about the horizontal axes, and the 3 translations, can be well determined by inversion methods.

4.4.3 Stations near Erimo

The closest region to the epicenter is located to the East of Samani, near Erimo town. There are a number of K-Net and Wise stations along the coastline in this area (see Figure 4.19). The largest displacements were recorded at these stations. Figures 4.28 and 4.29 present the deconvolved displacement and bandpassed velocity timeseries respectively.

The K-Net station HKD111 is very close to the GPS station Erimo1 (Figure 4.19). The

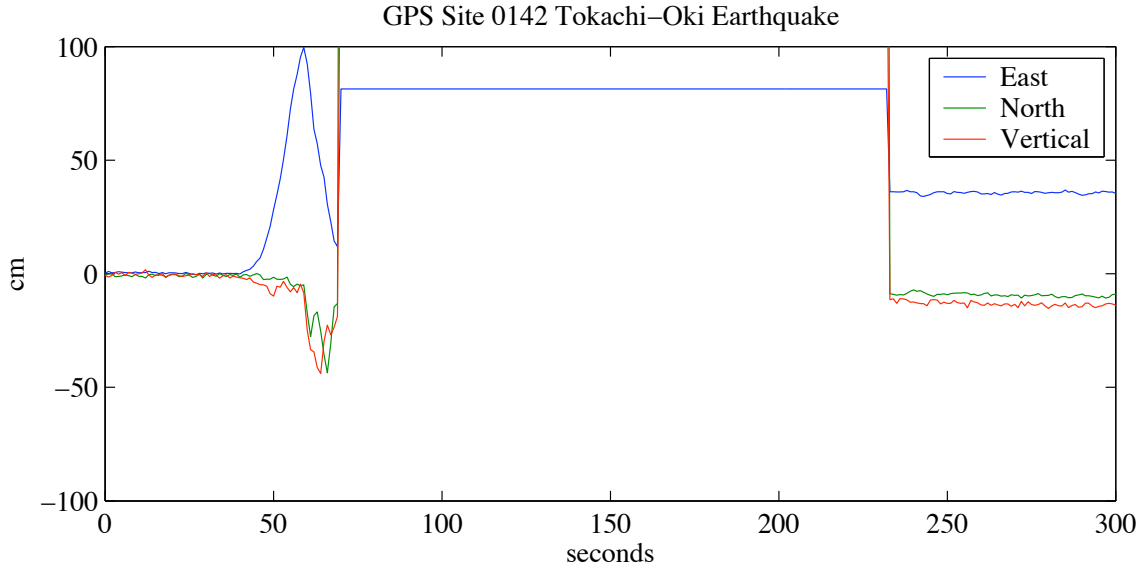

(a) 1*sps* GPS at Mitsuishi

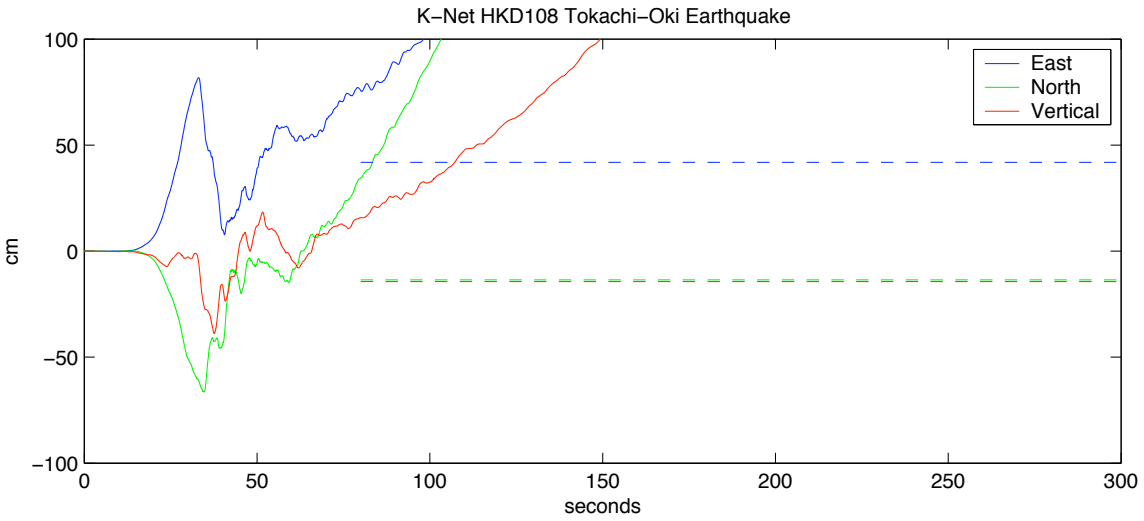

(b) 100*sps* Accelerometer at HKD108

Figure 4.26: High-rate GPS vs. accelerometer displacement timeseries for K-Net and GPS stations at Mitsuishi. GPS timing is 13*s* fast. 7*dy* average GPS offsets included on K-Net plot. high-rate GPS data was lost after 25*s* of the strong motion, and recovered about 170*s* later.

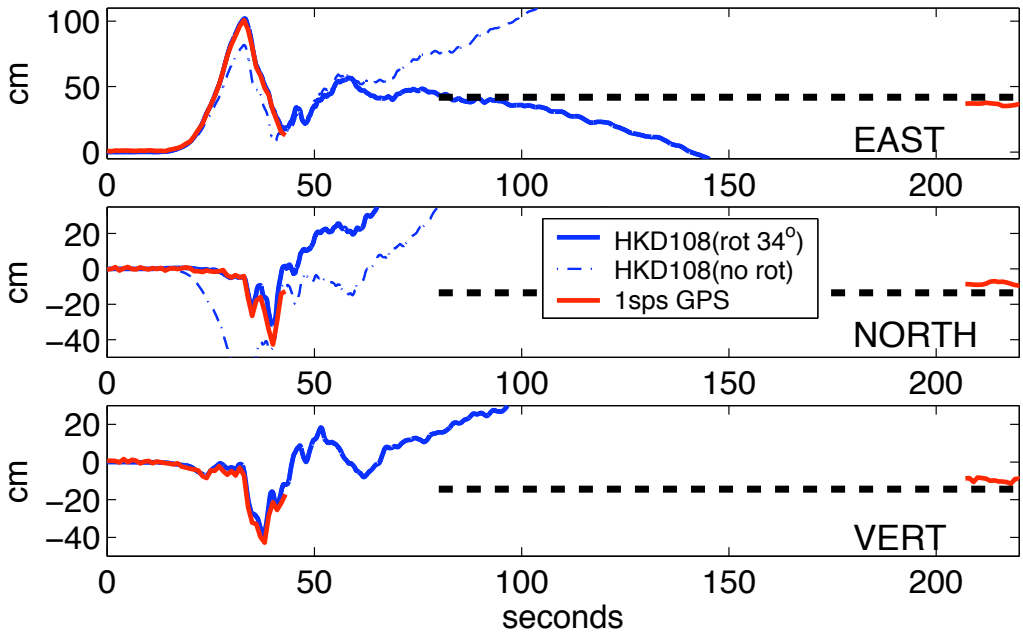

Figure 4.27: High-rate GPS vs. accelerometer displacement timeseries for K-Net and GPS stations at Mitsuishi. Accelerometer horizontal channels are rotated 34^o clockwise to best fit GPS. $7dy$ average GPS offsets included.

GPS station records a static displacement of $62.7cm$ to the East, $17.3cm$ to the South and $18.9cm$ of vertical drop. The final offsets estimates at this K-Net station are $48.4cm$ East, $18.1cm$ south, and $6.5cm$ vertical drop (though in retrospect, from Figure 4.28, this could easily have been chosen as $-20cm/s$, but the static offsets were estimated independently of the GPS). These are remarkably similar to the GPS. K-Net station HKD112 is the closest station to the epicenter, and is about $15km$ south-east of Erimo1, at the South-Eastern-most tip of Hokkaido. Permanent offsets determined at this station are also remarkably free of tilt, and are very similar to HKD111. The 2 other K-Net stations and the WISE stations located on the Eastern coastline, all show very large tilts, which in some cases even causes large non-physical trends on the vertical component.

Bandpassed velocities for these stations shown in Figure 4.29 confirm the similarity of K-Net stations HKD111 and HKD112, and show once again WISE stations may have inverted horizontal orientations. Motions from the WISE station i804k004 do not appear to be from a VSE-355EI instrument, as they are much smaller in magnitude than other nearby motions, and have higher frequency content.

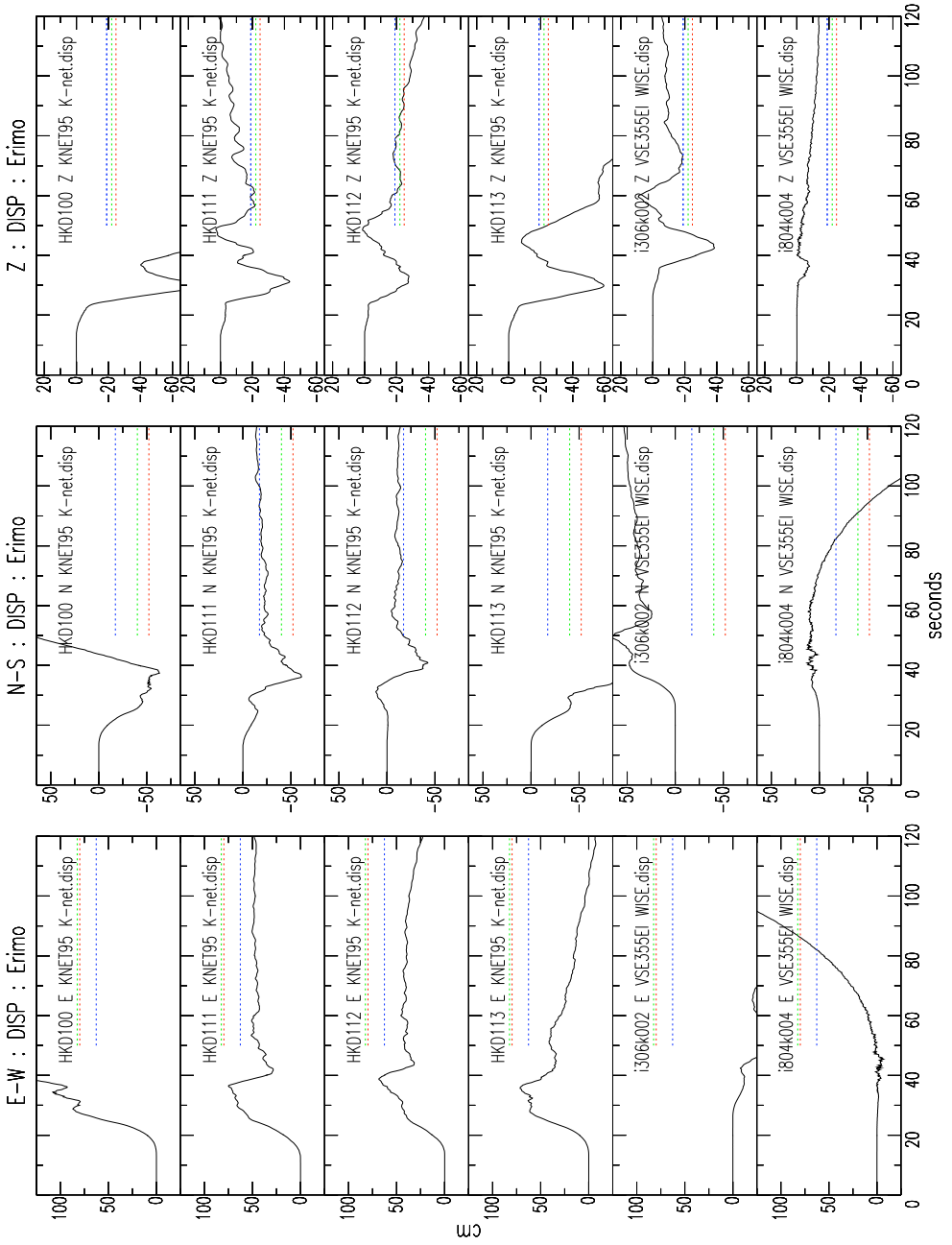

Figure 4.28: Displacements from stations near Erimo town. GPS station Erimo2 records 82.4*cm* East, 40.1*cm* South and 22.9*cm* vertical drop, Erimo1: 62.7*cm* East, 17.3*cm* South and 18.9*cm* vertical drop, Hiroo: 79.8*cm* East, 52.2*cm* South and 24.7*cm* vertical drop. All are plotted in horizontal lines. K-Net stations HKD111 and HKD112 have very similar final displacements for N-S and Z channels. Other stations perform poorly.

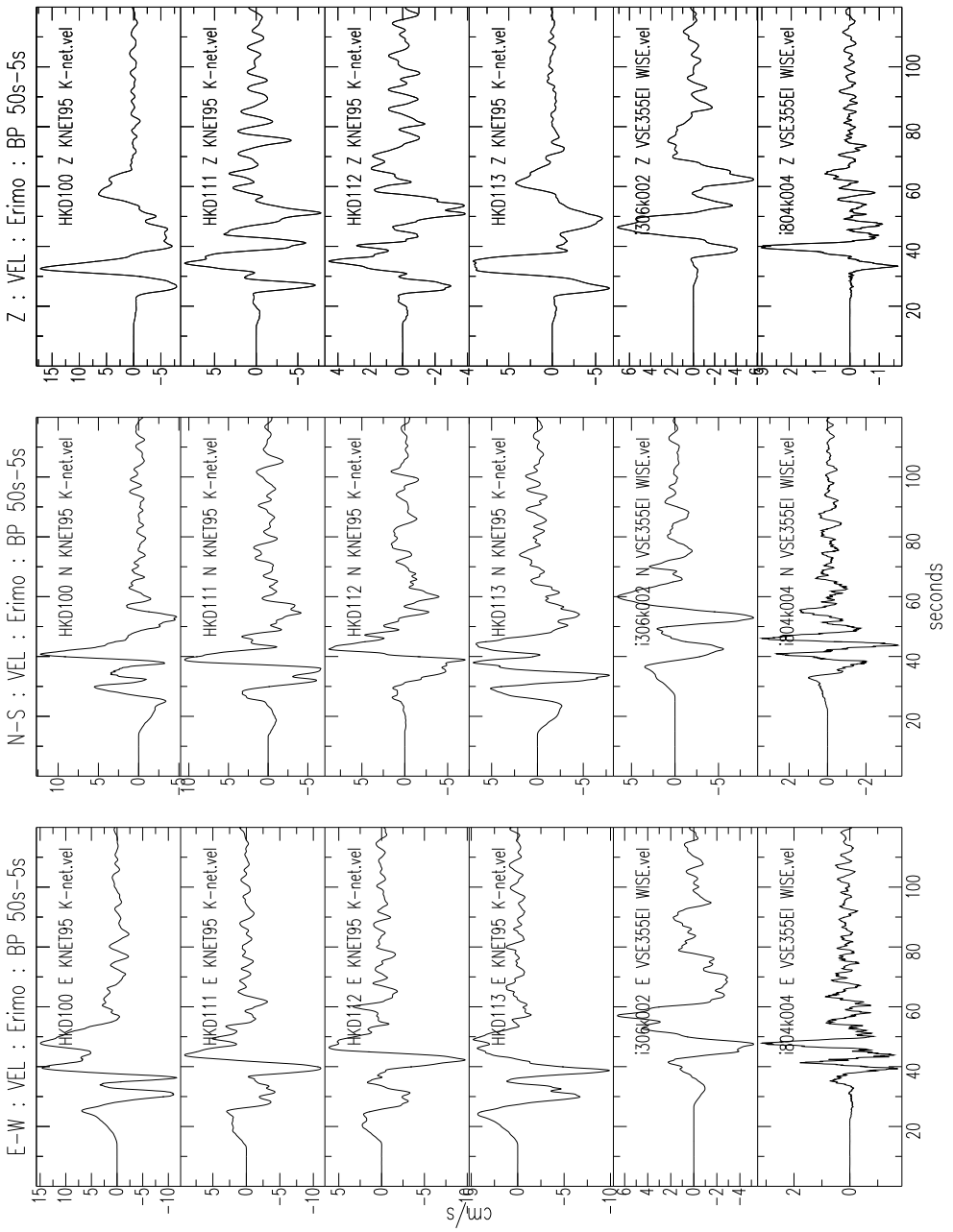

Figure 4.29: Velocity timeseries from the stations located near Erimo town. Bandpass from $50s$ — $5s$. Note similarities for all K-Net stations, WISE i306k002 may have horizontal channels inverted, i804k004 has an unexplained response.

Kristine Larson (*personal communication*) has again determined the 1sps high-rate GPS data from Erimo1. In Figure 4.30, this GPS data and the K-Net station HKD111 displacement timeseries are compared. The stations are just over 1km apart. This GPS station suffered a power outage after 25s of strong motion, and did not regain transmission until the evening, after the major aftershocks had occurred. Before this occurred, the E-W and vertical components very closely match, though once again the magnitudes of the E-W peaks are slightly lower for the seismic sensor. The N-S motions are similar, though as with the data in Figure 4.26, large offsets begin at the same time as E-W offset occurs for the accelerometer, and not until the vertical motions begin for the GPS. Figure 4.31 presents the same data with the a clockwise rotation of 20^o for the horizontal channels of the accelerometer, and the same timing corrections as made for Figure 4.27. The fit is much improved, with excellent phase and amplitude correspondence between the two sensors. Tilt is minor at the accelerometer station, as can be seen by the relatively stable displacements after the strong motion has passed. Even so, the 7day GPS averages do not closely match the final accelerometer timeseries displacements.

4.4.4 Stations near Urahoro

There are a number of stations in the vicinity of Urahoro, the F-Net station which records the highest velocities without any large spikes. This station is in a wide basin area in East Hokkaido (see Figure 4.32). This section analyses waveforms from the stations nearest Urahoro: F-Net station URH, K-Net stations HKD086 and HKD091, KiK-Net station TKCH07, and WISE stations i807k002 and i902k001. All these stations are within 20km of URH, which is 129km from the epicenter. This region suffered major structural damage during to the earthquake — landslides, widespread liquefaction and lateral spreading damaged infrastructure, and a tsunami caused significant damage at the local ports. Ground failure was not limited to the coastal areas.

Figures 4.33, 4.34 and 4.35 present the acceleration, velocity and displacement records from all the Urahoro region stations. Timing is not synchronised between stations. URH is deployed with a VSE-355G sensor. No channel from this station clips — there are no

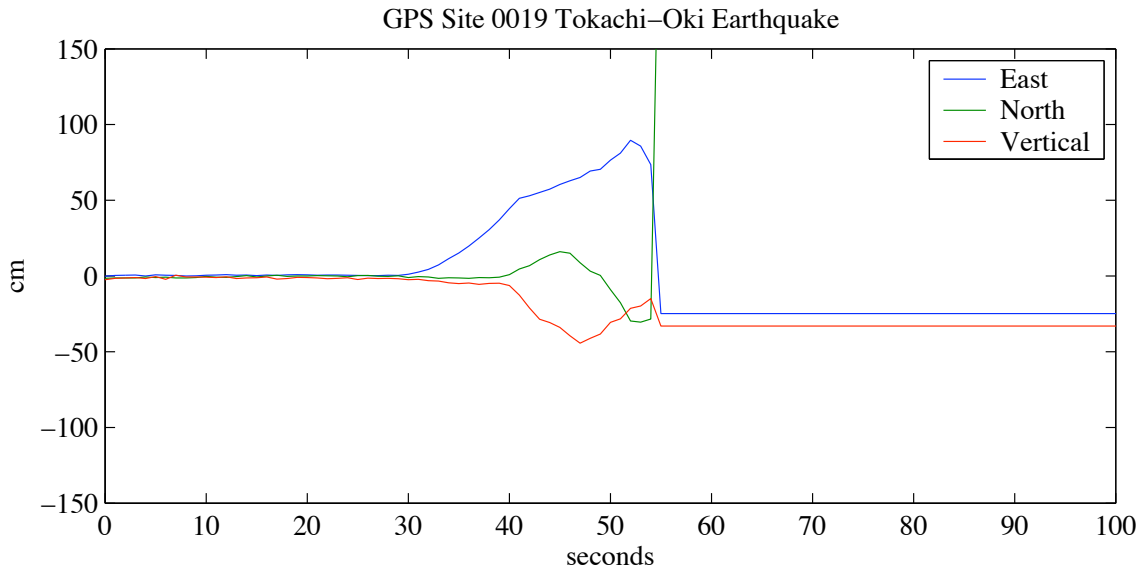

(a) 1*sps* GPS at Erimo1

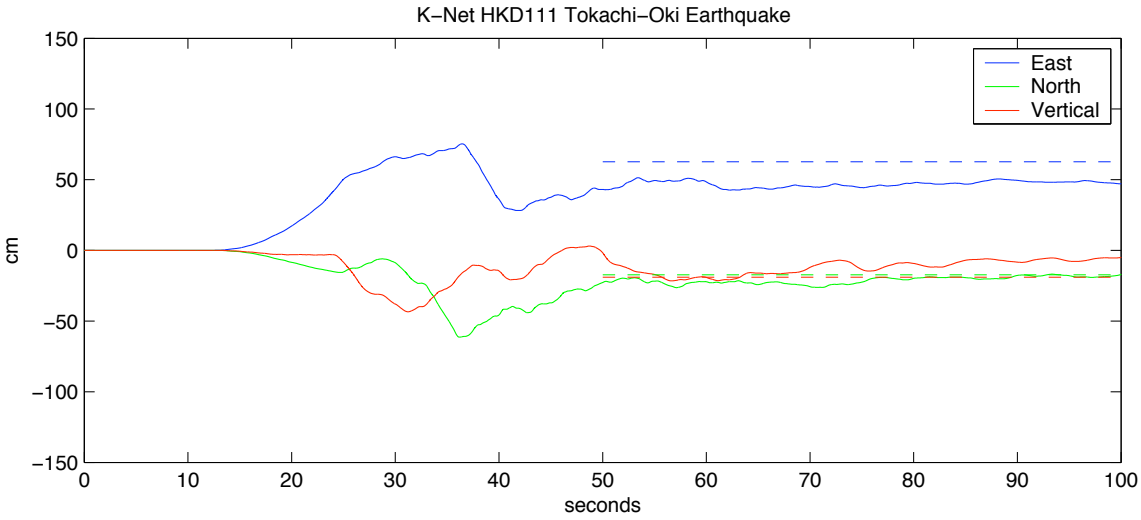

(b) 100*sps* Accelerometer at HKD111

Figure 4.30: High-rate GPS vs. accelerometer displacement timeseries for K-Net and GPS stations at Erimo. GPS timing is 13*s* fast. 7*dy* average GPS offsets included on K-Net plot.

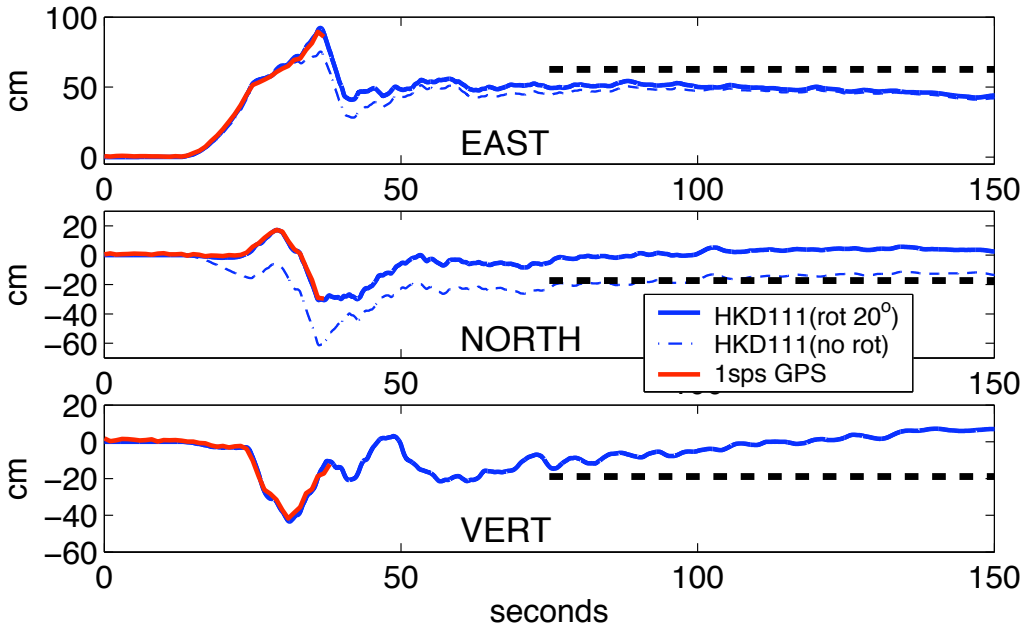

Figure 4.31: High-rate GPS vs. accelerometer displacement timeseries for K-Net and GPS stations at Erimo1. Accelerometer horizontal channels are rotated 20^o clockwise to best fit GPS. 7dy average GPS offsets included.

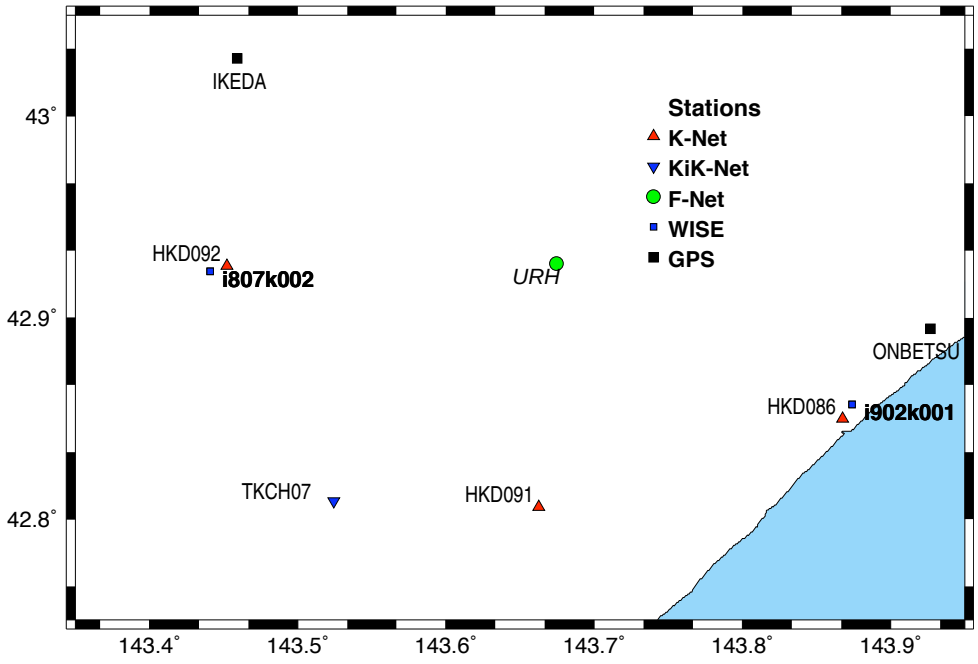

Figure 4.32: Stations near Urahoro. Blue stations from WISE, green: F-Net, red: K-Net, black triangle: KiK-Net, black square: GPS. All stations plotted are within 20km of URH, which is 129km from the epicenter.

unusually large high frequency peaks in either the velocity or acceleration timeseries. The maximum velocity is on the E-W component, recording $21.7 cm/s$. This level of velocity caused stations KSR and KMU to clip. Peak velocities on the other components are $17.4 cm/s$ N-S, and $12.9 cm/s$ Vertical.

This set of acceleration timeseries illustrates the variability in peak magnitude between closely spaced stations. At URH, accelerations are small, maximum $70 cm/s^2$, a little smaller but similar to the TKCH07 down-hole. Though these stations are buried, the other stations also have large variability, ranging from $750 cm/s^2$ to $250 cm/s^2$.

Velocities are quite large in this region. The N-S components of the up-hole KiK-Net station, and the WISE station i902k001 both record over $100 cm/s$.

All the accelerometers incur tilting during the earthquake. The stations all are located in wide flat basin, where widespread ground failure has been documented. Even the down-hole KiK-Net channels at TKCH07 show signs of tilting. GPS from the region indicates overall displacement of the order of $30 cm$ to the South-East, with a vertical drop of $\sim 8 cm$. The tectonic tilt from the differential vertical GPS is of the order of 0.0004^o, similar to previous observations. Trends observed in the E-W components of the velocity timeseries at TKCH07 up-hole and down-hole, HDK091 and i902k001 would be caused by tilts of the order of 0.1^o. HKD092 has a similar tilt, but only in the N-S direction. Even though there is major tilt in the E-W direction for the TKCH07 down-hole, N-S and Z channels record stable permanent offset comparable to the GPS. In the middle of all these tilting stations, the F-Net station URH produces very stable displacements comparable to GPS for all 3 channels.

Station HKD086, the K-Net instrument located on the coastline, has a very strange response, not easily interpreted by simple tilting alone. Figure 4.38 presents 3 components of acceleration and velocity timeseries data for the initial part of the record. From about $30 s$ into the record, frequency content changes dramatically, with very little high frequency content, associated with serious tilting in all three components. In the N-S direction, this fall of $800 cm/s$ is observed in only $15 s$, which corresponds to a tilt of over 3^o. In Figure 4.34, this tilt changes direction for all 3 components, indicating large, rapidly changing tilts. This appears to be a site that is liquefying. This is consistent with the widespread

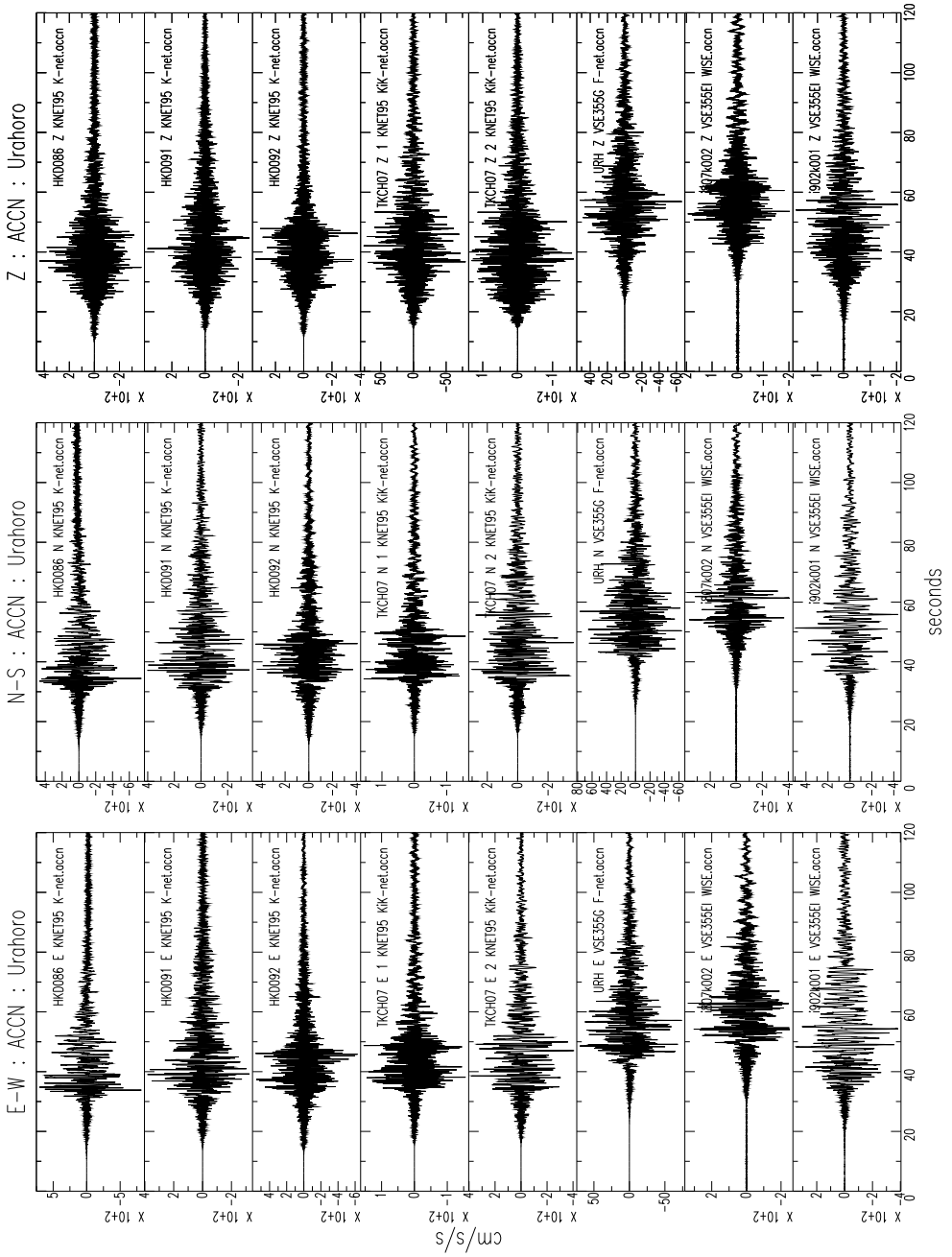

Figure 4.33: Acceleration timeseries from the stations located near Urahoro. Note the large variation acceleration magnitudes between these closely located stations. KiK-Net stations: '1': Down-Hole, '2': Up-Hole.

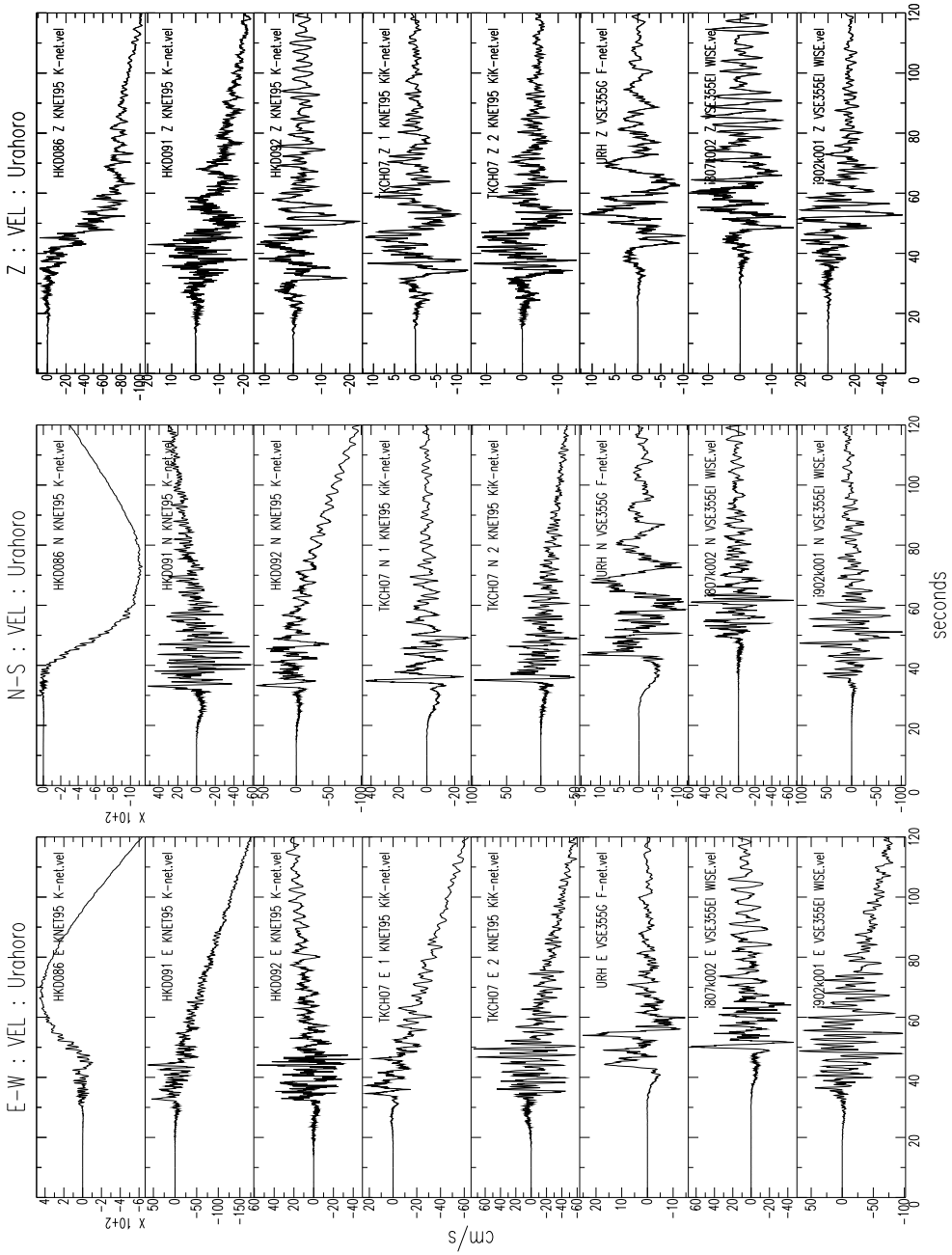

Figure 4.34: Velocity timeseries from the stations located near Urahoro. Tilting clearly affects all accelerometers bar N and Z KiK-Net down-hole. K-Net HKD086 liquefies. VSE i807k002 has resonances. KiK-Net stations: '1': Down-Hole, '2': Up-Hole.

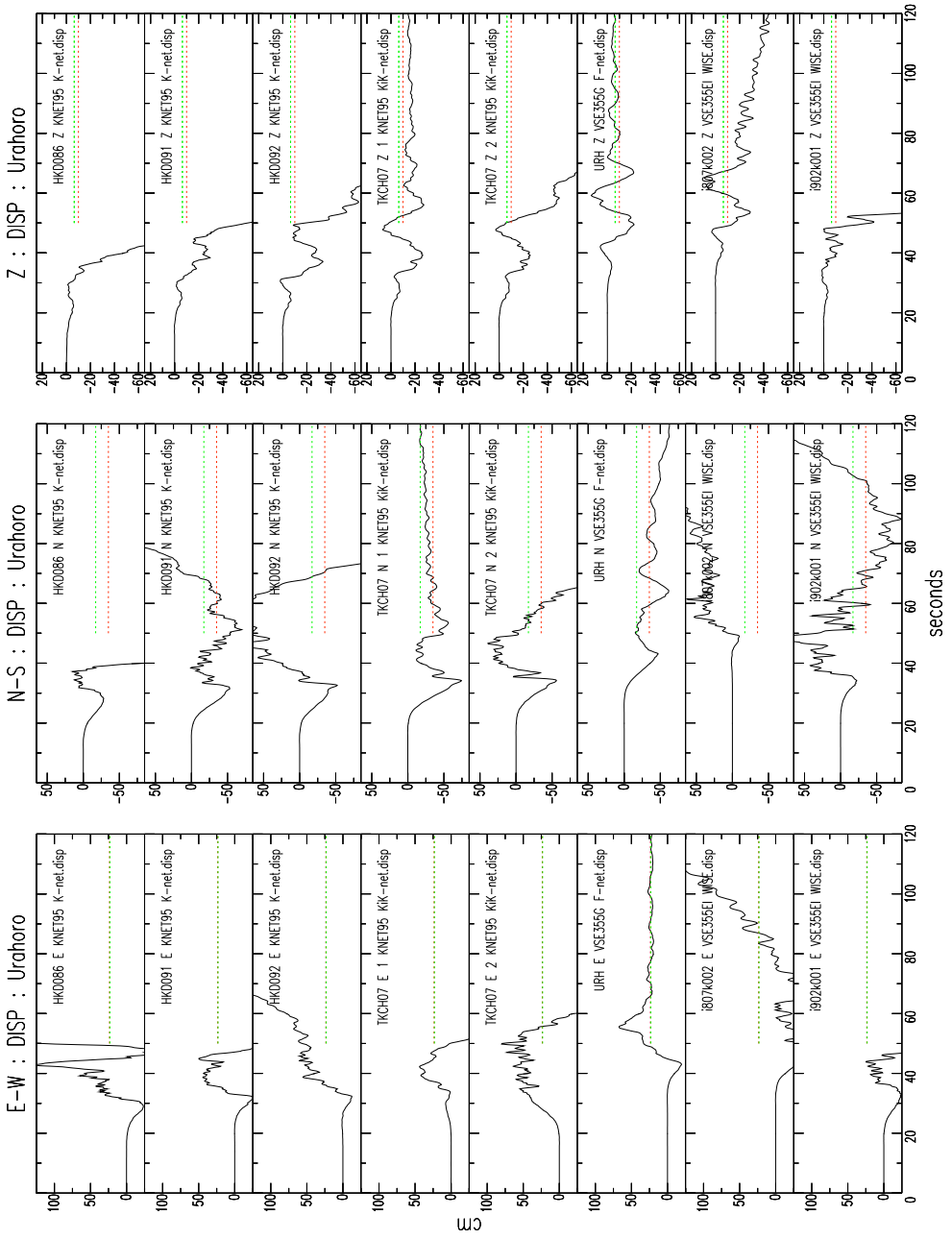

Figure 4.35: Displacements from stations near Urahoro. GPS stations — Ikeda: 23.6*cm* East, 34.9*cm* South, 10.0*cm* vertical drop, Onbetsu: 23.1*cm* East, 17.2*cm* South, 6.5*cm* vertical drop. Significant tilting for all accelerometers, including KiK-Net. F-Net station URH has good correlation with GPS . KiK-Net stations: '1': Down-Hole, '2': Up-Hole.

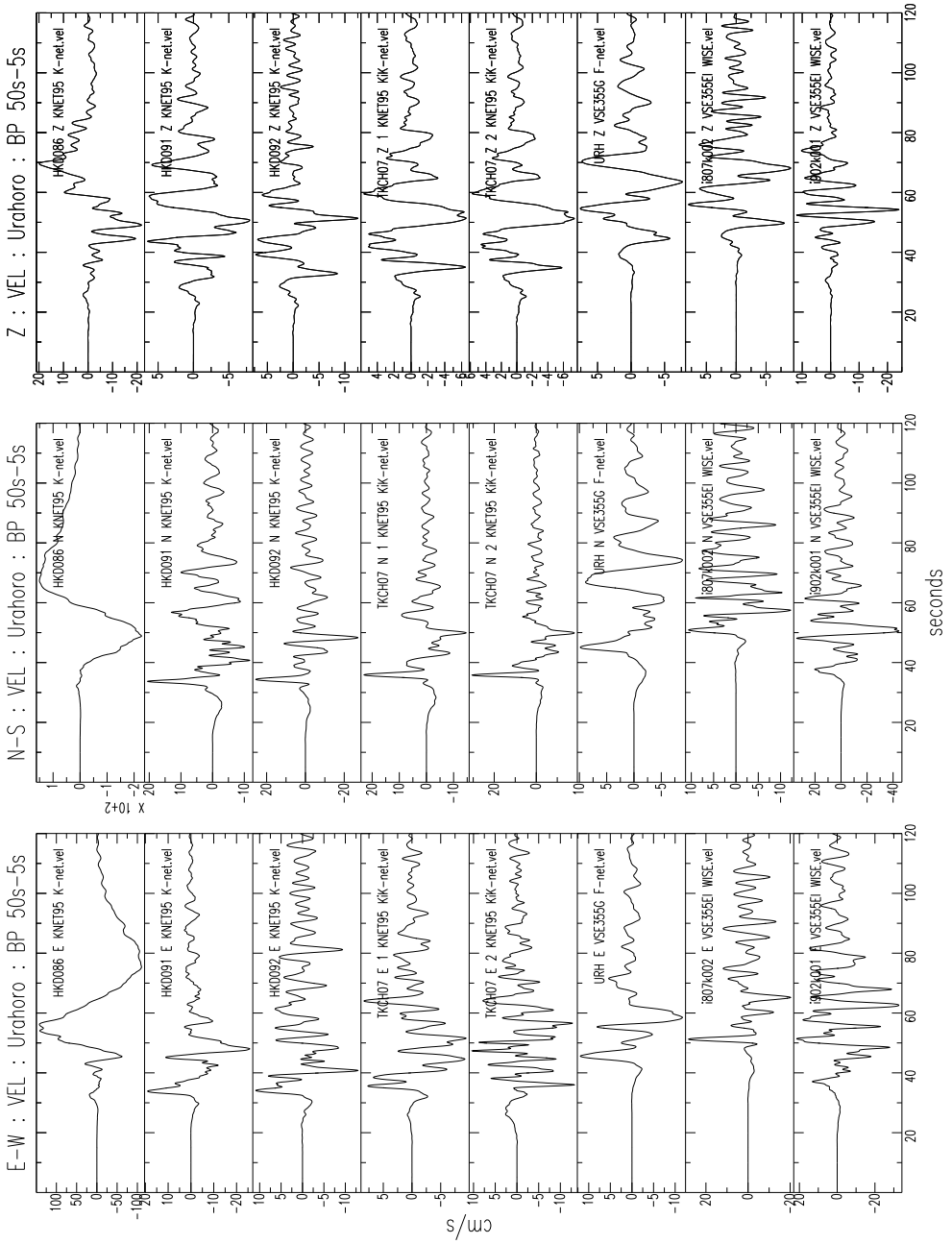

Figure 4.36: Velocity timeseries from the stations located near Urahoro. Bandpass from $50s$ — $5s$. Note basin resonance at most stations, not apparent at URH. KiK-Net stations: '1': Down-Hole, '2': Up-Hole.

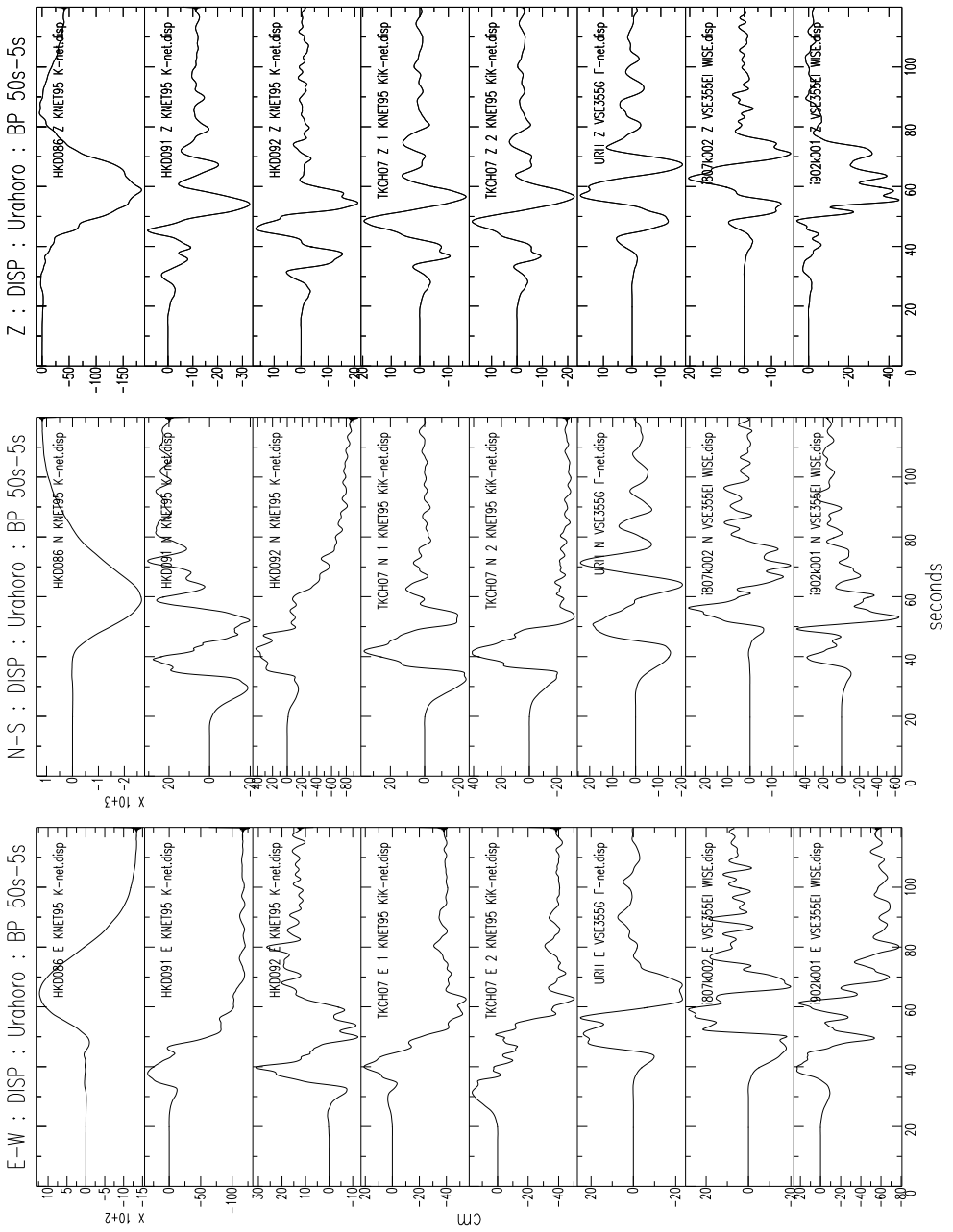

Figure 4.37: Displacement timeseries from the stations located near Urahoro. Bandpass from 50s — 5s. In this area, the 2 WISE stations appear correctly oriented. KiK-Net stations: '1': Down-Hole, '2': Up-Hole.

ground failure reported in this region.

A spectrogram of each component from the acceleration timeseries is presented in Figure 4.39. Each vertical line in the plot represents an FFT of 10s of the data beginning at the time it is plotted. It is clear from the plot that as the event progresses, the high frequency content is severely reduced, especially on the horizontal components.

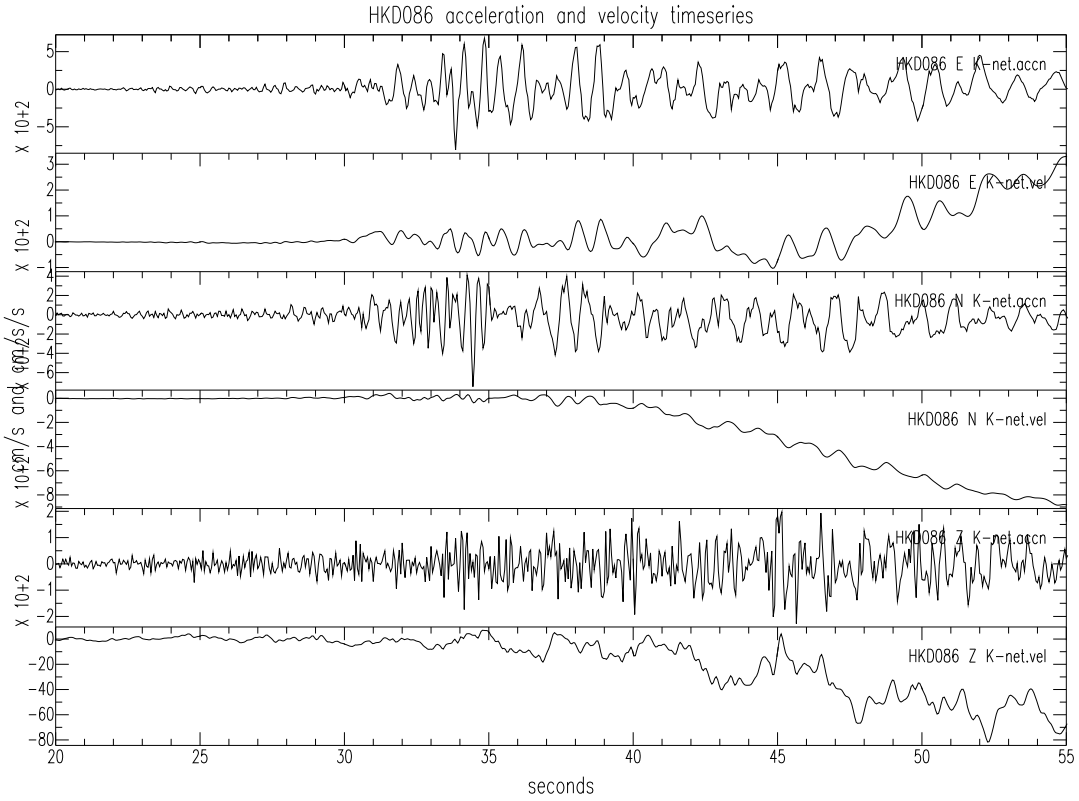

Figure 4.38: Velocity and acceleration timeseries from liquefaction site HKD086, K-Net. See Fig 4.32 for location. Note change in frequency content in the acceleration timeseries, and consequent very large tilts for all three components. One hypothesis is that liquefaction occurred at this site.

Figure 4.40 shows a similar spectrogram plot for nearby K-Net station HKD091, which does not have liquefaction. though dominant frequencies may also be low, there is not a complete attenuation of high frequencies like at HKD086.

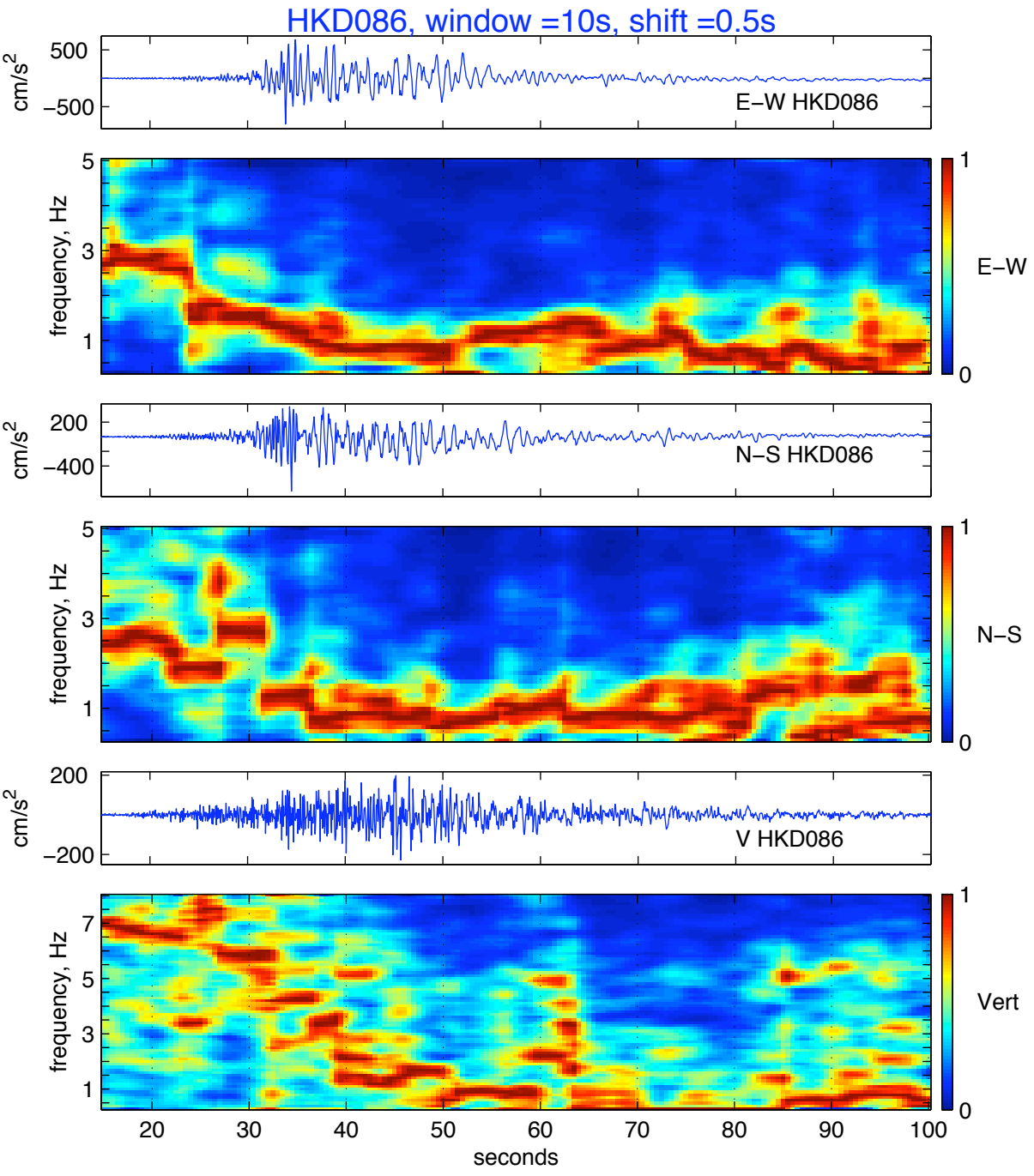

Figure 4.39: Acceleration timeseries and spectrogram for liquefaction site HKD086, K-Net. See Fig 4.32 for location. Frequency drop after about 30*s*, as site liquefies, with all high frequency attenuated.

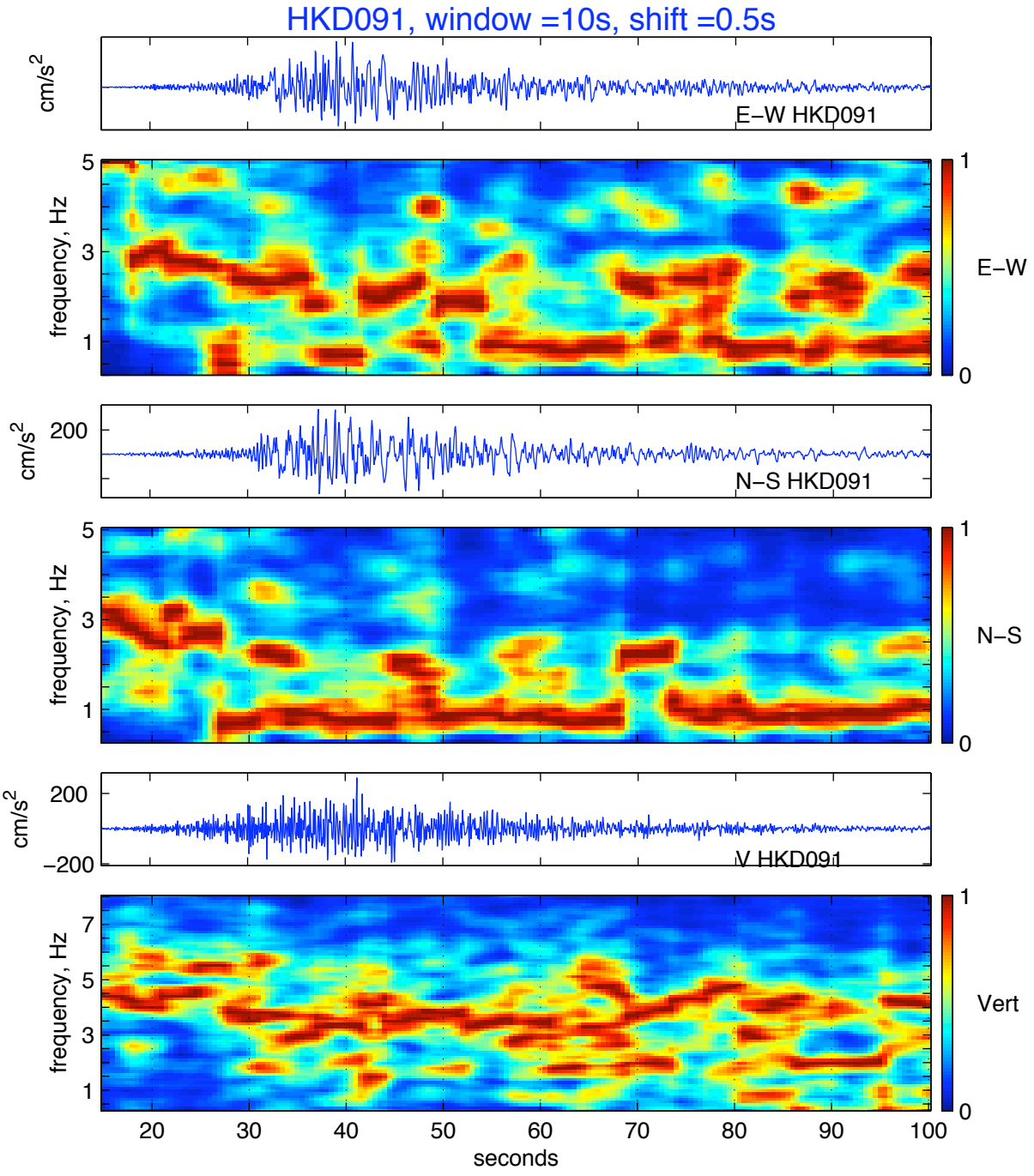

Figure 4.40: Acceleration timeseries and spectrogram for site HKD091, K-Net. See Fig 4.32 for location. Though tilting occurs at this site, no liquefaction occurs, and high frequencies are present in all components.

4.4.5 Stations near Obihiro

In Figures 4.7 and 4.8, it is clear the WISE stations to the West of Urahoro, in the wide flat basin, have recorded motions that appear to be of the correct order of magnitude, but with reversed polarities on the horizontal components. To investigate this, a cluster of stations around the town of Obihiro are examined. There are 3 WISE stations (i801k001, i801k004, i806k002), 2 KiK-Net stations (TKCH06, TKCH11), 1 K-Net (HKD095) and 1 GPS (Obihiro) stations within a few *km* of the town, which is about 160km from the epicenter — as shown in Figure 4.41. From the map in Figure 4.11, all the station are shown to lie in the flat basin, except KiK-Net TKCH11, which lies on the foothills of the mountain.

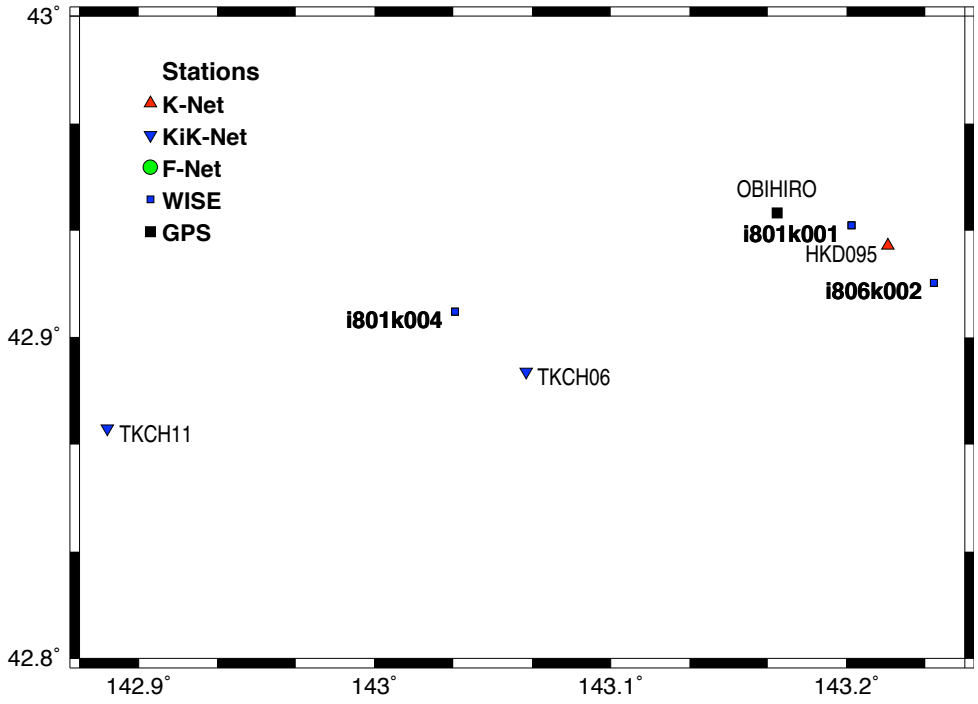

Figure 4.41: Stations near Obahiro. Blue stations from WISE, red: K-Net, black triangle: KiK-Net, black square: GPS. All stations plotted are within 15*km* of KiK-Net station TKCH06, which is 162*km* from the epicenter.

Figures 4.42, 4.43 show the band-passed velocity, and deconvolved displacement from these 8 sensors. Timing is not synchronised between networks. From the displacement timeseries, the WISE stations do all have the opposite polarity for the horizontal motions.

When we look at the velocity timeseries, these timeseries still appear reversed. Noting the similarity of the waveforms, and the close proximity of the stations, this is conclusive evidence that the polarity of the waveforms are reversed. Although the WISE stations once again do not provide a clear displacement field, the magnitudes of the best-guess offsets in Figures 4.7 are in general agreement with the GPS. Nonetheless, these examples do provide another reason for suggesting the WISE network is not appropriate for investigations into permanent ground displacement. Indeed, it also may be inappropriate to use this network to come to any conclusions regarding the functionality of the VSE series of seismometers in general.

Figure 4.42 also serves to illustrate again the stability and GPS compatibility of the displacements produced by the down-hole KiK-Net accelerometers. With very little tilt occurring at depths, the accelerometers perform very well. All the K-Net and WISE stations have unstable tilted displacements, with the surface KiK-Net instruments also showing some tilting. Even though the GPS station at Obihiro is $\sim 15km$ from TKCH06, and $\sim 30km$ from TKCH11, both KiK-Net down-hole sensor record static displacement almost identical to the GPS.

It is also interesting to note that though the static displacements from the 2 down-hole sites are very similar, the overall character of the ground motion is not. Kristine Larson (*personal communication*) has again determined the $1sps$ high-rate GPS data from Obihiro. In Figure 4.44, this GPS data and the 2 KiK-Net down-hole displacement timeseries are compared. The GPS and the TKCH06 site are located in the basin, where there are large displacement long period resonances measured both by the $1sps$ GPS, and the down-hole at $227m$ depth. These resonant waves are not seen at the nearby TKCH11 down-hole at $100m$ depth, located on the mountain side at the edge of the basin.

A spectrogram of the acceleration timeseries from both up-hole and down-hole from TKCH06, and the down-hole only from TKCH11, is presented in Figure 4.46. Each vertical line in the plot represents an FFT of $10s$ of the data beginning at the time it is plotted. The low frequency basin waves which dominate the TKCH06 station response are clearly observed in the spectrograms.

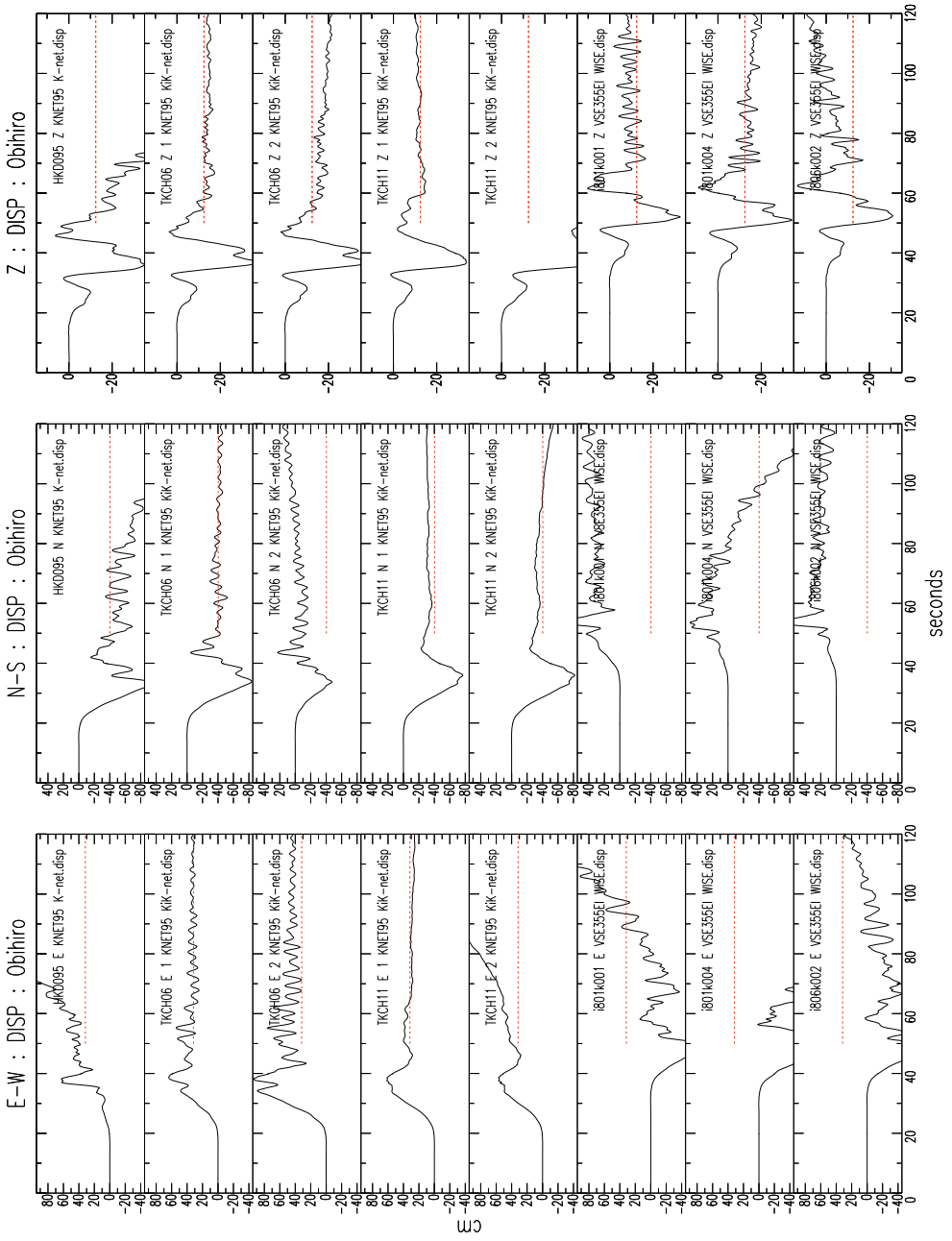

Figure 4.42: Displacements from stations near Obihiro. GPS Stn — Obihiro 31.7*cm* East, 40.3*cm* South, 12.4*cm* vertical drop. KiK-Net accelerometers, especially down-hole, have remarkably stable final offset, similar to GPS. KiK-Net stations: '1': Down-Hole, '2': Up-Hole.

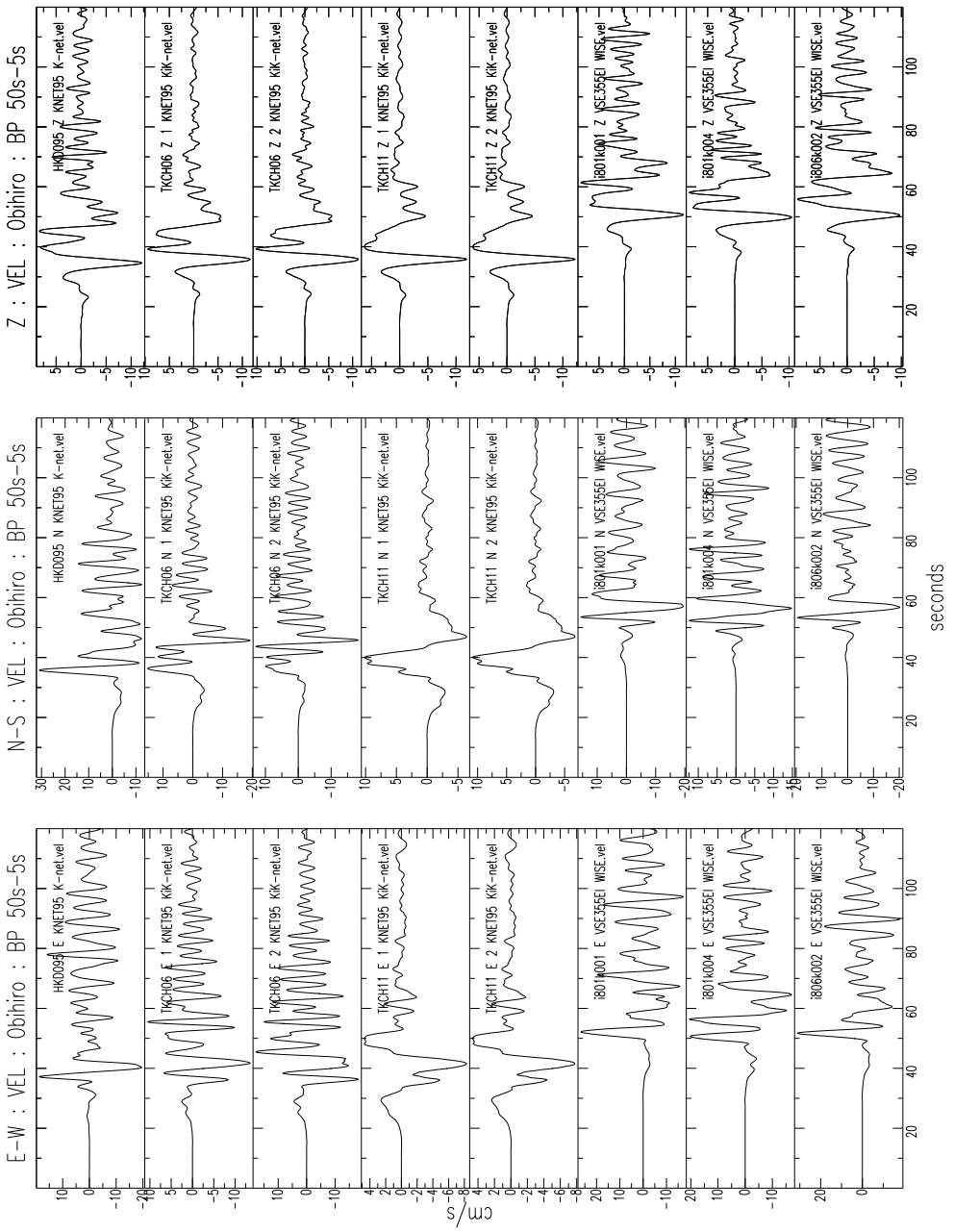

Figure 4.43: Velocity timeseries from the stations located near Obihiro. Bandpass from 50s — 5s. All stations in basin have large amplitude long period resonances at about 4s, which are not present on basin edge station TKCH11.

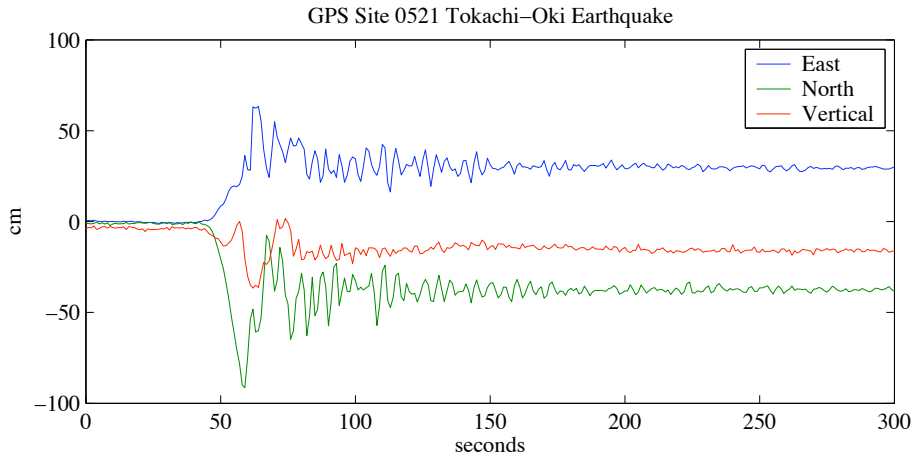

(a) 1*sps* GPS at Obihiro (Basin)

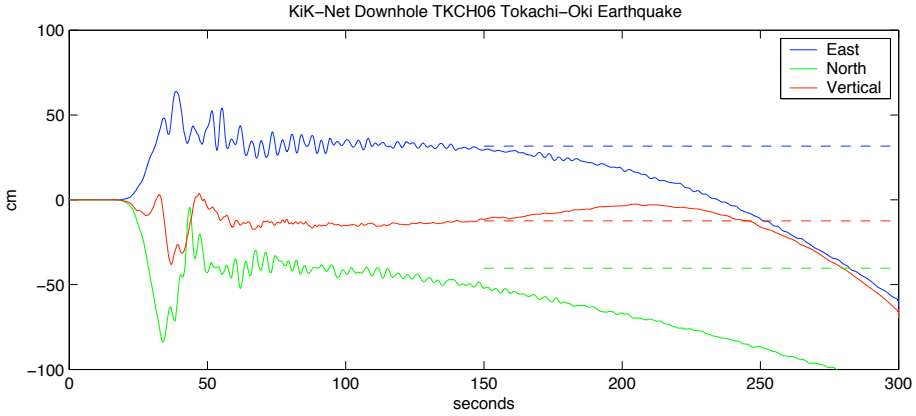

(b) 100*sps* accelerometer at TKCH06 down-hole (basin)

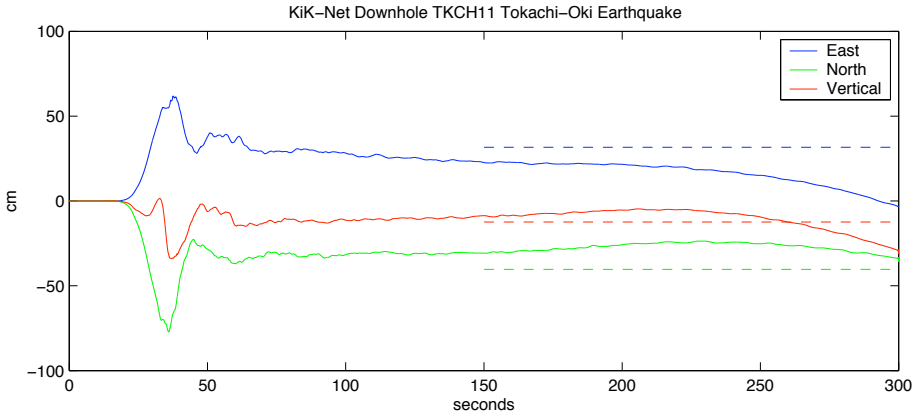

(c) 100*sps* accelerometer at TKCH11 down-hole (rock)

Figure 4.44: High-rate GPS vs. accelerometer displacement timeseries for KiK-Net and GPS stations near Obihiro. GPS timing is 13*s* fast. 7*dy* average GPS offsets included on KiK-Net plots.

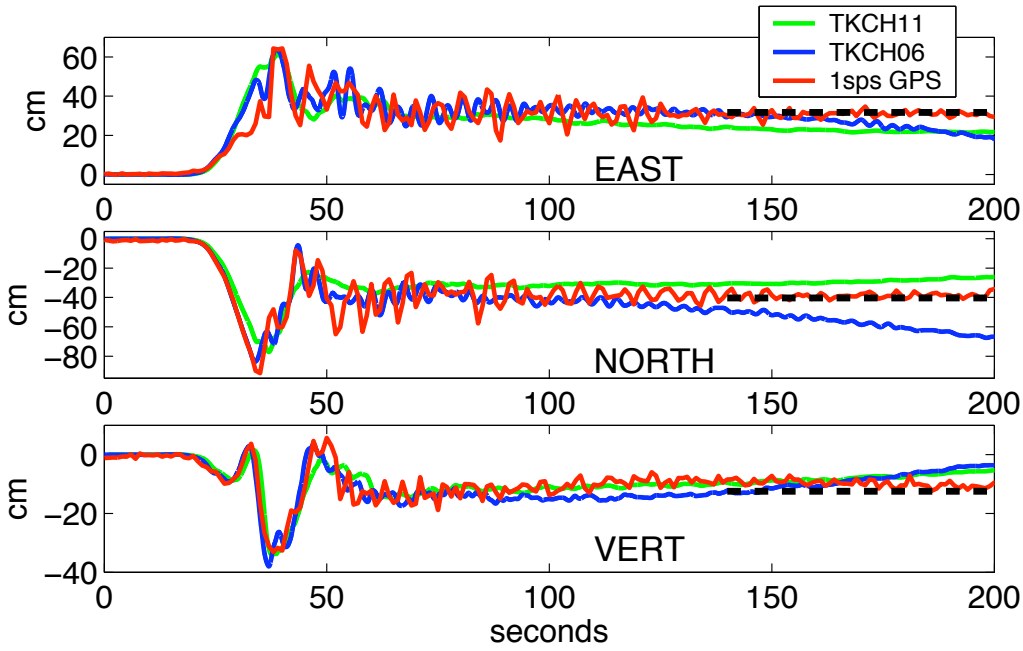

Figure 4.45: High-rate GPS vs. accelerometer displacement timeseries for KiK-Net and GPS stations near Obihiro. Accelerometer horizontal channels are not rotated. 7dy average GPS offsets are included.

4.5 Other F-Net stations on Hokkaido

The performance of the F-Net VSE-355G/G2 instruments in the near-field was not excellent, so the performance of the other F-Net stations on Hokkaido were analysed. After KMU, URH and KSR, the next closest station to the epicenter was HID, at 169km distance. This VSE-355G2 station recorded peak velocities of 16.6cm/s without the high frequency spikes seen at KMU and KSR. Upon deconvolution though, it appears this instrument also tilted. Figure 4.47 presents the displacement and velocity timeseries for both the deconvolved and un-deconvolved records. Deconvolved horizontal velocity timeseries have non-physical linear trends after 30s of strong motion, which is consistent with unexpected static offset in un-deconvolved horizontal displacements (see Figure 3.6. In the E-W component, this trend corresponds to a tilt of 0.01^o, much larger than the tectonic tilt as observed closer to the rupture. At this distance from the epicenter, with the vault setting, this size of tilting is unusual. It is likely this is a non-linear sensor response.

Figures 4.48 and 4.49 presents velocities and displacements from the remaining F-Net

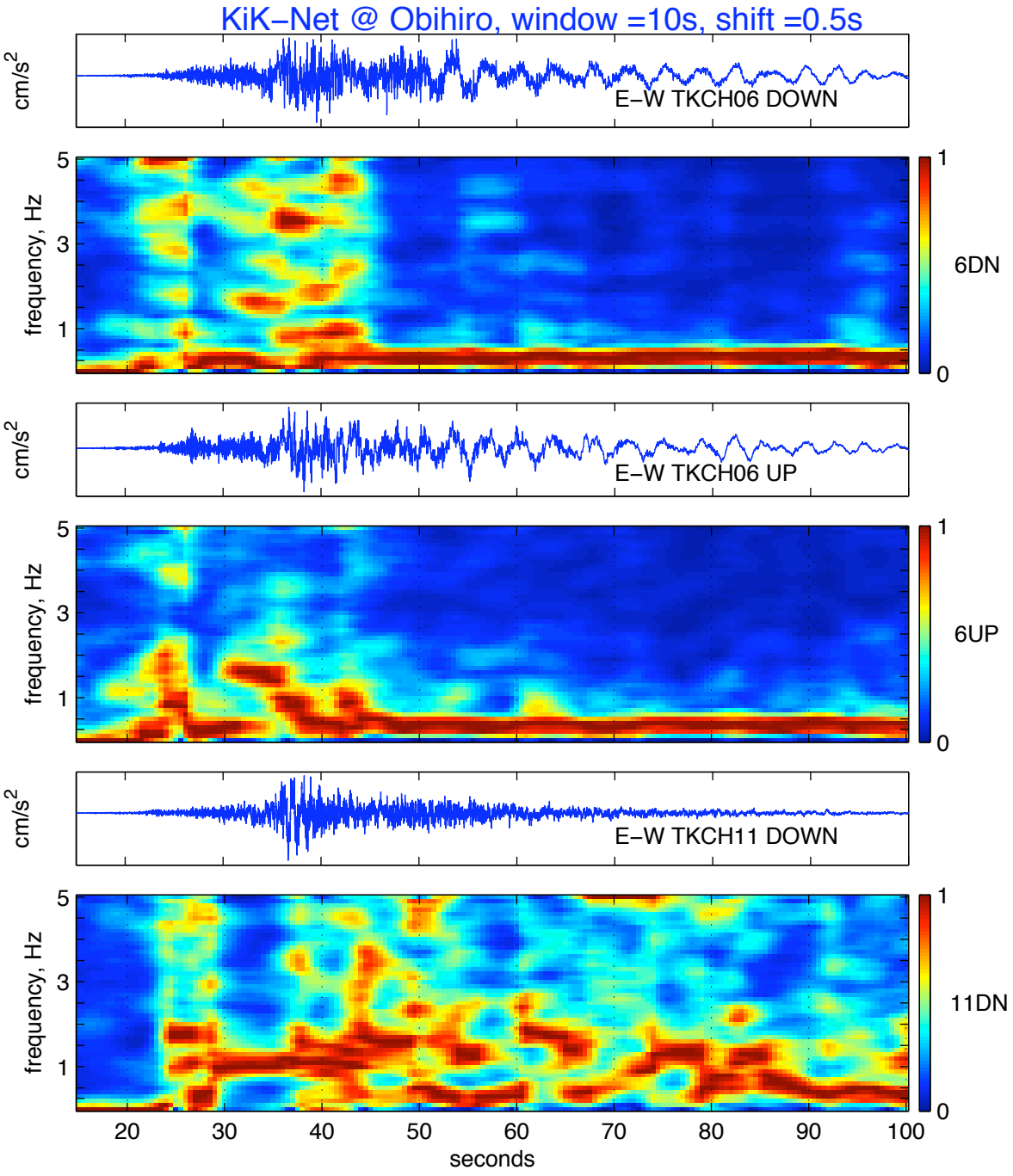

Figure 4.46: Acceleration timeseries and spectrogram for E-W component of KiK-Net sites TKCH06 and TKCH11. See Fig 4.41 for location. TKCH06 is located in the middle of the basin, and its response is dominated by basin waves, TKCH11 is on mountainous basin edge, and does not have these basin waves.

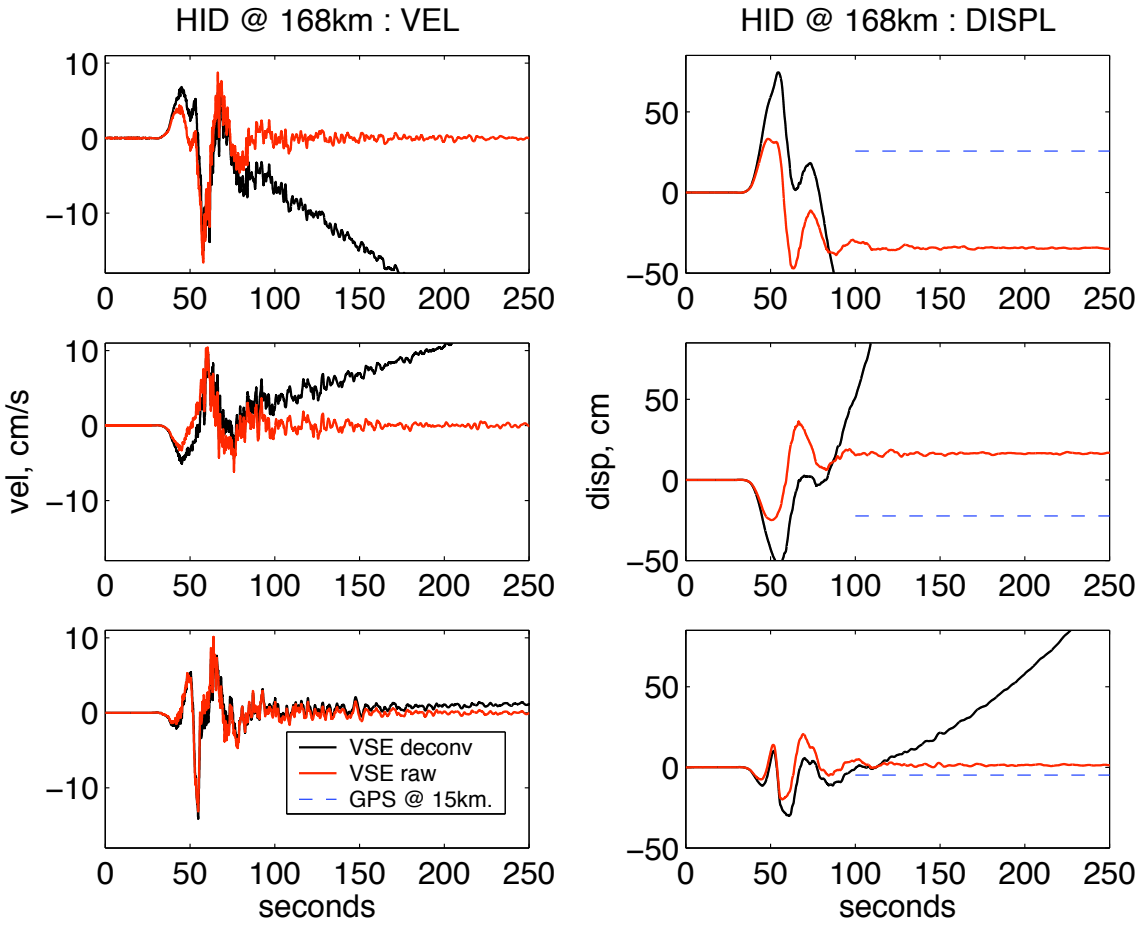

Figure 4.47: Comparison of deconvolved and raw velocity and displacement timeseries from VSE-355G2 at F-Net station HID, 169km from epicenter. GPS from Biratori station. Instrument performs poorly — note static offset in horizontal components of undeconvolved data. At this distance, and considering the station is location in a 30m deep vault, tilting is unlikely to be responsible. Note max velocity of 16.6cm/s is reached without clip. Top: E-W; middle: N-S; bottom: vertical.

stations on Hokkaido Island. Their locations can be seen on the map of Japan in Figure 4.50. The nearest GPS station to each station provides the expected static offset plotted. In general, the VSE does a good job in matching the GPS static offset, though tilts are observed even at large distances under small motions. This may be due to problems with sensor installation, or an unexpected non-linear sensor response. [Note these timeseries are 250s long, previous plots were only 120s long.]

Station IMG houses the only other VSE-355G sensor on Hokkaido, and the displacement derived from the sensor appears to be corrupted by tilting. It is not as stable as URH, which saw much larger motions and offsets, yet gave very good static offsets (see Figure 4.35). The East Component of KNP reached 15.1cm/s velocity, and this station also exhibits tilting after this value is reached, similar to at HID. The corresponding displacement is also not stable.

4.6 Teleseismic Motion around Japan

The earthquake provides an excellent opportunity to observe how large events may saturate broadband networks over a large area. As the F-Net network consists of stations with co-located broadband and strong motion (all VSE-355G/G2) instruments, velocities from both sets of instruments can be directly compared. In this study, for all earthquakes investigated, all F-Net data is obtained from the F-Net Website `www.fnet.bosai.go.jp/`. Each station's dataset comprises of channels from both the high-gain broadband sensor data, and the low-gain strong motion velocity sensor. A 45min time period of 1sps data, beginning at the onset of rupture is downloaded. The only processing of the data is the removal of the mean of the trace, and division by the station gain, as determined by sensitivity from SEED response files available on the F-Net Web-site. All F-Net instruments have a response flat to velocity between at least 0.0125Hz (80s) and 10Hz. The instruments deployed in F-Net at the time of the earthquake consist of STS-1's, STS-2's and CMG-1T's for the broadband sensor, and VSE-355G's and VSE-355G2's for the strong motion sensor. A summary of the instrument properties is in Table 2.1. As discussed in the previous Section, the VSE-355G is an earlier version of the VSE-355G2, with a similar frequency range, but lower dynamic

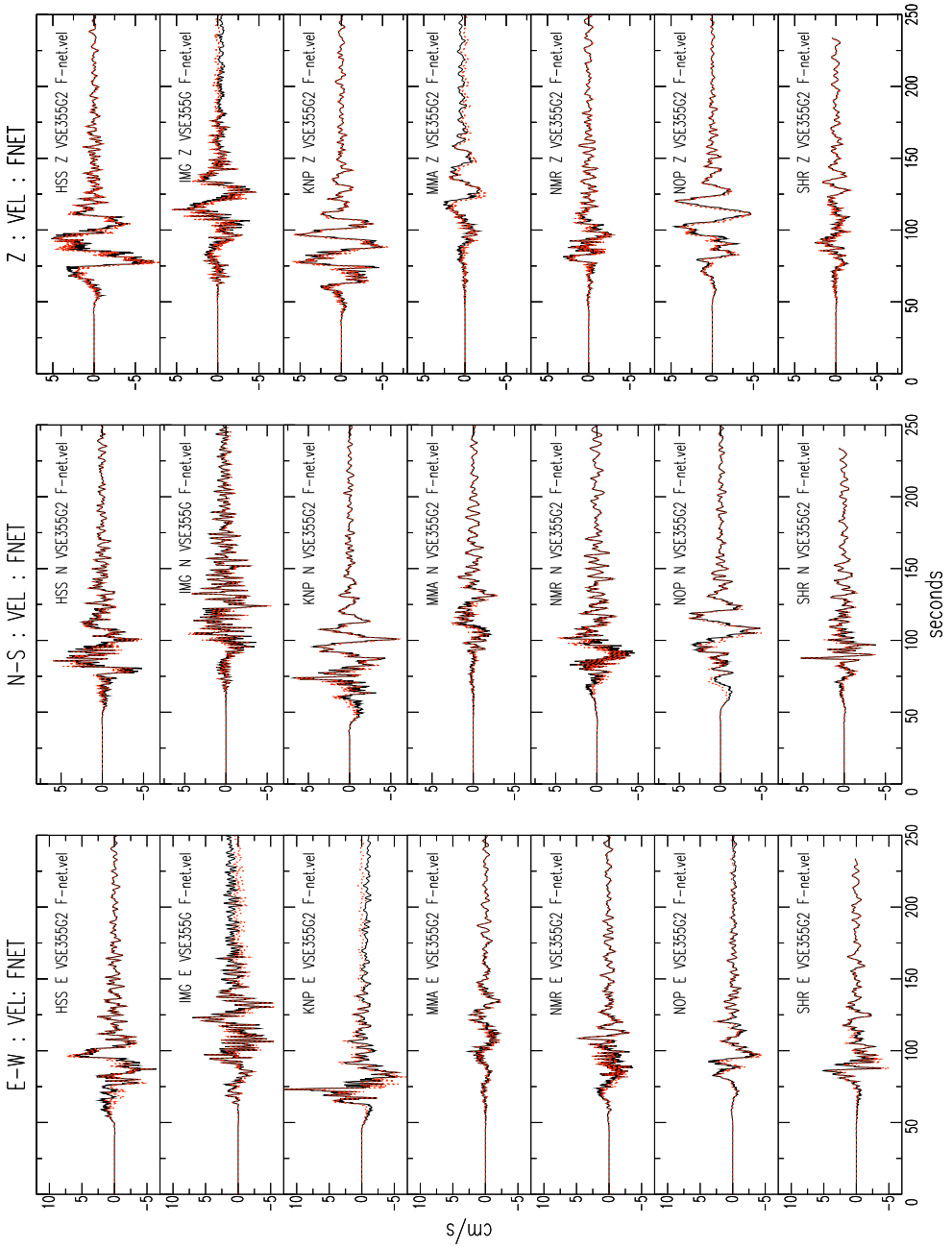

Figure 4.48: Velocity timeseries from other F-Net stations on Hokkaido Island. Solid lines are deconvolved data, dotted are raw VSE output. Max. velocity at KNP E-W component, where 13.1cm/s raw velocity is output, which is 15.1cm/s when deconvolved. No clipping is apparent. Very minor tilting is apparent over the 250s

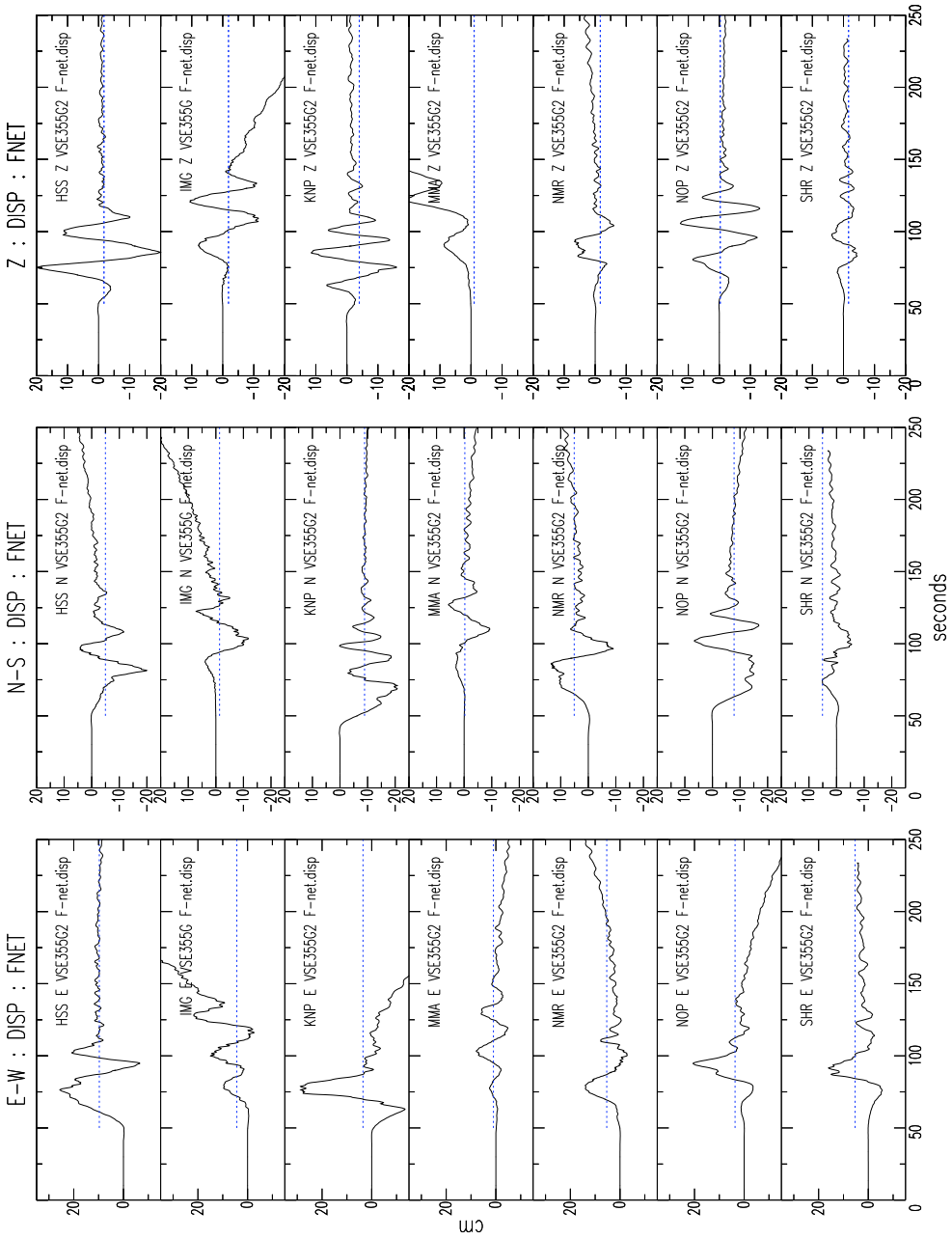

Figure 4.49: Displacement timeseries (deconvolved) from other F-Net stations on Hokkaido Island. Static offsets from nearest GPS stations are plotted as dotted lines.

range.

Figure 4.50 presents a summary plot of F-Net station performance throughout Japan during the M8.3 mainshock. Station performance is parameterised in the following manner:

Each of the 3 components is represented by a ratio K —

$$K_E = \frac{max(VSE[EW]velocity)}{max(Broadband[EW]velocity)} \tag{4.2}$$

$$K_N = \frac{max(VSE[NS]velocity)}{max(Broadband[NS]velocity)} \tag{4.3}$$

$$K_Z = \frac{max(VSE[Z]velocity)}{max(Broadband[Z]velocity)} \tag{4.4}$$

A station's performance can then be defined by the two parameters K_{max} and K_{min} —

$$K_{max} = max(K_E, K_N, K_Z) \tag{4.5}$$

$$K_{min} = min(K_E, K_N, K_Z) \tag{4.6}$$

For small motions below the broadband clip levels, and above the strong motion noise level, it is expected that $K_{max} \sim K_{min} \sim 1$. Due to some variation in instrument performance and calibration (station response files are being continuously maintained and updated, and quality control may not be perfect), a 'well operating station', observing motions within the fore-mentioned range, is defined as one with —

$$0.85 < K_{min}, \qquad \text{and} \qquad K_{max} < 1.15 \tag{4.7}$$

This allows a variation of 15% between the peak velocities from both sensors. A station with $K_{max} > 1.15$ has either clipped, has incorrect station gains, or a technical problem. A station with $K_{min} < 0.85$ has incorrect station gains, or a technical problem.

[Incorrect station gains are likely as quality control is not perfect - on the Web-site there are differences in sensors between the overall station summary table, and the individual station pages. Further, returned data would sometimes have incorrect starting values, beginning minutes into the record, and on a few occasions station coordinates on SAC files had different values to all station maps. eg: station SRN: 42.979N, 144.489E SAC header,

36.1987N, 136.6332E from station Web-page. A list of the stations with this problem is: AOG, KSR, HJO, NKG, NOP, OSW, SAG, SHR, SIB, SRN, STM, TYS, YNG. At another station, KZK, the broadband and strong motion are so different, it appears they are from different regions of Japan.]

In Figure 4.50, these 3 states are represented by colour symbols for each station. The closest station with un-clipped correct broadband recording of the event is HRO, with an STS-2, at 568km, with peak velocity of 0.69cm/s. The most distant station in the network that has a broadband instrument clipped, is station NAA, with an STS-1, at 924km distance. The E-W component of the VSE records 0.85cm/s, whilst the E-W STS-1 component clips at 0.76cm/s (see Figure 4.51). Figure 4.52 plots comparisons for all 3 components of the velocity and integrated displacement. It is noted there is no 'instrument response' in the displacement trace. This instrument response would be a long period signal in the clipped channel, similar to that observed in Figure 3.5, which is the response of the VSE to a δ-function in acceleration. This response is typically observed in sensor clipping, and its absence suggests the clipping at this channel may be due to datalogger saturation, rather than a sensor response.

In Figure 4.53 (SBT at 569km, with an STS-1) and Figure 4.54 (TYM at 834km, with an STS-1), clipping can be observed in the velocity trace. The integrated displacement timeseries contains the long period response attributed to the sensor clipping described above. It may be caused by a sudden deceleration of the mechanical sensor as it hits its 'stop', the limit of displacement of the pendulum.

Clipping of the broadband instruments due to shaking occurs at the stations indicated in Table 4.1. As discussed, stations as far away as 924km from the epicenter record velocities near 1cm/s and clip the STS-1. Though there are numerous other stations further away from the epicenter, which have $K_{max} > 1.15$ - as seen in Figure 4.50 — peak velocities are well below the broadband clip levels, and the high K_{max} is due to some station error. These stations are not included in Table 4.1.

In order to investigate whether these differences between the broadband and strong motion are caused by the strong motions or a systematic station error, F-Net data from smaller events (with subsequently smaller motions at distance), is analysed in a similar

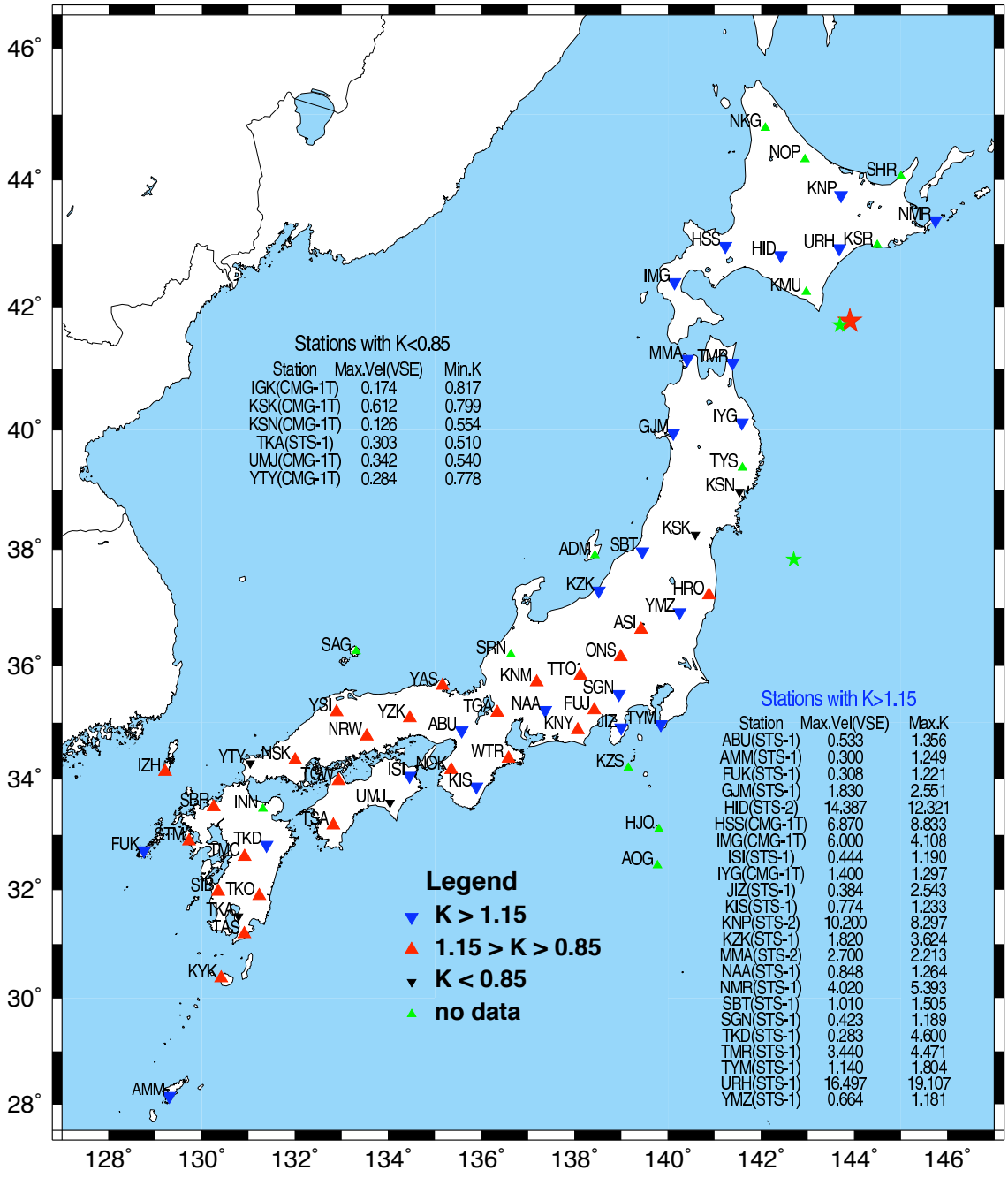

Figure 4.50: Comparison of velocity from F-Net instruments during M8.3 Tokachi-Oki earthquake. K: the ratio of maximum VSE (strong motion) velocity to maximum broadband velocity. This is determined for each of the 3 channels at each station. If $K > 1.15$ for any channel: generally indicates the broadband instrument has clipped, but can indicate incorrect station gain, or an instrument malfunction. $K < 0.85$: suggests instrument malfunction or other station problem. If $0.85 < K < 1.15$: the station appears well calibrated, in working order, and has not clipped. Problem stations have broadband instrument, max. observed VSE velocity (cm/s), and max/min K from all 3 channels tabulated.

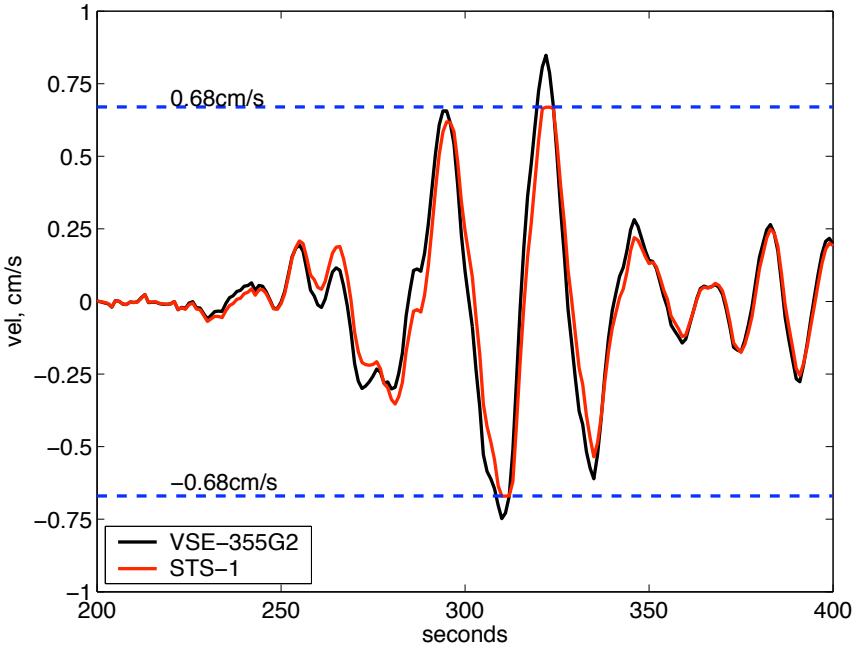

Figure 4.51: STS-1 E-W component from F-Net station NAA recording of M8.3 Tokachi-Oki, at 924km. STS-1 clips at 0.79cm/s.

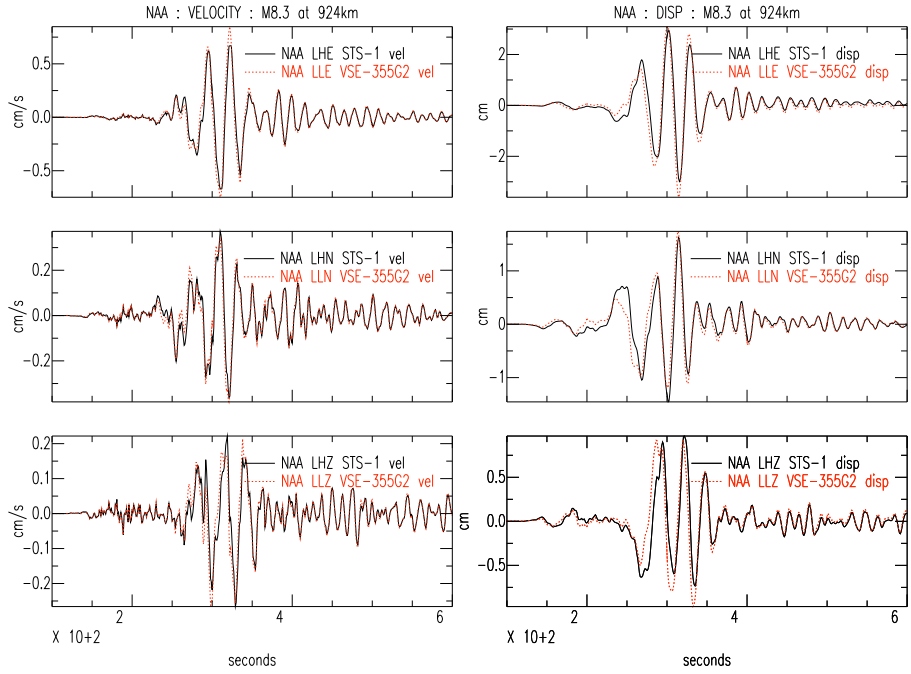

Figure 4.52: F-Net station NAA recording of M8.3 Tokachi-Oki, at 924km. 3 components of velocity and integrated displacement. Though STS-1 E-W component clips, no long period response observed in displacement, indicating saturation occurs in datalogger, not instrument.

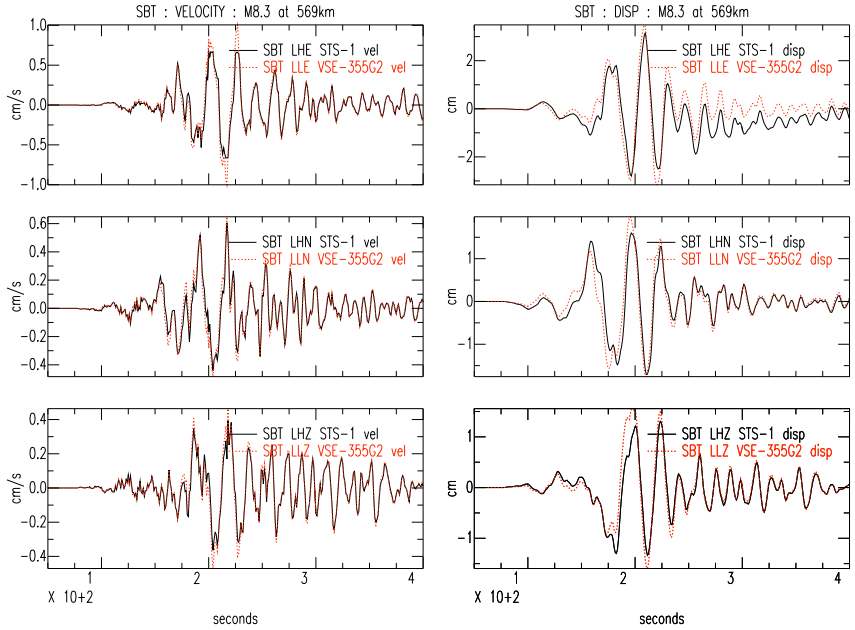

Figure 4.53: F-Net station SBT recording of M8.3 Tokachi-Oki, at 569*km*. All 3 components, in velocity and displacement. Clip in STS-1 E-W component, long period response observed in E-W displacement.

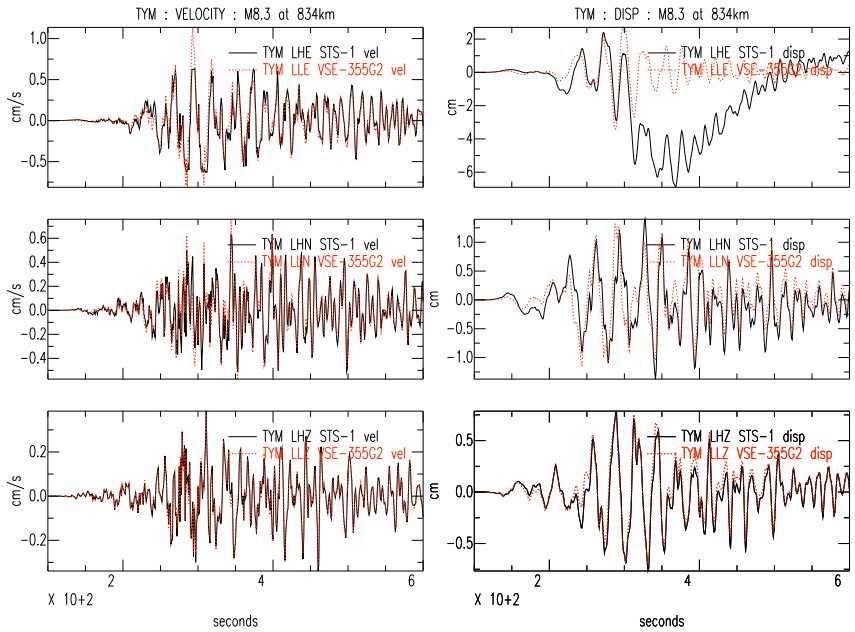

Figure 4.54: F-Net station TYM recording of M8.3 Tokachi-Oki, at 834*km*. All 3 components, in velocity and displacement. Clip at STS-1 E-W component, long period response observed in E-W displacement.

Station	**Distance** (km)	**Max VSE Velocity** (cm/s)	**Broadband Sensor**
URH	129	16.50	STS-1 **clips**
HID	169	14.39	STS-2 **clips**
KNP	221	10.20	STS-2 **clips**
TMR	223	3.44	STS-1 **clips**
NMR	232	4.02	STS-1 **clips**
HSS	257	6.87	CMG-1T **clips**
IYG	268	1.40	CMG-1T **clips**
MMA	300	2.70	STS-1 **clips**
IMG	318	6.00	CMG-1T **clips**
KSN	355	poor data	*wrong timing — ignore*
GJM	378	1.83	STS-1 **clips**
KSK	483	0.61	CMG-1T *NO CLIP*
HRO	568	0.69	STS-2 *NO CLIP*
SBT	569	1.01	STS-1 **clips**
YMZ	624	0.66	VSE-355G2 **clips**
KZK	679	1.82	STS-1 *DIFFERENT RECORDS?*
TYM	834	1.14	STS-1 **clips**
KNM	891	0.89	STS-2 *NO CLIP*
NAA	924	0.85	STS-1 **clips**

Table 4.1: Summary of F-Net station performance within 1000km of Tokachi-Oki

manner. Figure 4.55 presents data from the largest aftershock of the Tokachi-Oki earthquake, a M7.1 occurring $1hr, 18mins$ after the mainshock, very close to the epicentral area. Velocities from this earthquake were much smaller than from the mainshock, but still many stations to the west, up to a distance of $270km$, at IMG, have velocities over $1cm/s$, which is likely to clip the broadband instruments. Stations do not clip towards the north, even though they are closer to the epicenter. This is likely an indication that the directivity of the rupture was towards the West. Figure 4.56 is developed from F-Net data recorded from a M6.8 10 October 2003 earthquake located offshore of East Honshu.

Comparing all 3 maps shows there are many stations with pathological errors repeated for all earthquakes. Often the error appears to be simply a case of a difference in channel gains, as the strong motion and broadband signals for the same component are essentially a scalar multiple of each other. In some cases though, the errors are associated with unexpected instrument behaviour. This occurs both in the strong motion, and the high-gain broadband instruments (in the case of the high-gain broadband sensors, it is noted that from this dataset these errors only are observed for the STS-1 and CMG-1T, and not in the STS-2). One such example is in Figure 4.57, from station TKA at $1631km$, which the Z channel seems to have the same signal, with incorrect station gain. The magnitudes of the velocities recorded by the VSE are similar to those from nearby stations. The STS-1's reported gain seems too high if it clips at a minimum level of $0.59cm/s$. A permanent offset is also recorded on the displacement. This is associated with a broadband response to a step in acceleration, as illustrated in Figure 3.6. The large difference in magnitudes for the Z component is observed with both the M7.3 and M6.8 events. The STS-1 at TKD at $1487km$ from the M8.3(Figure 4.58) also shows similar behaviour, though in this case, STS-1 N-S and Z velocities appear too low. Again, the displacement timeseries show some non-linearity in the response, this time though an unknown long period wave (too long to be the instrument response illustrated in Figures 3.6 or 3.5) is observed in the N-S and Z channels. This performance is repeated again for both the M7.3 and M6.8 events.

A final example illustrates poor behaviour from a VSE-355G2, again during the M8.3, from station YMZ, at $624km$ (Figure 4.59). Here, though the velocity timeseries look identical, with the STS-1 not clipping at over $0.4cm/s$, the integrated displacements show the

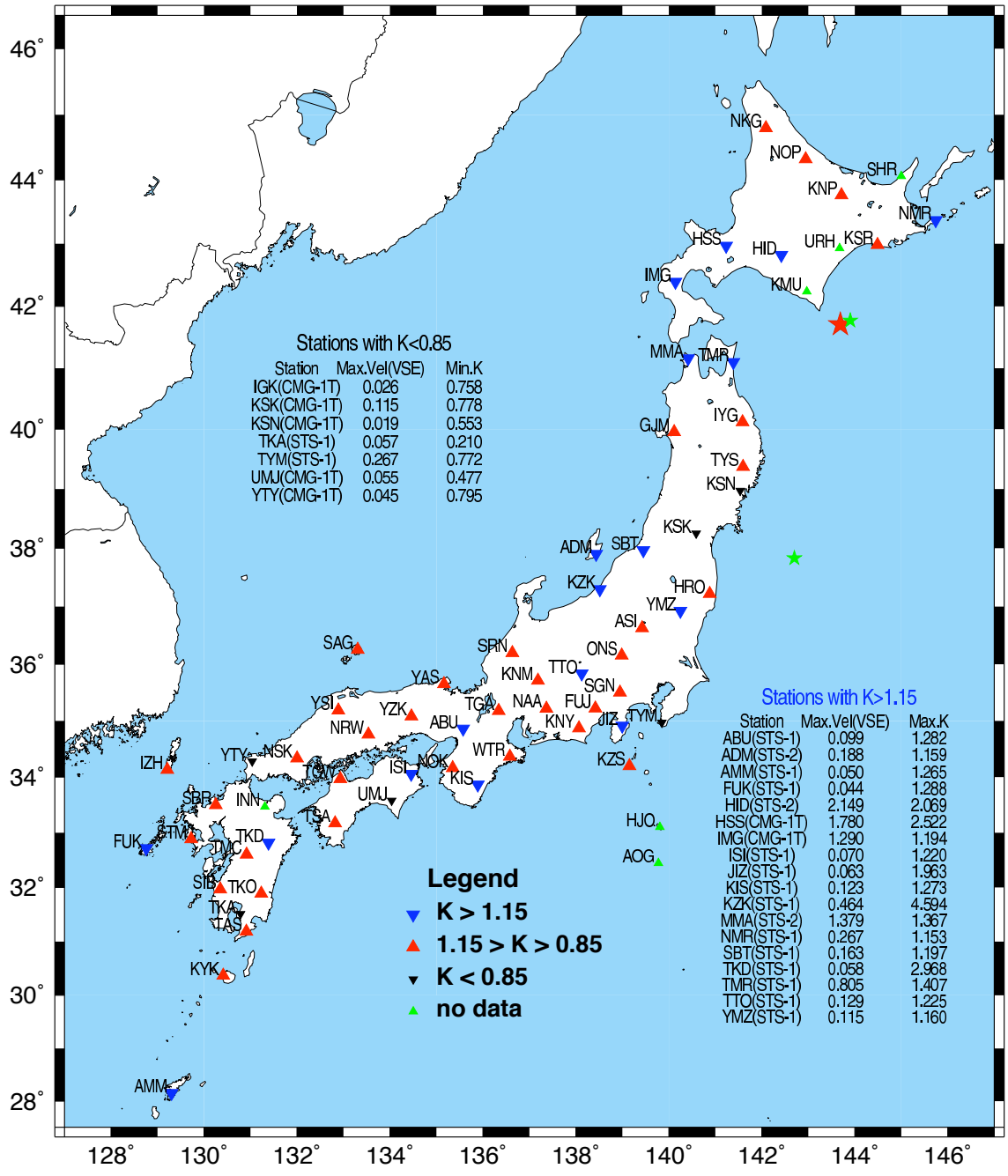

Figure 4.55: As Figure 4.50 for M7.1 25 September 2003 event, an aftershock of Tokachi-Oki.

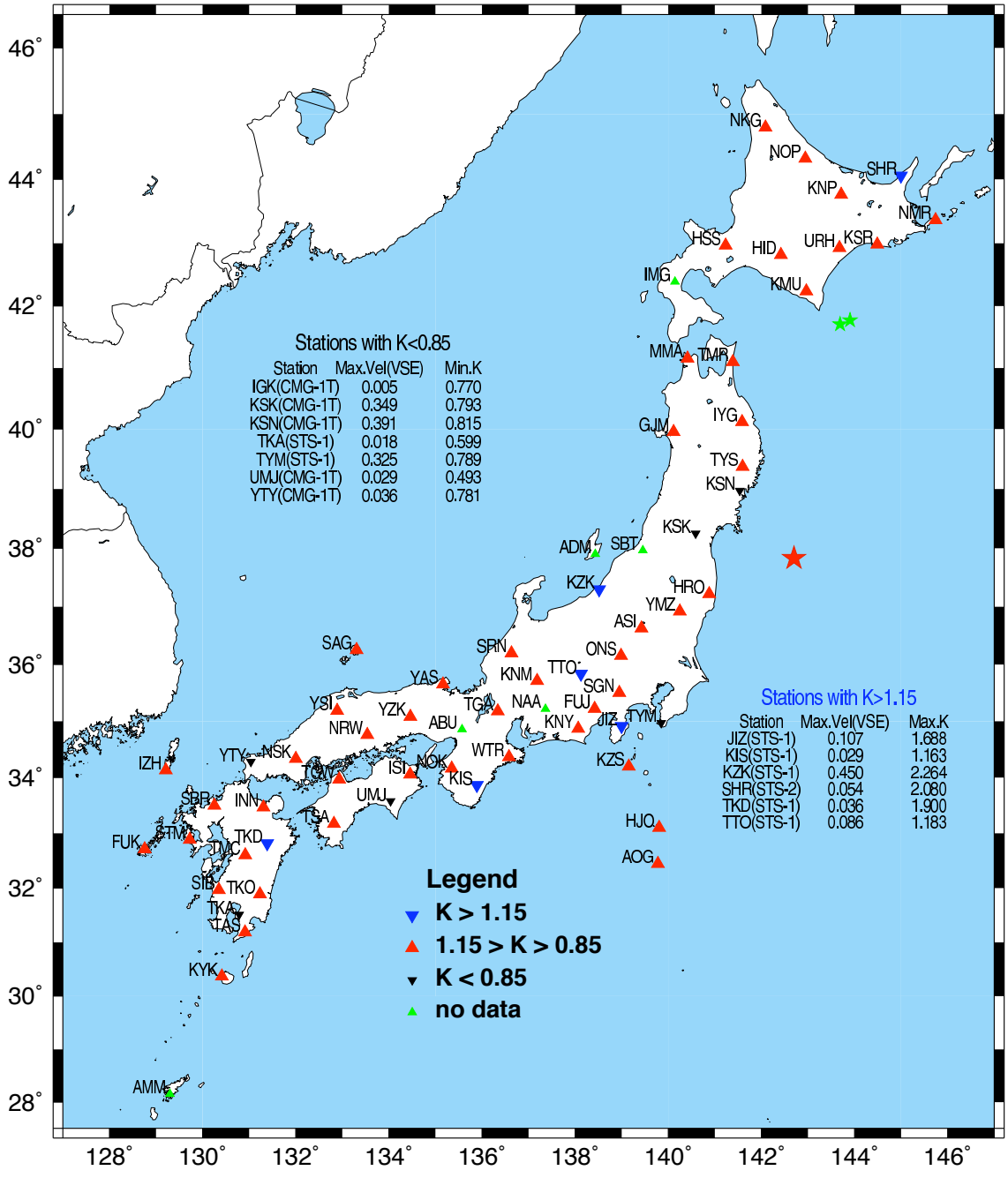

Figure 4.56: As Figure 4.50 for M6.8 10 October 2003 event, located off Honshu Island

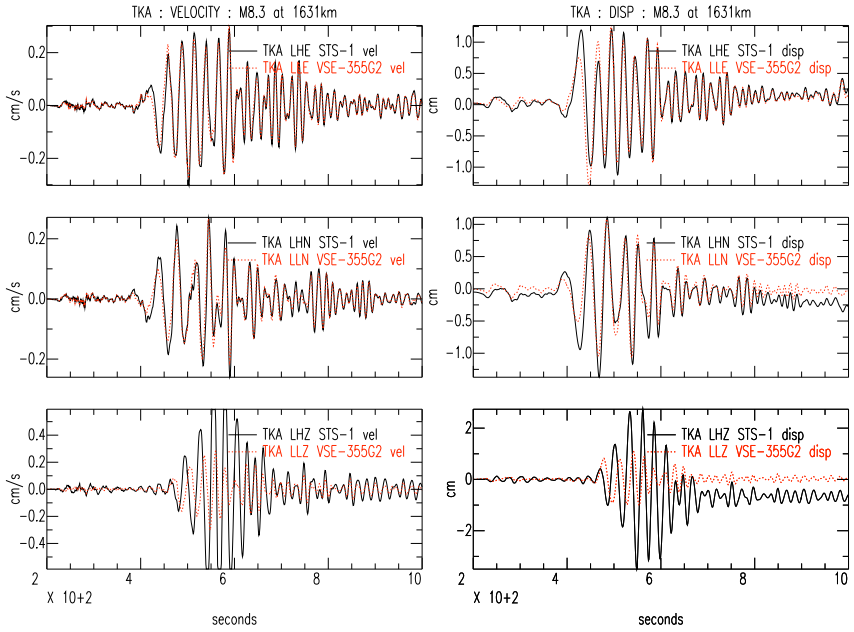

Figure 4.57: F-Net station TKA recording of M8.3 Tokachi-Oki, at 1631*km*. All components, in velocity and displacement. STS-1 Z component appears to have a low station gain, so velocity is too high, with unexplained static offset in corresponding displacement. Also STS-1 drift in N-S displacement.

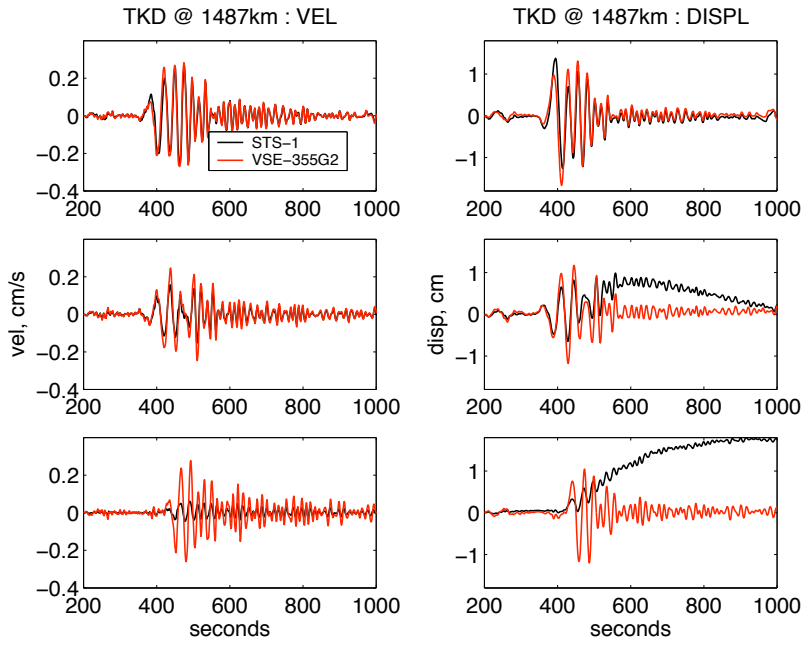

Figure 4.58: F-Net station TKD recording of M8.3 Tokachi-Oki, at 1487*km*. All components, in velocity and displacement. STS-1 Z and N-S component station gains appear to be too high. Unexplained long period drift in displacements. Top: E-W; middle: N-S; bottom: vertical.

VSE has recorded a permanent offset of near $2cm$ that is not physically realistic. Figure 3.6 shows a similar VSE response to a step in acceleration. These observations at YMZ cannot be due to tilt as the offset occurs only on the vertical channel, which is much less sensitive to tilt than the horizontal channels.

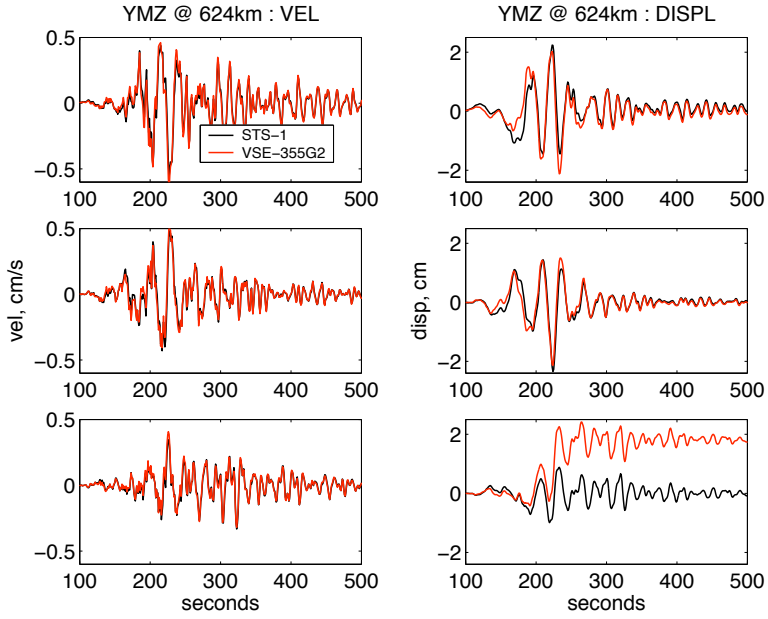

Figure 4.59: F-Net station YMZ recording of M8.3 Tokachi-Oki, at $624km$. All components, in velocity and displacement. VSE-355G2 Z component performance, similar offset in displacement to a step in acceleration. This also occurs in the M6.8 event, at $239km$, with max. vel of $0.22cm/s$. Top: E-W; middle: N-S; bottom: vertical.

Tables 4.2 and 4.3 present a summary of the station information for each earthquake. Instrument types, and K_{max}, K_{min} and peak strong motion velocity are given for each of the 3 earthquakes.

Though not directly relevant to the performance of the VSE, this dataset provides insight into the field performance of the broadband instruments. A general indication of where the actual clip levels of the broadband instruments in the field occur can be obtained by plotting the maximum strong motion velocity against the maximum broadband velocity, as shown in Figure 4.60. From the 3 events, there is a total of 185 station recordings, or 555 channels each of broadband and strong motion.

There is a lot of clutter about the black line in Figure 4.60, so in Figure 4.61, the same data is plotted this time with peak broadband velocity against the ratio of peak broadband

Station	Broad-Band	Strong Motion	Lat	Lon	M8.3				M7.1				M6.8			
					Dist	Kmax	Kmin	VSEmx	Dist	Kmax	Kmin	VSEmx	Dist	Kmax	Kmin	VSEmx
ABU	STS-1	VSE-355G2	34.9	135.6	1072	*1.36*	1.09	0.533	1055	*1.28*	1.08	0.099	-	-	-	-
ADM	STS-2	VSE-355G2	37.9	138.4	-	-	-	-	367	*1.16*	1.03	0.188	-	-	-	-
AMM	STS-1	VSE-355G	28.2	129.3	2010	*1.25*	1.18	0.300	1992	*1.26*	1.20	0.050	-	-	-	-
AOG	STS-2	VSE-355G2	32.4	139.8	-	-	-	-	-	-	-	-	654	1.02	1.00	0.057
ASI	STS-2	VSE-355G2	36.6	139.4	690	1.06	1.04	0.640	674	1.09	1.05	0.111	320	1.04	1.03	0.146
FUJ	STS-1	VSE-355G2	35.2	138.4	870	1.01	0.92	0.512	854	1.13	1.02	0.141	480	1.14	1.05	0.094
FUK	STS-1	VSE-355G	32.7	128.8	1674	*1.22*	1.12	0.308	1655	*1.29*	1.03	0.044	1388	1.12	1.00	0.021
GJM	STS-1	VSE-355G2	40.0	140.1	378	*2.55*	2.20	**1.830**	359	1.08	0.95	0.465	325	1.09	1.01	0.450
HID	STS-2	VSE-355G2	42.8	142.4	169	*12.32*	6.95	**14.387**	162	*2.07*	1.34	**2.149**	554	1.06	0.95	0.132
HJO	STS-2	VSE-355G2	33.1	139.8	-	-	-	-	-	-	-	-	587	1.03	0.98	0.052
HRO	STS-2	VSE-355G	37.2	140.9	568	1.09	1.03	0.692	554	1.12	1.06	0.133	174	1.06	1.02	0.315
HSS	CMG-1T	VSE-355G2	43.0	141.2	257	*8.83*	5.21	**6.870**	246	*2.52*	1.54	**1.780**	584	*1.15*	1.07	0.072
IGK	CMG-1T	VSE-355G	24.4	124.2	2652	0.92	*0.82*	0.174	2634	0.93	*0.76*	0.026	2302	0.89	*0.77*	0.005
IMG	CMG-1T	VSE-355G	42.4	140.1	318	*4.11*	3.53	**6.000**	303	*1.19*	1.06	**1.290**	-	-	-	-
INN	STS-2	VSE-355G2	33.5	131.3	-	-	-	-	-	-	-	-	1138	1.03	1.02	0.024
ISI	STS-1	VSE-355G2	34.1	134.5	1192	*1.19*	1.08	0.444	1174	*1.22*	1.04	0.070	853	1.13	1.02	0.039
IYG	CMG-1T	VSE-355G2	40.1	141.6	268	*1.30*	0.89	**1.400**	250	1.03	0.93	0.303	272	1.02	0.94	0.254
IZH	STS-2	VSE-355G2	34.1	129.2	1542	1.06	1.01	0.341	1523	1.05	1.02	0.056	1282	1.07	1.00	0.044
JIZ	STS-1	VSE-355G2	34.9	139.0	874	*2.54*	1.04	0.384	859	*1.96*	0.95	0.063	464	*1.69*	1.00	0.107
KGM	CMG-1T	VSE-355G	26.8	128.2	2198	1.05	1.01	0.223	2180	1.06	1.00	0.040	1832	1.07	1.03	0.008
KIS	STS-1	VSE-355G2	33.9	135.9	1125	*1.23*	0.94	0.774	1108	*1.27*	0.98	0.123	756	*1.16*	0.94	0.029
KMU	CMG-1T	VSE-355G2	42.2	143.0	-	-	-	-	-	-	-	-	490	1.03	0.99	0.161
KNM	STS-2	VSE-355G2	35.7	137.2	891	1.05	0.96	**0.893**	873	1.04	0.95	0.137	546	1.07	0.95	0.068
KNP	STS-2	VSE-355G2	43.8	143.7	221	*8.30*	5.01	**10.200**	228	1.11	0.98	0.418	664	1.02	1.00	0.097
KNY	STS-2	VSE-355G2	34.9	138.1	920	1.04	1.02	0.467	904	1.11	1.01	0.105	530	1.09	0.95	0.093
KSK	CMG-1T	VSE-355G	38.3	140.6	483	0.94	*0.80*	0.612	466	0.81	*0.78*	0.115	191	0.84	*0.79*	0.349
KSN	CMG-1T	VSE-355G	39.0	141.5	-	-	-	-	355	0.58	*0.55*	0.019	163	0.88	*0.81*	0.391
KSR	STS-2	VSE-355G2	43.0	144.5	-	-	-	-	156	1.03	1.02	0.602	592	1.06	0.93	0.099
KYK	STS-2	VSE-355G2	30.4	130.4	1750	1.10	1.05	0.336	1732	1.08	0.94	0.053	1401	1.07	0.96	0.013
KZK	STS-1	VSE-355G2	37.3	138.5	679	*3.62*	2.52	**1.820**	662	*4.59*	1.93	0.464	374	*2.26*	1.64	0.450
KZS	STS-2	VSE-355G2	34.2	139.2	-	-	-	-	1015	1.04	0.99	0.100	587	1.03	0.98	0.182
MMA	STS-2	VSE-355G2	41.2	140.4	300	*2.21*	2.12	**2.700**	281	*1.37*	1.02	**1.379**	419	1.13	1.00	0.252
NAA	STS-1	VSE-355G2	35.2	137.4	924	*1.26*	0.99	**0.848**	907	1.14	1.02	0.145	-	-	-	-
NKG	STS-2	VSE-355G2	44.8	142.1	-	-	-	-	367	1.06	1.04	0.449	776	1.05	0.94	0.081
NMR	STS-1	VSE-355G2	43.4	145.7	232	*5.39*	3.18	**4.020**	249	*1.15*	1.07	0.267	666	1.12	1.08	0.056
NOK	STS-2	VSE-355G2	34.2	135.4	1130	1.07	1.01	0.553	1112	1.05	1.02	0.103	777	1.08	1.03	0.037
NOP	STS-2	VSE-355G2	44.3	142.9	-	-	-	-	296	1.00	0.98	0.373	721	1.05	1.01	0.110
NRW	CMG-1T	VSE-355G	34.8	133.5	1194	1.08	1.01	0.378	1175	1.04	0.98	0.079	890	1.09	1.01	0.037
NSK	STS-2	VSE-355G2	34.3	132.0	1329	1.08	1.00	0.373	1310	1.05	1.00	0.057	1038	1.04	0.99	0.034

Table 4.2: Summary of F-Net station performance during large earthquakes in Autumn, 2003. Epicenters plotted on maps in Figures 4.50, 4.55 and 4.56. Distances of station from epicentre are in *km*, maximum velocities are from the strong motion instrument, in cm/s.

Station	Broad-Band	Strong Motion	Lat	Lon	M8.3				M7.1				M6.8			
					Dist	Kmax	Kmin	VSEmx	Dist	Kmax	Kmin	VSEmx	Dist	Kmax	Kmin	VSEmx
ONS	CMG-1T	VSE-355G	36.2	139.0	756	0.95	0.91	0.564	739	0.96	0.87	0.086	380	0.96	0.90	0.103
OSW	STS-2	VSE-355G2	27.1	142.2	-	-	-	-	1627	1.03	1.00	0.017	1192	1.04	1.01	0.018
SAG	STS-2	VSE-355G2	36.3	133.3	-	-	-	-	1083	1.05	1.02	0.071	853	1.05	1.02	0.054
SBR	STS-1	VSE-355G	33.5	130.3	1512	1.14	1.09	0.308	1493	1.09	1.04	0.050	1224	1.10	1.04	0.030
SBT	STS-1	VSE-355G2	38.0	139.5	569	*1.50*	1.07	**1.010**	552	*1.20*	1.05	0.163	-	-	-	-
SGN	STS-1	VSE-355G2	35.5	138.9	819	*1.19*	1.01	0.423	803	1.09	1.02	0.081	423	1.09	1.02	0.103
SHR	STS-2	VSE-355G2	44.1	145.0	-	-	-	-	-	-	-	-	718	*2.08*	1.07	0.054
SIB	STS-2	VSE-355G2	32.0	130.4	1622	1.05	1.01	0.347	1604	1.05	1.00	0.065	1301	1.02	0.99	0.025
SRN	STS-2	VSE-355G2	36.2	136.6	-	-	-	-	865	1.03	0.99	0.116	569	1.07	1.00	0.095
STM	STS-2	VSE-355G2	32.9	129.7	1594	1.06	1.05	0.335	1575	1.04	1.03	0.050	1299	1.03	1.02	0.028
TAS	STS-2	VSE-355G2	31.2	130.9	1650	1.06	0.97	0.335	1632	1.04	1.03	0.053	1308	1.04	0.96	0.017
TGA	STS-2	VSE-355G2	35.2	136.3	985	1.05	0.96	0.762	967	1.05	0.99	0.137	641	1.04	1.00	0.061
TGW	STS-2	VSE-355G2	34.0	132.9	1295	1.05	1.03	0.331	1276	1.07	1.03	0.091	979	1.03	1.02	0.030
TKA	STS-1	VSE-355G2	31.5	130.8	1631	1.00	*0.51*	0.303	1613	0.94	*0.21*	0.057	1296	0.90	*0.60*	0.018
TKD	STS-1	VSE-355G2	32.8	131.4	1487	*4.60*	1.07	0.283	1469	*2.97*	1.10	0.058	1168	*1.90*	1.02	0.036
TKO	STS-2	VSE-355G2	31.9	131.2	1572	1.04	1.02	0.372	1554	1.05	1.00	0.077	1237	1.03	0.99	0.025
TMC	STS-2	VSE-355G2	32.6	130.9	1535	1.07	0.99	0.306	1516	1.07	1.05	0.066	1218	1.05	0.99	0.027
TMR	STS-1	VSE-355G2	41.1	141.4	223	*4.47*	2.29	**3.440**	204	*1.41*	1.21	**0.805**	380	1.10	0.98	0.213
TSA	CMG-1T	VSE-355G	33.2	132.8	1366	1.05	1.00	0.363	1348	1.10	1.02	0.080	1034	1.03	1.01	0.036
TTO	STS-1	VSE-355G	35.8	138.1	828	1.11	1.03	0.666	812	*1.23*	1.00	0.129	464	*1.18*	0.99	0.086
TYM	STS-1	VSE-355G2	35.0	139.8	834	*1.80*	0.97	**1.140**	820	1.13	*0.77*	0.267	408	0.90	*0.79*	0.325
TYS	STS-2	VSE-355G2	39.4	141.6	-	-	-	-	314	1.06	1.00	0.348	197	1.05	0.97	0.361
UMJ	CMG-1T	VSE-355G	33.6	134.0	1257	0.79	*0.54*	0.342	1240	0.79	*0.48*	0.055	914	0.83	*0.49*	0.029
URH	STS-1	VSE-355G	42.9	143.7	129	*19.11*	13.68	**16.497**	-	-	-	-	572	1.08	1.01	0.144
WTR	STS-2	VSE-355G2	34.4	136.6	1042	1.04	0.86	0.773	1026	1.04	1.02	0.137	672	1.06	1.03	0.043
YAS	STS-2	VSE-355G2	35.7	135.2	1019	1.05	1.00	0.530	1000	1.03	0.98	0.106	715	1.05	1.03	0.064
YMZ	STS-1	VSE-355G2	36.9	140.2	624	*1.18*	1.14	0.664	608	*1.16*	1.02	0.115	239	1.12	1.00	0.219
YNG	STS-2	VSE-355G2	24.4	123.0	-	-	-	-	2705	1.03	1.01	0.037	2384	1.07	1.01	0.013
YSI	STS-2	VSE-355G2	35.2	132.9	1206	1.05	1.01	0.391	1187	1.07	1.04	0.062	926	1.07	1.03	0.057
YTY	CMG-1T	VSE-355G	34.3	131.0	1400	0.96	*0.78*	0.284	1381	0.93	*0.80*	0.045	1121	0.95	*0.78*	0.036
YZK	CMG-1T	VSE-355G	35.1	134.5	1108	1.06	1.03	0.410	1090	1.04	1.02	0.091	798	1.03	1.01	0.059
ZMM	STS-2	VSE-355G2	26.2	127.3	2299	1.08	0.97	0.194	2281	1.07	0.94	0.029	1936	1.04	*0.85*	0.009

Table 4.3: Table 4.2 continued. Summary of F-Net station performance during large earthquakes in Autumn, 2003. Epicenters are located in Figures 4.50, 4.55 and 4.56.

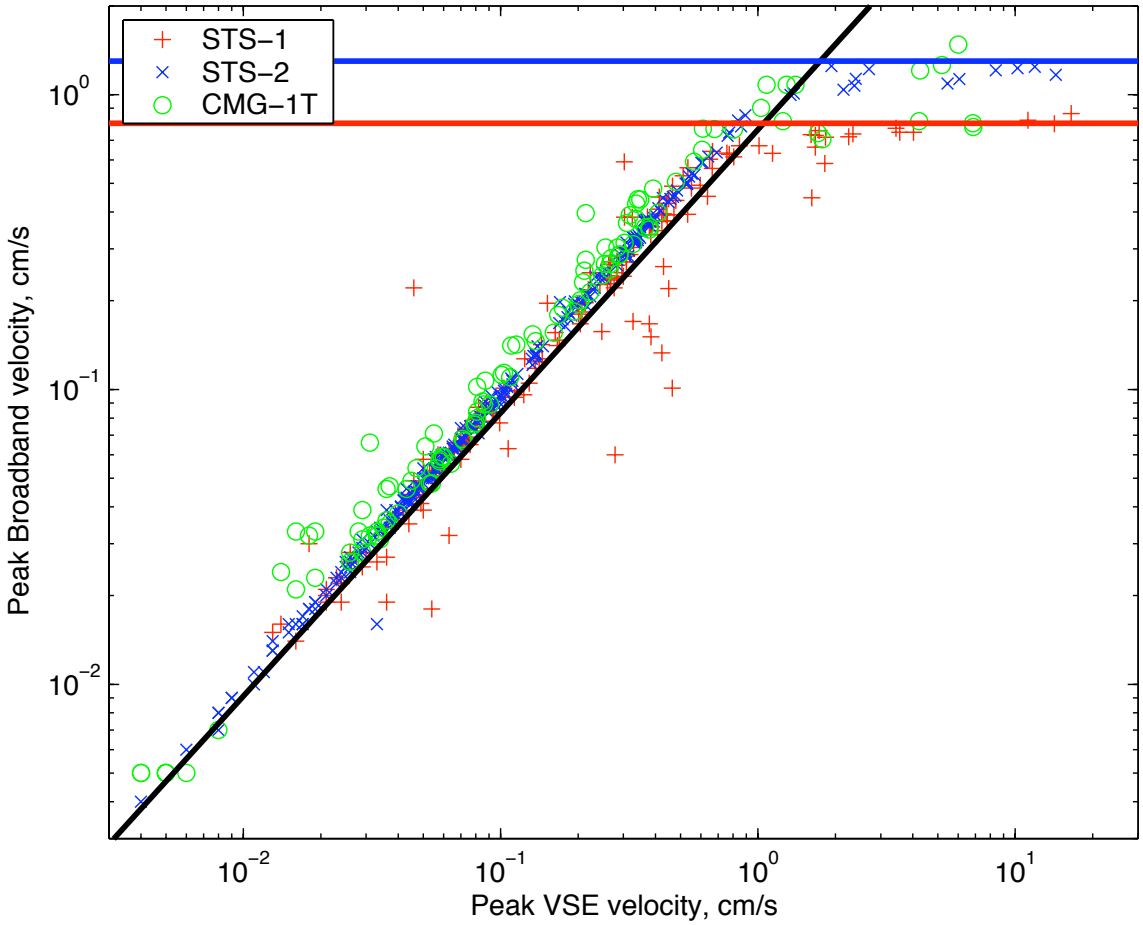

Figure 4.60: F-Net data from the 3 earthquakes: Comparison of peak broadband velocity against peak strong motion (VSE) velocity for each of 555 channels. Stations with STS-1 represented by: red plus; STS-2: blue cross; CMG-1T: green circles. The black line represents equal velocities for both instruments, the line on which data below clip is expected to fall on. Blue line is expected clip for STS-2 (and CMT-1T), at $1.3 cm/s$, red line is expected clip for STS-1, at $0.8 cm/s$

velocity to peak strong motion velocity for each component (equivalent to $1/K_E$, $1/K_N$ and $1/K_Z$). It is clear there is a lot of variation for the CMG-1T stations, though there is a bias to ratios above 1. There is some cluster of events just above a ratio of 1.6, which is the expected ratio if an STS-1 gain has been assigned to the CMG-1T. [From Table 2.1, we see sensitivity of STS-1 is $\sim 2500V/m/s$, and an STS-2 and CMG-1T have $1500V/m/s$, a ratio of 1.66.] The STS-1 also has a lot of variation, though ratios tend to be less than 1, and some clustering below a ratio of 0.6, which is consistent with a station gain of the STS-1 replaced with that of an STS-2. The STS-2 has much less variation, and has an average ratio of ~ 1.

The ratios for all instruments tend to drop sharply as they approach the expected clip levels, which indicates clipping. In fact, many of the instruments seem to clip at levels below the expected clip, but for the STS-1 and STS-2, the clip occurs within 80% of the expected clip for almost all instruments. This is observed in Figure 4.61 with the clustering of STS-2 channels between the two vertical blue lines, and for the STS-1 channels between the two vertical red lines. It is noted there is no exceedance of the expected clip for any of these channels. In contrast, the CMG-1T has a much broader range of apparent clipping, from $0.7cm/s$ to $1.45cm/s$.

In order to investigate the mean and standard deviation for the broadband stations below clipping, all data within 80% of the STS-2 clip for the STS-2 channels, and within 80% of the STS-1 clip for the CMG-1T and STS-1 channels is disregarded. The resultant data set may be summarised as:

	STS-2	STS-1	CMG-1T
# channels	252	141	96
$\left[\frac{peakBBvel}{peakVSEvel}\right]$ mean	0.971	0.930	1.116
$\left[\frac{peakBBvel}{peakVSEvel}\right]$ std. deviation	0.049	0.384	0.232

These means and standard deviations confirm that in this network, the STS-2 is a more consistent and reliable instrument then the STS-1 and CMG-1T.

It is noted that since all broadband components are compared with the the VSE-355G/G2, they are thus also sensitive to any variations from the VSE sensor calibration.

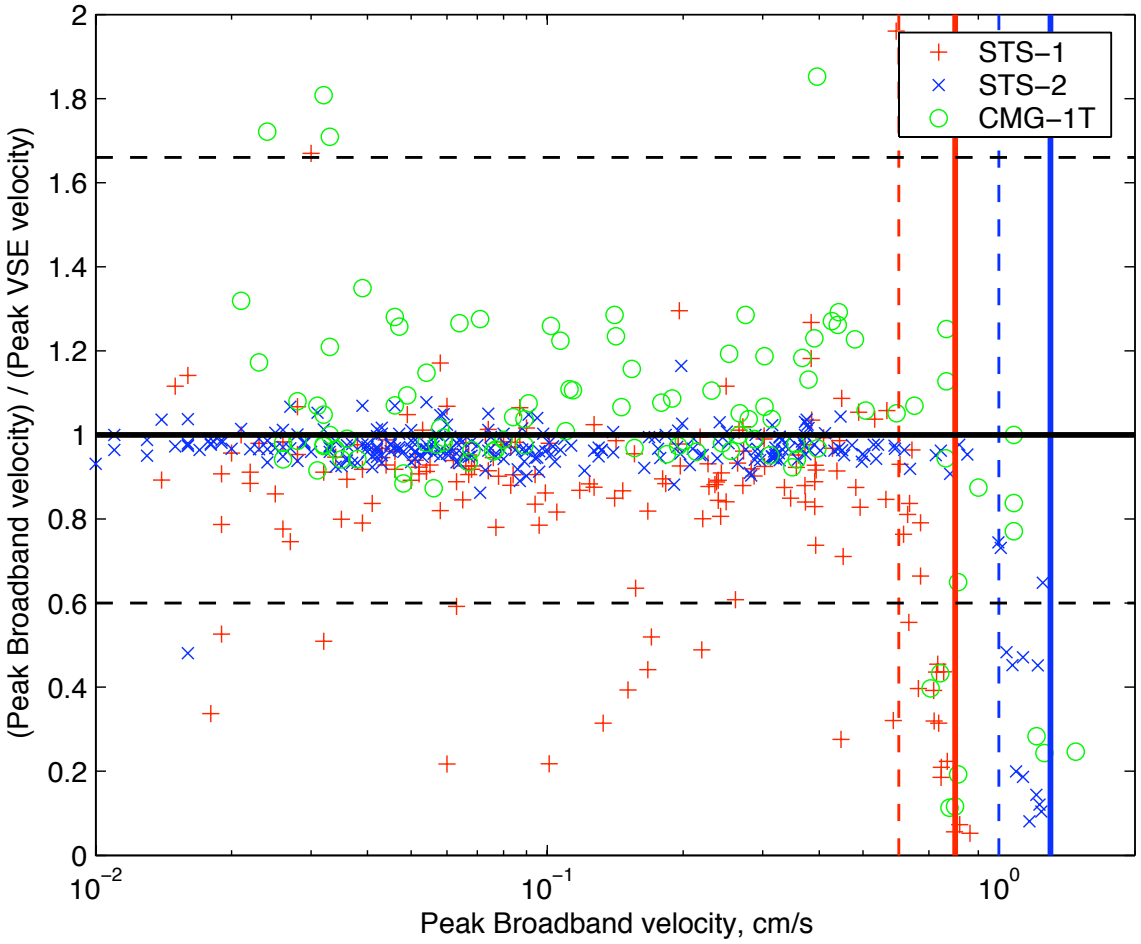

Figure 4.61: F-Net data from the 3 earthquakes: Comparison of peak velocity ratios against peak broadband velocity for each of 555 channels. STS-1: red plus; STS-2: blue cross; CMG-1T: green circles. The solid black line is expected ratio, 1. Dotted lines are expected ratios if simple instrument gain errors have occurred. Blue line: expected clip for STS-2, CMT-1T ($1.3 cm/s$), red line: expected clip for STS-1 ($0.8 cm/s$). Dotted red, blue lines are at 80% of these clip levels.

Figure 4.62 shows there is no correlation between component and deviation from expected behaviour. Any correlation trends more with instrument type, as seen in Figure 4.61.

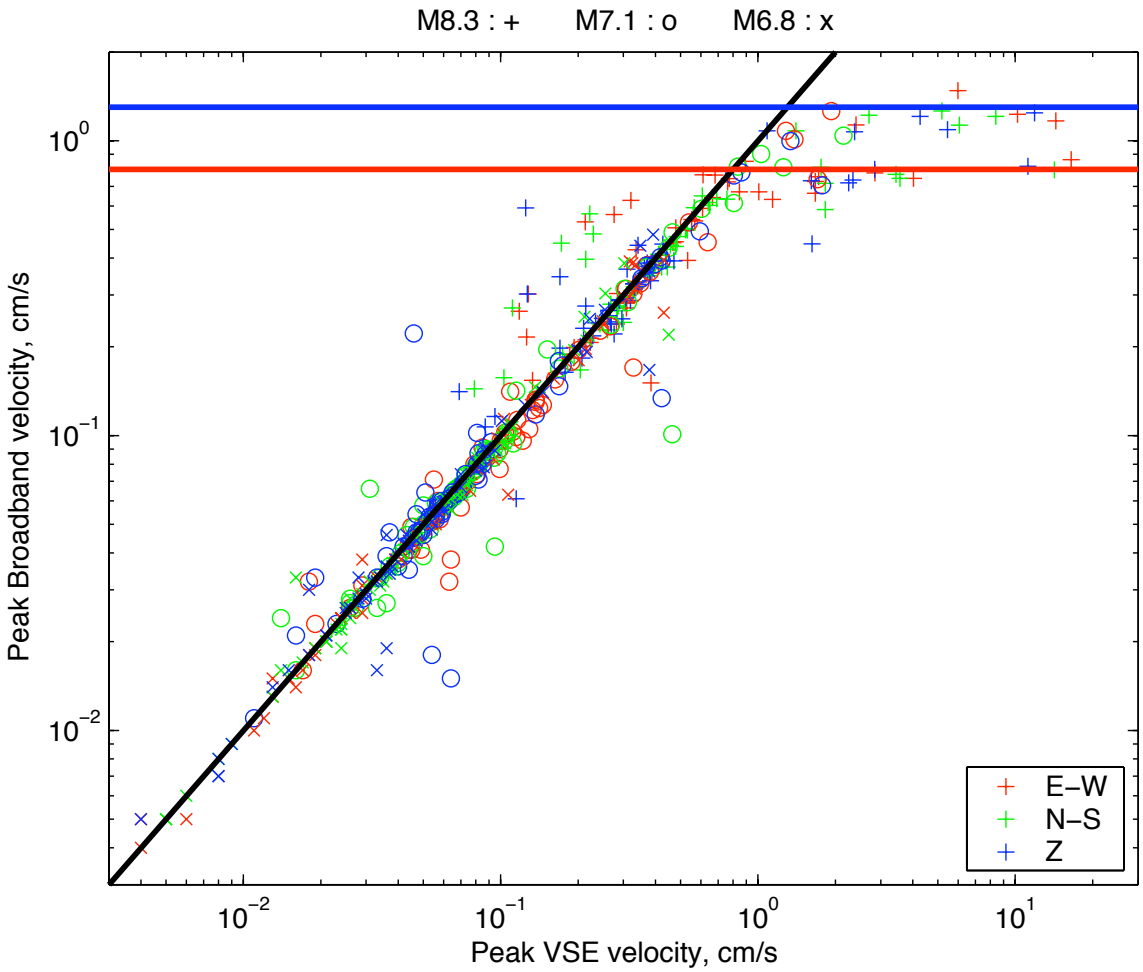

Figure 4.62: F-Net data from the 3 earthquakes: Comparison of peak broadband velocity against peak strong motion (VSE) velocity for each of 555 channels. As Figure 4.60, with colours representing channel orientations rather than broadband instrument type. Observe no error trending with individual components.

Finally, this dataset can be used to observe how the velocity decays with distance from the epicenter. Figure 4.63 shows on a log scale there appears to be a roughly linear decay of velocity with distance. The distance range here is from $100km$ to $3000km$. A least squares fit to the data shows this decay rate of velocity amplitude with distance varies in the form of $vel \propto 1/r^n$, with n varying from 1.65 (M6.8) to 1.26 (M7.1). This is roughly consistent with the expected values of 1.42 (rock sites) and 1.62 (basin sites), developed from regression

analysis using a catalogue of southern California events (Cua, 2004).

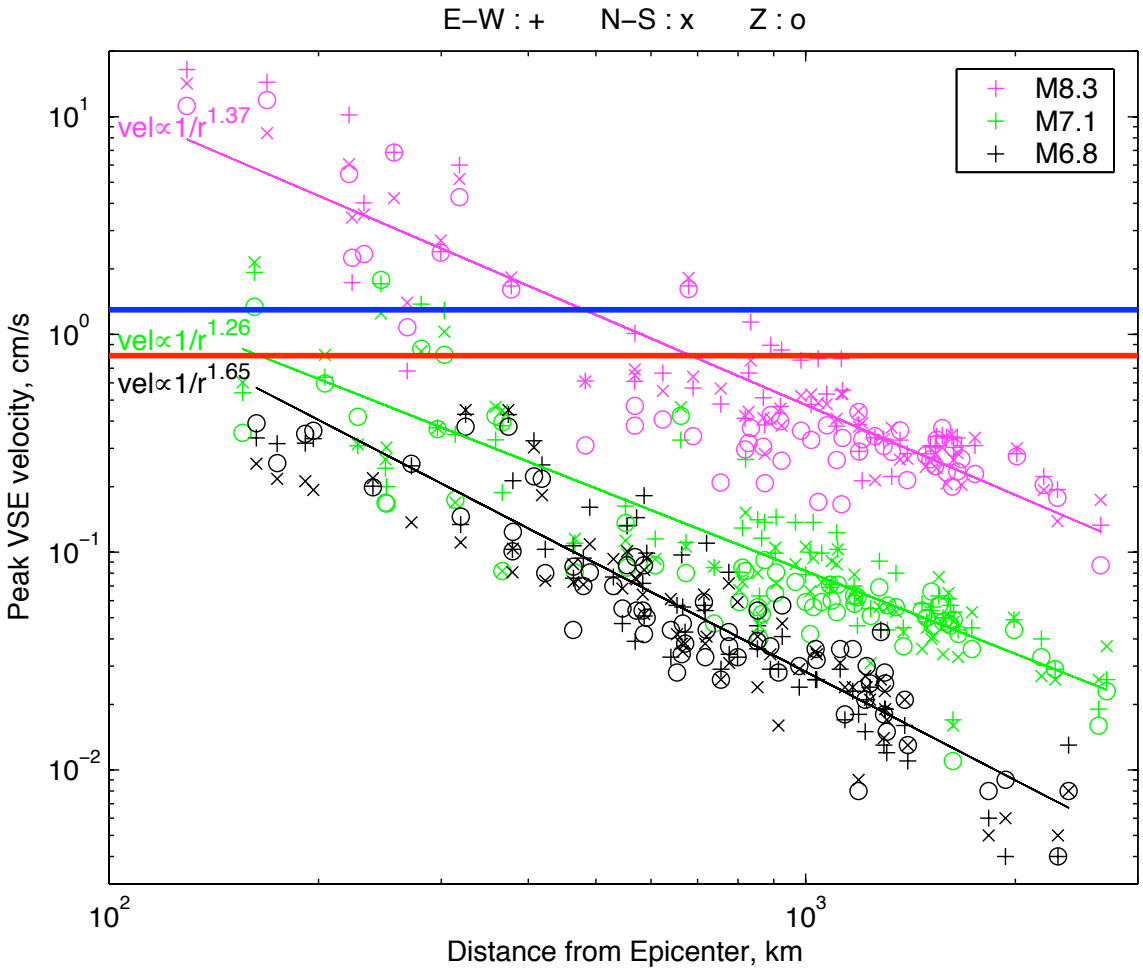

Figure 4.63: Comparison of peak strong motion velocity against distance from the epicenter for the three earthquakes, using F-Net data. Blue line: expected STS-1 and CMG-1T clip, red line: expected STS-1 clip. In M8.3, signals out to 1000km clip the STS-1. Compare ratios of velocity decay with distance to relationship of $vel \propto 1/r^n, n = 1.42(rock), 1.62(basin)$ from Cua (2004).

4.7 Summary

The many results of the analysis of the strong and weak motions recorded over Japan from the M8.3 25 Sept 2003 Tokachi-Oki earthquake are summarised below —

• Seismic data is available from 4 main networks. Nationwide Networks run by NIED are: 1. F-Net — a 24-bit broadband network with strong motion (VSE-355G/G2) and

high-gain velocity sensors co-located in vaults. About 100 stations throughout Japan, separated by about $100km$. 2. K-Net — a dense 24-bit strong motion accelerometer network with 1000 stations nationwide, at $20km$ intervals. Free-field sites, but often noisy urban locations. 3. KiK-Net — an up-hole down-hole network of 24-bit accelerometers, with minimum borehole depth of $100m$. 650 stations nationwide, located a quiet sites, often hard-rock. A final network local to Hokkaido run by the Civil Engineering Research Institute of Hokkaido consists of over 100 16-bit stations of strong motion VSE255EI instruments, with a corner at $56s$. Stations are located on civil infrastructures such a road embankments, bridges, and large buildings.

• F-Net VSE-355G2 instruments, identical to the instrument tested in this thesis, also exhibit low clip levels during the earthquake. As in the lab, once velocities reach about $16cm/s$, spikes in frequency associated with non-physical ground displacements occur. Only 2 VSE-355G2 recorded velocities significantly above this clipping velocity, and both had this problem (Figures 4.13 and 4.20). Another recorded $16.6cm/s$ and did not clip (Figure 4.47). A VSE-355G recorded $25cm/s$ without clipping, though this was the only sensor of this type to measure velocities above $14cm/s$ (Figure 4.29). VSE-355EI sensors in the WISE network record over $100cm/s$ without clipping (Figure 4.15).

• GPS data is recorded by GEONET, and is freely available over the Web at a sample rate of one data point per day. Many seismic stations are located in close proximity to GPS stations, and large permanent offsets are recorded ($> 1m$) over a wide area (Figures 4.5 and 4.6). These well recorded large displacements provide an important dataset for understanding how permanent displacements may be determined during strong ground motions.

• Strong motion seismic data, whether recorded by accelerometers or strong motion velocity sensors, is very sensitive to ground tilts, which cannot be readily distinguished from ground translation. A tilt of 0.003^o in an accelerometer, or strong motion velocity instrument, will produce a $10cm$ offset from the true displacement after only $20s$. Tilts larger than this are widespread in the observed seismic data.

• The expected tectonic tilts are determined from the vertical co-seismic deformation between GPS stations. In the most severely displaced regions, these tilts are very small (of

the order of 0.0005^o). This is too minor to significantly obscure permanent displacements of many *cm*, widespread over most of the island of Hokkaido. As many seismic stations do have offsets compatible with larger tilts, they may be due to local site failure. Landslides, lateral spreading, and liquefaction were indeed observed over large regions near the epicenter.

• In sites where little ground tilting occurs, such as many down-hole KiK-Net and vaulted F-Net stations, and also some up-hole KiK-Net K-Net stations, permanent ground displacements from the seismic data is very similar to displacements measured by GPS (Figures 4.28, 4.35 and 4.42).

• high-rate GPS ($1sps$) is not freely available from GEONET, but was obtained for a sample of station from Kristine Larson. Preliminary analysis of this dataset shows excellent correlation with GPS for many stations. A methodology to combine the high-rate GPS data and the seismic data, which is easily affected by tilting, can lead to a complete understanding of ground motions — translations and displacements, at a given site.

• There are numerous KiK-Net sites in the region, where very small amounts of tilt is observed by the deep down-hole sensors, with the up-hole sensors recording local site tilting due to a variety of effects, which could include liquefaction and lateral spreading. In general, tectonic tilts determined from GPS data are shown to be almost negligible compared to the observed tilts.

• Though the WISE network is very dense, with many strong motion velocity sensors in the near source region (F-Net only has 4 stations that record over $10cm/s$), this network is unfortunately inappropriate for the studies undertaken here. Sensor component alignment appears to be unreliable. Also, the sensors are not located in 'free-field' sites (as this network is installed to monitor civil infrastructure) many have obvious structural resonances, or suffer site failure. Further, the sensor characteristics are not as broadband as other sensors used in this study, with a corner at $56s$ instead of at least $80s$. This increases the sensor noise for permanent displacement estimation.

• Regional ground motions from Tokachi-Oki observed over the length of Japan by the broadband F-Net stations show that high-gain broadband instruments have all saturated within $500km$ of the rupture, and some saturate at distances up to $1000km$ from the epicen-

ter (Figure 4.50).

• The Tokachi-Oki, and other large earthquakes, provide an excellent dataset for estimating the state-of-health of the sensors in a seismic network. By comparing timeseries from the broadband and strong motion sensors, which have been excited above the noise level over a very broad area, incorrect station gains, or faulty sensors, can be readily identified. Pathological errors in station gains were found for the CMG-1T and STS-1 broadband sensors. It is not known whether this is characteristic of the sensor, or is isolated to F-Net in particular (Figures 4.50, 4.55, 4.56 and 4.61).

• The large number of saturated broadband instruments provide insight into the overall performance of broadband sensors at levels near clipping. The STS-2 and STS-1 are shown to reliably clip at, or within 80%, of their expected clip levels ($1.3 cm/s$ and $0.8 cm/s$ respectively). There was a larger variation in clipping for the CMG-1T (Figure 4.61).